PERFORMANCE ASSESSMENT OF LIME-POZZOLAN MORTARS WITH STRAW AGGREGATE FOR SOUND AND THERMAL INSULATION PURPOSES

A THESIS SUBMITTED TO
THE GRADUATE SCHOOL OF NATURAL AND APPLIED SCIENCES
OF
MIDDLE EAST TECHNICAL UNIVERSITY

BY

MİYASE MERVE KAPLAN

IN PARTIAL FULFILLMENT OF THE REQUIREMENTS
FOR
THE DEGREE OF MASTER OF SCIENCE
IN
BUILDING SCIENCE IN ARCHITECTURE

SEPTEMBER 2019

Approval of the thesis:

PERFORMANCE ASSESSMENT OF LIME-POZZOLAN MORTARS WITH STRAW AGGREGATE FOR SOUND AND THERMAL INSULATION PURPOSES

submitted by **MİYASE MERVE KAPLAN** in partial fulfillment of the requirements for the degree of **Master of Science in Building Science, Department of Architecture, Middle East Technical University** by,

Prof. Dr. Halil Kalıpçılar
Dean, Graduate School of **Natural and Applied Sciences** _____

Prof. Dr. Cana Bilsel
Head of Department, **Architecture** _____

Assoc. Prof. Dr. Ayşe Tavukçuoğlu
Supervisor, **Architecture Dept., METU** _____

Prof. Dr. Mehmet Çalışkan
Co-Supervisor, **Mechanical Engineering Dept., METU** _____

Examining Committee Members:

Prof. Dr. Sinan Turhan Erdoğan
Civil Engineering Dept., METU _____

Assoc. Prof. Dr. Ayşe Tavukçuoğlu
Architecture Dept., METU _____

Prof. Dr. Emine Nevin Caner Saltık
Architecture Dept, METU _____

Prof. Dr. Ceyhan Kayran İşçi
Chemistry Dept., METU _____

Assoc. Prof. Dr. Semra Arslan Selçuk
Architecture Dept., Gazi University _____

Date: 05.09.2019

I hereby declare that all information in this document has been obtained and presented in accordance with academic rules and ethical conduct. I also declare that, as required by these rules and conduct, I have fully cited and referenced all material and results that are not original to this work.

Name, Surname: Miyase Merve Kaplan

Signature:

ABSTRACT

PERFORMANCE ASSESSMENT OF LIME-POZZOLAN MORTARS WITH STRAW AGGREGATE FOR SOUND AND THERMAL INSULATION PURPOSES

Kaplan, Miyase Merve
Master of Science, Building Science, Department of Architecture
Supervisor: Assoc. Prof. Dr. Ayşe Tavukçuoğlu
Co-Supervisor: Prof. Dr. Mehmet Çalışkan

September 2019, 143 pages

The main concern of the study is to propose lime-based straw-mixed mortars with pozzolanic additives to be used as qualified building materials, particularly for sound and thermal insulation purposes and to assess their performance properties in this regard. Compositional properties of a specific type of traditional exterior plaster were inspiring for the production of porous lime-based straw-mixed mortar samples with high thermal resistivity and sound absorption properties. Several mortar mixtures, mainly composed of lime as binder, wheat straw fibers as aggregate and metakaolin as the pozzolanic additive, were prepared in various "binder: pozzolanic additive: straw" ratios. Comprehensive laboratory analyses were conducted on those newly-produced samples to determine their performance properties. The lowest bulk density and thermal conductivity and the highest porosity and sound absorption characteristics were achieved at the straw-mixed samples with the binder: straw ratio of 3:1. The L3W1 and LM3W1 samples have low but still enough flexural and compressive strength while LM3W1 is stiffer than L3W1. The sample L3W1 with weighted sound absorption coefficient (αw) value of 0.40 has higher sound absorption than the sample LM3W1 while the sample LM3W1 with thermal conductivity (λ) value of 0.06 W/mK is more thermal resistive than the sample L3W1. Since stiffness and strength characteristics are crucial for building materials, further analyses can be performed to

prepare lime-based straw-mixed pozzolanic (LMW) mixtures with a higher content of straw for the development of more thermal resistive and sound absorptive materials coated with protective and breathable plasters having higher water impermeability.

Keywords: Lime, Pozzolan, Bio-Aggregate, Insulation, Material

ÖZ

SES VE ISI YALITIMI AMACIYLA ÖNERİLEN SAMAN AGREGALI PUZOLAN KATKILI KİREÇ HARÇLARININ PERFORMANS ANALİZLERİ

Kaplan, Miyase Merve
Yüksek Lisans, Yapı Bilimleri, Mimarlık Bölümü
Tez Danışmanı: Doç. Dr. Ayşe Tavukçuoğlu
Ortak Tez Danışmanı: Prof. Dr. Mehmet Çalışkan

Eylül 2019, 143 sayfa

Çalışmanın temel amacı, saman içeren puzolan katkılı kireç esaslı harçların, özellikle ses ve ısı yalıtımı amacıyla kullanılabilecek nitelikli yapı malzemeleri olarak önerilmesi ve bu çerçevede performans özelliklerinin değerlendirilmesidir. Özel bir geleneksel dış sıva türünün ham madde ve temel fiziksel özellikleri, yüksek ısıl dirençli ve ses yutma özellikli, gözenekli, kireç esaslı saman içerikli harç örneklerinin üretiminde ilham verici olmuştur. Bu çerçevede, birbirinden farklı "bağlayıcı: puzolanik katkı: saman" oranına sahip, ana bağlayıcısı saf kireç olan, metakaolin katkılı ve saman içerikli harç karışımları hazırlanmıştır. Üretilen harç örneklerinin performans özeliklerini saptamak amacıyla kapsamlı laboratuvar analizleri yapılmıştır. En düşük birim hacim ağırlığı ve ısıl iletkenlik ile en yüksek gözeneklilik ve ses yutma özellikleri, bağlayıcı: saman oranı 3:1 olan örneklerde elde edilmiştir. L3W1 ve LM3W1 örnekleri, düşük fakat yeterli eğilme ve basınç dayanımı değerlerine sahipken, LM3W1 örneği daha rijittir. Ağırlıklı ses yutma katsayısı (αw) değeri 0.40 olan L3W1 örneği, LM3W1 örneğinden daha yüksek bir ses yutma özelliğine sahipken, ısıl iletkenlik (λ) değeri 0.06 W/mK olan LM3W1 örneği daha yüksek bir ısıl direnç göstermektedir. Yapı malzemeleri açısından rijitlik ve mukavemet özellikleri çok önemli olduğu için, gelecek çalışmalar daha yüksek oranlarda saman içeren, yüksek ısıl direnç ve ses yutma özellikleri olan, nefes alan ve düşük su emme

kapasitesine sahip bir katmanla korunmuş, kireç esaslı puzolan katkılı saman içeren (LMW) malzeme örnekleri hazırlamak üzere şekillenmelidir.

Anahtar Kelimeler: Kireç, Puzolan, Bio-Agrega, Yalıtım, Malzeme

To every woman who runs with the wolves

ACKNOWLEDGMENTS

I would like to express my deepest gratitude to my supervisor Assoc. Prof. Dr. Ayşe Tavukçuoğlu for her academic guidance, constant encouragement, and sacrifices. I also would like to express my sincere thanks to my co-supervisor Prof. Dr. Mehmet Çalışkan for his invaluable support with his deep knowledge, and patience. I am truly honored to call myself as their student and complete this thesis with them.

I would like to thank the METU Materials Conservation Laboratory for providing such an exceptional working environment for me during my studies. I also would like to thank MEZZO Studio, Mezzo Team and METU Central Laboratory for their valuable help and technical support during acoustical and thermal experimentations.

I should extend my gratitude to my dearest friends for their constant support and help during my graduate journey. It is truly a privilege to share all those moments with them. Thank you for all the great books I read and all the good music I listened to.

Finally, I am grateful to my loving family, my beautiful mother Ferda Kaplan, my big-hearted father Dr. Nejdet Kaplan and my amazing sister Dr. Mehveş Kaplan who have always believed in me even when I doubt myself. Thank you for supporting me with love and patience throughout my life. Thank you for constantly reminding me of the importance of positivity and being kind. Thank you for raising me right. This thesis is dedicated to them.

TABLE OF CONTENTS

ABSTRACT v

ÖZ vii

ACKNOWLEDGMENTS x

TABLE OF CONTENTS xi

LIST OF TABLES xiv

LIST OF FIGURES xvii

LIST OF ABBREVIATIONS xxiv

LIST OF SYMBOLS xxv

CHAPTERS

1. INTRODUCTION 1

1.1. Argument 3

1.2. Aim and Objectives 3

1.3. Disposition 4

2. LITERATURE REVIEW 5

2.1. Resource Efficiency in the Context of Building Materials 5

2.2. Insulation Materials Commonly-Used in Construction Practice 8

2.2.1. Thermal Properties of Some Insulation Materials 14

2.2.2. Sound Absorption Properties of Some Insulation Materials 16

2.2.3. Basic Physical and Mechanical Properties of Some Building Insulation Materials 19

2.3. Thermal and Acoustic Characteristics of Bio-Fibers 22

2.3.1. Wheat Straw as a Promising Bio-Fiber Ingredient in Thermal and Sound Insulation Materials 24

2.4. Lime Mortars Throughout History 26
2.4.1. Pozzolanic Admixtures 29
2.4.2. Pozzolanic Reaction 30
2.4.3. Carbonation Reaction 31
2.4.4. Metakaolin 31
2.5. Lime-Based Pozzolanic Mortars Used in Anatolia 33
3. MATERIAL AND METHOD 37
3.1. Sample Preparation 37
3.1.1. Traditional Exterior Plaster Sample as an Inspiring Material 38
3.1.2. Lime-Pozzolan Mortars with Straw Aggregate 39
3.2. Determination of Basic Physical Properties 50
3.3. Determination of Physicomechanical Properties 54
3.4. Determination of Mechanical Properties 56
3.5. Determination of Acoustical Properties 57
3.6. Determination of Thermal Properties 59
3.7. Determination of Compositional Properties 63
3.8. Determination of Pozzolanic Activity 64
3.9. Determination of Mineralogical and Microstructural Properties 66
4. RESULTS 69
4.1. Performance and Compositional Properties of the Traditional Exterior Plaster Sample 69
4.2. Some Raw Material Characteristics of Straw Aggregate, Metakaolin Additive, and Lime Binder Used in the Mixture of Newly-Produced Mortars 73
4.3. Basic Physical Properties of New Mortar Samples 76
4.4. Physicomechanical Properties of New Mortar Samples 81
4.5. Mechanical Properties of New Mortar Samples 83

4.6. Acoustical Properties of New Mortar Samples 85

4.7. Thermal Properties of the New Mortar Samples 88

4.8. XRD Analyses Results for the Confirmation of Pozzolanic Reaction Products Formation in New Mortar Samples 96

4.9. Cross-Section Image Analyses of New Mortar Samples 108

5. DISCUSSION 115

5.1. Potentials and Limitations of Newly-Produced Mortar Samples to be Used as Construction Materials 115

5.2. Performance Evaluation of Newly-Produced Mortar Samples in Comparison to Some Commonly-Used Thermal and Sound Insulation Materials 122

5.3. Impact of Straw Aggregate and Metakaolin Additive on Performance Properties of Newly-Produced Mortar Samples 126

5. CONCLUSION 129

REFERENCES 133

LIST OF TABLES

TABLES

Table 2.1. Thermal characteristics of the conventional and alternative building insulation materials 16

Table 2.2. Sound absorption coefficients of the conventional and alternative building insulation materials 19

Table 2.3. Basic physical and mechanical properties of the conventional and alternative building insulation materials 21

Table 2.4. Thermal conductivity and sound absorption coefficient values of unprocessed plant-based natural fibers at specific density and thicknesses 23

Table 3.1. Lime: metakaolin: wheat straw proportions in the mixtures and flow diameters, fractions by weight 43

Table 3.2. Material properties, performed experiments and followed analyses methods 49

Table 3.3. Water vapor permeability classes for building materials according to SD and RT values 54

Table 3.4. Evaluation of pozzolanic activity by conductivity measurements.....66

Table 4.1. The aggregate content by weight (%) and binder /aggregate ratio of the historical mortar sample (SK.Pe.6) 70

Table 4.2. Physical, physicomechanical properties, water vapor permeability and pozzolanic activity characteristics of historical mortar sample 73

Table 4.3. Pozzolanic activity measurements of wheat straw and metakaolin with saturated lime method..... 76

Table 4.4. Pozzolanic activity measurements of wheat straw and metakaolin with electrical conductivity method 76

Table 4.5. The bulk density, effective porosity, and water absorption capacity values of the straw-mixed lime-based (LW) and straw-mixed lime-pozzolan (LMW) samples 78

Table 4.6. The equivalent air layer thickness of water vapor diffusion (SD, m), water vapor diffusion resistance index (μ, unitless), and water vapor transmission rate (RT, g/hm^2) values of the straw-mixed lime-based (LW) and straw mixed lime-pozzolan (LMW) samples..... 80

Table 4.7. The ultrasonic pulse velocity (UPV, m/s) and corresponding modulus of elasticity (MoE, MPa) values of the new mortar samples 82

Table 4.8. The flexural strength and compressive strength values of the straw-mixed lime-based (LW) and straw-mixed lime-pozzolan (LMW) samples..... 84

Table 4.9. Sound absorption coefficient (α) values of the newly-produced mortar samples in octave band central frequencies (Hz) 86

Table 4.10. Noise reduction coefficient (NRC) and weighted sound absorption coefficient (αw) values of the newly-produced mortar samples 86

Table 4.11. Thermal conductivity, specific heat, thermal diffusivity, and thermal effusivity values of new mortar samples in relation to density and thickness values 89

Table 4.12. Temperature differences during 60 seconds of heating period and the heating rates of the straw-mixed lime-based mortar samples together with rock wool, glass wool, EPS, AAC insulation block, wood, and marble samples 91

Table 4.13. Temperature differences during 60 seconds of cooling period and the cooling rates of the straw-mixed lime-based mortar samples together with rock wool, glass wool, EPS, AAC insulation block, wood, and marble samples 92

Table 4.14. Temperature differences during 60 seconds of heating period and the heating rates of the straw-mixed lime-pozzolan mortar samples together with rock wool, glass wool, EPS, AAC insulation block, wood, and marble samples.....94

Table 4.15. Temperature differences during 60 seconds of cooling period and the cooling rates of the straw-mixed lime-pozzolan mortar samples together with rock wool, glass wool, EPS, AAC insulation block, wood, and marble samples.....95

Table 5.1. Physical, physicomechanical, and mechanical properties of newly-produced straw-mixed lime-pozzolan mortar samples..... 118

Table 5.2. NRC, αw, α_{mid}, α_{high}, and λ values of straw-mixed lime-pozzolan mortar samples 121

Table 5.3. Sound absorption coefficient and NRC values of straw-mixed lime-pozzolan mortar samples of this study and commonly-used conventional and alternative insulation materials 123

Table 5.4. Thermal conductivity, specific heat, and thermal diffusivity values of straw-mixed lime-pozzolan mortar samples of this study and commonly-used conventional and alternative insulation materials..... 125

LIST OF FIGURES

FIGURES

Figure 2.1. Cross section images of wheat straw fibers 25

Figure 3.1. Original lime mortar samples collected from the traditional Kemer Village house 39

Figure 3.2. Raw materials preparation **a)** wheat straw fibers **b)** metakaolin 41

Figure 3.3. Curing conditions and setup inside climate chambers 44

Figure 3.4. Curing and dehydration spaces **a)** climate chambers **b)** desiccators 44

Figure 3.5. Samples produced for sound absorption coefficient measurements according to ISO 10534-2:1998 46

Figure 3.6. Samples produced for compressive and flexural strength measurements according to TS EN 1015-11:2000 47

Figure 3.7. Samples produced for thermal conductivity measurements 48

Figure 3.8. a) Water-immersed samples prepared for the determination of bulk density, effective porosity, and water absorption capacity **b)** Samples prepared for the determination of equivalent air thickness of water vapor permeability and water vapor diffusion resistance index 51

Figure 3.9. a) Flexural strength test setup **b)** Compressive strength test setup 57

Figure 3.10. a) Material sample inside impedance tube sample holder **b)** Standard curve and classes defined by TS EN ISO 11654:2000 59

Figure 3.11. Active infrared thermography measurement setup and material samples 63

Figure 3.12. Pozzolanic activity test with saturated lime method **a)** before chemical titration with EDTA **b)** after chemical titration with EDTA 65

Figure 4.1. The particle size distribution of aggregates of the traditional exterior plaster sample by weight 70

Figure 4.2. The aggregate content of the traditional lime-based straw-mixed mortar (SK.Pe.6) 70

Figure 4.3. The cumulative passing percentage of grains of SK.Pe.6..... 71

Figure 4.4. XRD traces of SK.Pe.6 (Q: quartz, C: calcite, T: tobermorite (CSH))... 71

Figure 4.5. Cross-section images of SK.Pe.6..... 72

Figure 4.6. XRD traces of wheat straw (<0.125 mm in grain size) 74

Figure 4.7. XRD traces of $Ca(OH)_2$ (<0.125 mm in grain size) 74

Figure 4.8. XRD traces of kaolin (<0.125 mm in grain size) 75

Figure 4.9. XRD traces of metakaolin (<0.125 mm in grain size)..... 75

Figure 4.10. The graph showing the bulk density (g/cm^3) and effective porosity (% by volume) values of the straw-mixed lime-based (LW) and straw-mixed lime-pozzolan (LMW) samples 78

Figure 4.11. The graph showing the equivalent air layer thickness of water vapor diffusion ($SD_{3\ cm}$, m) and water vapor diffusion resistance index (μ, unitless) values of the straw-mixed lime-based (LW) and straw mixed lime-pozzolan (LMW) samples 80

Figure 4.12. The graph showing the upper range and lower range of ultrasonic pulse velocity values ($UPV_{LOW\text{-}RANGE}$, $UPV_{UP\text{-}RANGE}$) of the new mortar samples and their UPV values obtained with a slight pressure ($UPV_{w/PRESS}$) 82

Figure 4.13. The graph showing the UPV values obtained with a slight pressure ($UPV_{w/PRESS}$) and corresponding modulus of elasticity values belonging to the new mortar samples 83

Figure 4.14. The graph showing the flexural strength (kPa) and compressive strength (kPa) values of the straw-mixed lime-based (LW) and straw mixed lime-pozzolan (LMW) samples..... 84

Figure 4.15. Sound absorption coefficients of the new mortar samples..... 87

Figure 4.16. Sound absorption coefficients of the straw-mixed lime-based (LW) mortar samples 87

Figure 4.17. Sound absorption coefficients of the straw-mixed lime-pozzolan (LMW) mortar samples 88

Figure 4.18. Thermal conductivity values of new material samples 90

Figure 4.19. View of the straw-mixed lime-based mortar samples together with marble and wood samples and rock wool, glass wool, expanded polystyrene, autoclaved aerated concrete thermal insulation samples (on the left top), its IR image taken at the ambient conditions of 25.3ºC and 31%RH before heating period was started – initial IR image (on the left bottom); the last IR image of the heating period after the uniform heating with halogen lamp for a period of 200s (on the right bottom); and the

differential IR image showing the temperature difference between the initial and the last IR images for the heating period of 200s (on the right top)..... 91

Figure 4.20. View of the straw-mixed lime-based mortar samples together with marble and wood samples and rock wool, glass wool, expanded polystyrene, autoclaved aerated concrete thermal insulation samples (on the left top), its IR image taken at the ambient conditions of 25.3ºC and 31%RH after the uniform heating with halogen lamp for a period of 200s – initial IR image (on the left bottom); the last IR image of the cooling period when halogen lamps were switched off for a period of 200s (on the right bottom); and the differential IR image showing the temperature difference between the initial and the last IR images for the cooling period of 200s (on the right top) 93

Figure 4.21. View of the straw-mixed lime-pozzolan mortar samples together with marble and wood samples and rock wool, glass wool, expanded polystyrene, autoclaved aerated concrete thermal insulation samples (on the left top), its IR image taken at the ambient conditions of 24.3ºC and 33%RH before heating period was started – initial IR image (on the left bottom); the last IR image of the heating period after the uniform heating with halogen lamp for a period of 218s (on the right bottom); and the differential IR image showing the temperature difference between the initial and the last IR images for the heating period of 218s (on the right top)..... 94

Figure 4.22. View of the straw-mixed lime-pozzolan mortar samples together with marble and wood samples and rock wool, glass wool, expanded polystyrene, autoclaved aerated concrete thermal insulation samples (on the left top), its IR image taken at the ambient conditions of 24.3ºC and 33%RH after the uniform heating with halogen lamp for a period of 218s – initial IR image (on the left bottom); the last IR image of the cooling period when halogen lamps were switched off for a period of 180s (on the right bottom);, and the differential IR image showing the temperature difference between the initial and the last IR images for the cooling period of 180s (on the right top)..... 96

Figure 4.23. XRD traces of L1W0-outer powder (P: Portlandite, C: Calcite) 98

Figure 4.24. XRD traces of L1W0-inner powder (P: Portlandite, C: Calcite)..... 98

Figure 4.25. XRD traces of L9W1-outer powder (P: Portlandite, C: Calcite, T: Tobermorite) 99

Figure 4.26. XRD traces of L9W1-inner powder (P: Portlandite, C: Calcite, T: Tobermorite) 99

Figure 4.27. XRD traces of L7W1-outer powder (P: Portlandite, C: Calcite, T: Tobermorite) 100

Figure 4.28. XRD traces of L7W1-inner powder (P: Portlandite, C: Calcite, T: Tobermorite) 100

Figure 4.29. XRD traces of L5W1-outer powder (P: Portlandite, C: Calcite, T: Tobermorite) 101

Figure 4.30. XRD traces of L5W1-inner powder (P: Portlandite, C: Calcite, T: Tobermorite, Q: Quartz) 101

Figure 4.31. XRD traces of L3W1-outer powder (P: Portlandite, C: Calcite, T: Tobermorite, Q: Quartz) 102

Figure 4.32. XRD traces of L3W1-inner powder (P: Portlandite, C: Calcite, T: Tobermorite, Q: Quartz) 102

Figure 4.33. XRD traces of LM1W0-outer powder (P: Portlandite, C: Calcite, T: Tobermorite) 103

Figure 4.34. XRD traces of LM1W0-inner powder (P: Portlandite, C: Calcite, T: Tobermorite) 103

Figure 4.35. XRD traces of LM9W1-outer powder (P: Portlandite, C: Calcite, T: Tobermorite, Q: Quartz) 104

Figure 4.36. XRD traces of LM9W1-inner powder (P: Portlandite, C: Calcite, T: Tobermorite, Q: Quartz) 104

Figure 4.37. XRD traces of LM7W1-outer powder (P: Portlandite, C: Calcite, T: Tobermorite, Q: Quartz) 105

Figure 4.38. XRD traces of LM7W1-inner powder (P: Portlandite, C: Calcite, T: Tobermorite, Q: Quartz) 105

Figure 4.39. XRD traces of LM5W1-outer powder (P: Portlandite, C: Calcite, T: Tobermorite, Q: Quartz) 106

Figure 4.40. XRD traces of LM5W1-inner powder (P: Portlandite, C: Calcite, T: Tobermorite, Q: Quartz) 106

Figure 4.41. XRD traces of LM3W1-outer powder (P: Portlandite, C: Calcite, T: Tobermorite, Q: Quartz) 107

Figure 4.42. XRD traces of LM3W1-inner powder (P: Portlandite, C: Calcite, T: Tobermorite, Q: Quartz) 107

Figure 4.43. Magnified images of L1W0 taken by stereomicroscope (top left: exterior surface with 25x, top right: cross-section image with 7x, bottom left: cross-section image with 12.5x, bottom right: cross-section image with 25x) 109

Figure 4.44. Magnified images of L9W1 taken by stereomicroscope (top left: exterior surface with 25x, top right: cross-section image with 7x, bottom left: cross-section image with 12.5x, bottom right: cross-section image with 25x) 109

Figure 4.45. Magnified images of L7W1 taken by stereomicroscope (top left: exterior surface with 25x, top right: cross-section image with 7x, bottom left: cross-section image with 12.5x, bottom right: cross-section image with 25x)..... 110

Figure 4.46. Magnified images of L5W1 taken by stereomicroscope (top left: exterior surface with 25x, top right: cross-section image with 7x, bottom left: cross-section image with 12.5x, bottom right: cross-section image with 25x)..... 110

Figure 4.47. Magnified images of L3W1 taken by stereomicroscope (top left: exterior surface with 25x, top right: cross-section image with 7x, bottom left: cross-section image with 12.5x, bottom right: cross-section image with 25x)..... 111

Figure 4.48. Magnified images of LM1W0 taken by stereomicroscope (top left: exterior surface with 25x, top right: cross-section image with 7x, bottom left: cross-section image with 12.5x, bottom right: cross-section image with 25x)..... 111

Figure 4.49. Magnified images of LM9W1 taken by stereomicroscope (top left: exterior surface with 25x, top right: cross-section image with 7x, bottom left: cross-section image with 12.5x, bottom right: cross-section image with 25x)..... 112

Figure 4.50. Magnified images of LM7W1 taken by stereomicroscope (top left: exterior surface with 25x, top right: cross-section image with 7x, bottom left: cross-section image with 12.5x, bottom right: cross-section image with 25x)..... 112

Figure 4.51. Magnified images of LM5W1 taken by stereomicroscope (top left: exterior surface with 25x, top right: cross-section image with 7x, bottom left: cross-section image with 12.5x, bottom right: cross-section image with 25x)..... 113

Figure 4.52. Magnified images of LM3W1 taken by stereomicroscope (top left: exterior surface with 25x, top right: cross-section image with 7x, bottom left: cross-section image with 12.5x, bottom right: cross-section image with 25x)..... 113

LIST OF ABBREVIATIONS

ABBREVIATIONS	
LCA	Life cycle assessment
PUR	Polyurethane
EPS	Expanded polystyrene
XPS	Extruded polystyrene
WHO	World Health Organization
TL	Transmission loss
NRC	Noise reduction coefficient
XRD	X-Ray diffraction
RH	Relative humidity
SD	Equivalent air thickness of water vapor permeability
RT	Water vapor transmission rate
UPV	Ultrasonic pulse velocity
MoE_{dyn}	Dynamic modulus of elasticity

LIST OF SYMBOLS

SYMBOLS

λ	Thermal conductivity
U-Value	Thermal transmittance
c	Specific heat capacity
D	Thermal diffusivity
e	Thermal effusivity
μ	Water vapor diffusion resistance coefficient
φ	Porosity
ρ	Density
μ-value	Water vapor diffusion resistance factor
α	Sound absorption coefficient
αw	Weighted sound absorption coefficient
α_{mid}	Average sound absorption coefficient (500-1000 Hz)
α_{high}	Average sound absorption coefficient (1000-2000
θ	Water absorption coefficient
σ_f	Flexural strength
σ_c	Compressive strength
ν_{dvn}	Poisson's ratio
ΔT	Temperature difference

CHAPTER 1

INTRODUCTION

Globally, the construction industry is one of the biggest exploiters of the world's natural resources due to the increasing demand for raw materials for material productions. Worldwide, the most extracted minerals are all associated with the building sector, some of which are on the verge of depletion (Valero-Delgado, 2014). The construction sector, together with buildings, has the highest shares of non-renewable energy consumption and greenhouse gas emissions (Eurostat, 2018; Global Alliance for Buildings and Construction, 2018; IEA, 2018). The building sector is one of the biggest polluters of the environment as well. The realization of the depletion of the world's sources led to the emergence of the sustainability concept. Various studies were conducted to reveal the overall environmental impact of building materials with the life cycle assessment methodology. Obtained data proved that the most common building materials, used in today's society, cannot be regarded as environmentally responsible or sustainable due to the high levels of non-renewable energy consumption, global warming potential, and toxicity rates (Asdrubali, Schiavoni & Horoshenkov, 2012). Several conventional building materials are harmful to human health since they directly influence indoor air quality (WHO, 2002).

Energy consumption rates of buildings are directly related to the properties of building envelopes. Heating and cooling-related activities have the largest share of building-related energy consumptions. For this reason, thermal insulation is vital to lower energy demands, to sustain energy efficiency, and to ensure structures' durability. Acoustical insulation has a primary influence on human health and comfort since noise is a major urban threat. Generally, thermal insulation materials are also used for acoustical applications. Commercially dominant thermal and sound insulation materials are known to be harmful to the environment and human health due to the non-renewable raw material demand, embodied energy backgrounds, high amounts of

CO_2 emissions during manufacturing, and toxicity rates (Asdrubali *et al.,* 2012; Jelle, 2011).

This realization awoke an interest in alternative insulation materials produced from renewable bio-sources and recycled sources. Even though low-impact insulation materials are already commercialized and in use, their market share is highly limited. Several studies were conducted on bio-fibers to reveal their true potential to be used within thermal and sound insulation material compositions. Traditionally, straw fibers have been used for various building applications from load-bearing walls to bio-aggregates for lime-based mortars and plasters.

From a historical perspective, mortars applied on the facades of structures naturally acted as insulation layers. Throughout history, lime has been used as a primary building material until the determination of the true nature of hydraulic behavior, which led to the discovery of cement (Veiga, 2017). Development of Portland cement caused lime-based mortars fall into disuse, which caused the disappearance of artisanal knowledge about traditional construction techniques (Barbero-Barrera *et al.,* 2013). Awareness about environmental sustainability and compatibility problems of cement mortars revive the interest of lime-based mortars with pozzolanic additives and bio aggregates to be used as a building component.

In the last years, historical lime-based mortars were questioned to re-discover their potentials. In Anatolia, lime-based mortars with pozzolanic additives were commonly used. Studies show that traditional lime-based mortars are still durable and functioning. To overcome well-known inconveniences of lime-based mortars, pozzolanic additives, especially calcined clays, were used to enhance mechanical performances. Moreover, plant fibers were used as natural reinforcing agents within various mortar compositions. Traditional mortars promoted thermal and acoustical comfort.

Learning from the past; it is possible to create new low-impact material compositions to be used for thermal and sound insulation purposes, which can also be compatible with the historic fabric. Therefore, this study deals with the development of lime-based

straw-mixed building materials with or without pozzolanic additives to be used for thermal and sound insulation purposes and the assessment of performance characteristics of those products.

1.1. Argument

A literature survey was conducted on lime-based mortars about their thermal and acoustic behavior and the effects of bio-fiber and pozzolanic additive utilizations into the mortar compositions. Even though the straw as a bio-aggregate and the metakaolin as pozzolanic additive were widely used within lime-based compositions throughout the historical context, there is no comprehensive study in the literature that shows individual and combined effects of straw and metakaolin in the lime-based mortar mixtures. There is a lack of knowledge about thermal and sound insulation properties of those kinds of products. Performance properties of lime-based mortars are investigated mostly in terms of mechanical behavior, mineralogical properties and pozzolanic behavior. Moreover, pozzolanic activity and behavior of straw fibers within lime-based compositions have not been examined yet. Bio-aggregate and pozzolanic additive utilization within lime-based mortars without any other additive, aggregate or chemical component is an inspiring research topic that needs comprehensive research effort.

1.2. Aim and Objectives

The main aim of the research is to develop new lime-based straw-mixed porous building materials with and without metakaolin having potentials for thermal and acoustical insulation purposes.

By the end of the study, it is expected to:

— Determine performance properties of traditional exterior plaster sample obtained from Kemer Village (Salihli/Manisa) to be used as an inspiration source for the formulation of new material composition;
— Develop some types of lime-based products with wheat straw and metakaolin;

— Examine basic physical, physicomechanical, mechanical, mineralogical, and microstructural properties of the newly-produced products to discuss their potentials to be used as building materials;
— Assess their performance properties with a focus on thermal and acoustical features, such as sound absorption coefficient and thermal conductivity;
— Evaluate overall performance characteristics of lime-based products to discuss their potentials and limitations particularly for their use as building insulation materials;
— Discuss the individual and combined impact of wheat straw and metakaolin on the performance properties of lime-based products.

The results achieved are expected to contribute to building materials technology and to guide improving low-impact materials and their performances for their specific uses as thermal and sound insulation materials.

1.3. Disposition

This study is composed of 6 chapters in which this introduction is the first where the motivation and content of this study are described. The second chapter, literature review, presents a review of present studies and data on resource efficiency in the context of building materials, insulation materials used in construction practice and their performance properties, thermal and acoustic characterization of bio-fibers with a special focus on wheat straw, lime mortar use throughout history, and lime-based mortars with pozzolanic additives from the Turkish context. The third chapter, material and method, explains the procedure of sampling and conducted laboratory experiments according to various standards. The fourth chapter, results, reports obtained performance properties data of the traditional lime-based mortar sample and the newly-produced lime-based straw mixed products. The fifth chapter, discussion, compares to obtained results to discuss the overall performances of the newly-produced material samples. Finally, the sixth chapter, conclusion, briefly summarizes the importance of the study with recommendations for further studies.

CHAPTER 2

LITERATURE REVIEW

In this chapter, a brief literature survey is presented regarding resource efficiency in the context of building materials, thermal and sound insulation materials commonly used in the construction sector and their performance properties, as well as thermal and sound insulation characteristics of bio-fibers with a special focus on wheat straw. Moreover, literature findings of lime mortars and pozzolanic admixtures used in lime-based mortars, especially metakaolin, are presented. Lastly, the history and usage of lime-based mortars with pozzolanic additives in Anatolia are briefly summarized.

2.1. Resource Efficiency in the Context of Building Materials

Several models depend on different paradigms have been studied by researchers to predict the correlation between overall capacity and consumption rates of non-renewable resources of Earth's crust. Starting from the very first attempts, it was concluded that the human use of essential resources has surpassed sustainable rates (Meadows *et al*., 1972; Meadows *et al.*, 1992). Even though studied models and generated predictions have been widely questioned, research efforts were particularly effective to remind that Earth's sources are finite, would be depleted and must be preserved. This realization led to the international recognition of the concept of sustainability. In 1987, the World Commission on Environment and Development published a milestone report titled "Our common future", also known as Brundtland Report which defines sustainability as the "development that meets the needs of the present without compromising the ability of future generations to meet their own needs" (Brundtland,1987).

Valero-Delgado (2014) points out that worldwide the most extracted minerals are iron ore, aluminum, copper, zinc, magnesium, limestone, and gypsum all of which are closely linked with the building industry. Analyses about the state of depletion of the world's mineral resources reveal that some traditional building material sources like

tin, zinc or copper are under the danger of scarcity because of exponential use over the last decade (Valero-Delgado, 2014). On the other hand, some commodities like limestone, gypsum, sand or clay are very abundant in the crust so no scarcity problems are foreseen either now or in the medium to long term (Valero-Delgado, 2014).

Recent energy trends reveal that the buildings and construction sector, among all other industries, are responsible for the largest shares of energy consumption and greenhouse gas emissions. According to 2017 statics, it is estimated that construction industry along with buildings consume more than 35% of global primary energy, emits approximately 40% of energy-related CO_2 worldwide and generates almost 35% of total waste of European Union countries (Eurostat, 2018; Global Alliance for Buildings and Construction, 2018; IEA, 2018). The magnitude of the global building industry also shows that interventions through more sustainable development may effectively promote resource efficiency and reduce undesired environmental impacts.

Building-related emissions can be examined under three main categories; direct emissions from fossil fuel combustions in the buildings, indirect emissions from power and heat generations and embodied carbon or CO_2 emissions from the use of building materials. 28% of the annual buildings-related CO_2 emissions caused only by the material used in buildings (Global Alliance for Buildings and Construction, 2018). The primary contributor to this type of emission is cement and steel production which have high process emissions and are used in large quantities, followed by the production of aluminum, glass and insulation materials (Global Alliance for Buildings and Construction, 2018). Even though many countries have comprehensive regulations about direct and indirect emissions, awareness about embodied carbon is increasing recently.

Huberman and Pearlmutter (2008) conclude that depending on the building's life expectancy and its energy-efficiency level for operation, the embodied energy commonly accounts for in the range of 10% to 60% of the total energy used during the structure's lifetime. The utilization of environmentally responsible building materials has turned into a major subject to accomplish the objective of sustainable construction and energy-efficient design. In reaction to ever-increasing material demand,

consciousness about abiotic depletion potential, global warming potential, toxicity potential of construction materials and their sustainability rates have contributed to introducing life cycle assessment (LCA) investigations. The strategy used to survey the environmental impacts of a given material is known as life cycle assessment (LCA) and incorporates the complete life cycle of the product, procedure or activity, in other words, the extraction and processing of raw materials, manufacturing, transportation and distribution, use, maintenance, recycling, reuse and final disposal (Pacheco-Torgal, 2014). This technique quantifies and compares material and energy inflows and material emissions outflows from a life cycle perspective for advancement opportunities and provides guidelines for the choice of construction materials (Ding, 2014). The life cycle assessment of building materials is crucial to develop environmental profiles of materials. LCA studies are guiding to understand the importance and effectiveness of environmentally responsible building materials which may assist to significantly decrease greenhouse gas emissions and energy consumptions.

The most common methods to assess the environmental impact of materials are cradle-to-grave (LCA) and cradle-to-gate approaches. The first technique accounts for every stage of a product's life from the raw material extraction to the disposal or recycling of the product. The second strategy discusses the product's lifecycle partially, from raw material extraction until the material's transportation from the production plants to the customers.

Certain impact categories are defined for environmental impact studies. Embodied energy is the sum of the total direct and indirect energy used in the entire lifecycle of a product (Asdrubali, 2009). Depending on the methodology followed, embodied energy may also be named as primary energy consumption or cumulative energy demand. Embodied energy is typically measured in megajoules of energy per kilogram of the product (MJ/kg). Non-renewable cumulative energy demand is defined as the total amount of non-renewable energy used during the complete lifecycle of a product. It is also expressed with MJ/kg. Global Warming Potential is a measure that expresses the relation between the amount of heat trapped by a certain mass of gasses emitted

and the amount of heat trapped by a comparable carbon dioxide mass over a specific time. It is expressed as a factor of CO_2.

Materials continue to affect the environment even after installation. Material selection plays a vital role in designating indoor air quality. Since people spend lots of their time inside enclosed spaces, indoor conditions have significant effects on the health, comfort, and performance of users. The emission of volatile organic compounds from building materials that potentially give off damaging gasses for a significant period can considerably harm human health. Moreover, maintenance, removal, and disposal of materials that contain harmful substances arise questions about safety. Materials with embodied pollution cannot be regarded as sustainable.

The building sector is one of the biggest exploiters of Earth's resources and one of the biggest polluters of the environment. The industry is therefore obliged to confront many issues about environmental policies and must take serious actions about sustainable development. In creating the objective of the environmentally responsible construction sector, the selection and use of suitable building materials are fundamental.

2.2. Insulation Materials Commonly-Used in Construction Practice

A building's energy consumption depends heavily on the features of its envelope (Schiavoni, D'Alessandro, Bianchi & Asdrubali, 2016). Enhancing the thermal performance of buildings is essential since energy demand for heating and cooling activities constitutes a considerable portion of overall energy demand. In this regard, thermal insulation materials represent a key factor together with improving appliance performance and modifying occupant behavior to sustain energy efficiency and to control embodied emissions.

In addition to the reduction of energy consumption and greenhouse gas emissions, thermal insulation is necessary to ensure the structure's durability, to contribute to the prevention of possible building damage and to reduce the operational costs. Along with thermal properties, embodied energy, overall environmental impact, fire resistance,

water vapor permeability, and toxicity are very significant for the selection procedure of the most appropriate insulation material.

Noise is a major urban threat for human health together with the air quality. Studies show that chronic exposure to noise has serious negative impacts on the auditory organs, blood pressure and cognitive performance (European Environment Agency, 2014). Other than obvious physical disturbances, noise also triggers stress, discomfort, disturbance and insomnia (European Environment Agency, 2014). Acoustical comfort is one of the major requirements for human well-being since poor acoustic conditions may cause unhealthy environments. Since noise-related problems are directly or indirectly interfering with the individual's health and comfort, acoustic insulation gains importance.

Worldwide, commonly used conventional thermal and sound insulation products from mineral, petroleum or plastics origin which dominate the market are mineral wools, polyurethane foam, expanded polystyrene, and extruded polystyrene boards. Mineral wools cover rock wool and glass wool. Rock wool is produced by melting several types of volcanic rocks such as dolostone, basalt, and diabase, at around 1600 °C (Schiavoni *et al*., 2016). It is estimated that rock wool has 30% share of European building insulation market (Asdrubali, 2006). Glass wool is manufactured at a temperature around 1400 °C by blending natural sand and borosilicate glass where the heated mass is pulled through rotating nozzles to create fibers (Jelle, 2011). For both rock wool and glass wool, acquired mineral fibers bound together using binders, generally phenolic resin and starches and oils of food-grade to eliminate dust (Schiavoni *et al*., 2016). Mineral wool products are manufactured in batt, board and pipe sections.

Polyurethane (PUR) is manufactured by an exothermic reaction between di- or poly-isocyanate and polyol (alcohol with multiple hydroxyl groups) (Schiavoni *et al*., 2016; Jelle, 2011). Polyurethane products are available as rigid foam panels and pipe sections or PUR can be used as an expanding foam for in situ applications to infill cavities around building components.

Expanded polystyrene (EPS) is obtained from the expansion of small polystyrene grains (from petroleum) with an expansion gas like pentane (Jelle, 2011). EPS products are available as panels. It is highly flammable and hazardous in case of fire because of the possible release of dangerous gasses. EPS is a thermal insulation material whose acoustic properties are not significant due to closed porosity and low density (Schiavoni *et al.*, 2016). Extruded polystyrene (XPS) is obtained from the expansion of melted polystyrene (from petroleum) with an expansion gas like pentane or carbon dioxide, where the mass of polystyrene is extruded by the pressure release through a nozzle causing the mass to expand (Jelle, 2011). XPS normally costs 10-30% more than EPS (Schiavoni *et al.*, 2016).

Performance and cost cannot be only parameters for the selection of building materials. In terms of resource efficiency, energy consumption, embodied emissions, and toxicity rates, currently used thermal and sound insulation materials that dominate the construction sector cannot be regarded as environmentally responsible or sustainable (Asdrubali *et al.,* 2012). Global market share of natural, recycled or sustainable materials for insulation purposes is not sufficient, according to 2011 statics, mineral wools (52% of the market share) and plastics (41%) prevail the market (Asdrubali, D'Alessandro & Schiavoni, 2015).

Current commercially dominant thermal and sound insulation materials, e.g. mineral wools, polyurethane foams, expanded polystyrene (EPS) or extruded polystyrene (XPS), have known to be potentially harmful to the environment and human health not only for production and construction workers but also occupants. The research on man-made vitreous fibers show that glass wool and rock wool may give serious damage to lungs through inhalation, may cause fibrosis, skin and eye irritations and sick-building syndrome (WHO, 2002).

Polyurethane foam production depends on petrochemicals, and it may contain respiratory irritants and cause occupational asthma (Asdrubali *et al.,* 2012). Moreover, since polyurethane when burning releases very poisonous substances like hydrogen cyanide (HCN), it is extremely dangerous in case of fire (Jelle, 2011). Primary energy demand, global warming potential and water footprint of EPS and polyurethane foam

are the greatest among other conventional and alternative natural insulation materials because of the high level of industrial processing (Bribian, Capilla & Uson, 2011). Discarded polystyrene isn't biodegradable and is resistant to photolysis. XPS represents very similar characteristics with EPS regarding disposal, reuse and combustion problems.

In addition to synthetic materials, awareness towards resource efficiency, embodied carbon and health issues increased the attention given towards environmentally responsible and sustainable alternatives produced from bio-fibers, forest residues, and recycled materials.

Cellulose insulation, cork boards, wood fiber insulation panels, hemp boards, kenaf panels, flax boards or sheep wool rolls represent environmentally friendly insulation materials with low environmental impact, low cost and good performances, all are commercially available.

Cellulose insulation is made from processed paper waste or wood fibers together with certain chemicals like boric acid or borax to improve material properties (Jelle, 2011). Cellulose is usually preferred as filler material for cavities either as dense panels or as a loose-fill insulation product.

Cork is the bark of a tree (Quercus suber or cork oak) that is native to southwest European countries like Spain and Portugal and northwest African countries like Tunisia and Morocco. Obtaining cork is a renewable process since it is extracted without damaging the tree. The inner structure of natural cork allows cork-based insulation products to be light, elastic and thermally and acoustically insulating since cork consists of spherical light granules containing air (Berardi & Iannace, 2015). Cork granules are expanded to cork boards under high pressure and employing steam which releases the resins held within the granules. Cork-based materials are available as boards and loose-fill insulation products.

The waste from the wood products industry is the main constituent of the production of wood fiber insulation boards that are used for cavity insulation. Wood fibers are

bounded with an agent such as aluminum sulfate to protect the product from biologic attacks.

Hemp (Cannabis sativa) is an annual bast fiber plant whose fibers are used in the textile industry for ages. Hemp fibers are known to be safe, recyclable, biodegradable and naturally resistant to insect attacks (Pedroso, de Brito & Silvestre, 2017). Recently, bast fibers of hemp are used as a raw material for thermal and sound insulation material production. For the manufacture of insulation products, hemp fibers are usually treated with soda or boron salts to improve fire resistance and then the composition is subjected to heat-setting to form a robust panel (Berardi & Iannace, 2015). Excessive water exposure leads hemp-based insulation materials to degrade (Pedroso *et al.,* 2017).

Kenaf (Hibiscus cannabinus) is a fast-growing annual plant, widespread in African and Asian countries. To produce kenaf-based insulation panels, kenaf fibers are usually mixed with polyester fibers to improve robustness. Kenaf-based insulation products are available as panels or boards.

Flax (Linum usitatissimum) is a plant that is also known as linseed. It is an ancient source of fiber. Flax consists mainly of cellulose and its fibers have a higher capacity to trap air, leading in desirable characteristics for insulation (Schiavoni *et al.,* 2016). The flax fibers are twice as durable as fibers of polyester (Pedroso *et al.,* 2017). To improve fire resistance, flax fibers are treated with certain chemicals. Fibers can be mixed with polyester fibers as binding agents to improve mechanical strength or may be manufactured without any addition. Flax-based insulation products are available as boards or rolls.

Wool is predominantly composed of a variety of amino acids whose molecular structure contributes to the fiber resilience (Berardi & Iannace, 2015). Sheep wool is a traditional building insulation material known to the world since ancient times. Virgin or recycled wools may be used for the production of insulation materials with or without certain additives. Wool has a positive impact on indoor air quality thanks

to its distinct ability to absorb noxious gases and it is incombustible. Sheep wool-based products are usually available as mats or rolls.

Even though natural fiber-based products are compatible with commonly-used synthetic alternatives, these fibers present some negative characteristics such as wettability and absorbability characters due to their open pore structure, vulnerability to biological attacks and also the high level of flammability (Zach, Hroudova, Brozovsky, Krejza & Gailius, 2013). However, with the help of the chemical treatment of fibers, these characteristics could be modified.

Environmental impact analysis on common insulation products that is based on cradle-to-gate methodology reveals that, for the same thickness value, PUR foam (135 MJ/kg) has the highest embodied energy, closely followed by XPS (130 MJ/kg) and EPS (125 MJ/kg) (Pedroso *et al.,* 2017).

Cumulative energy demands of rock wool (20 MJ/kg) and glass wool (35 MJ/kg) are considerably lower than the other synthetic materials and some alternative materials such as hemp mat (40 MJ/kg) and flax mat (50 MJ/kg) (Pedroso *et al.,* 2017). Asdrubali (2006) presents that the non-renewable cumulative energy demand of EPS is the highest, while it is the lowest for flax fiber rolls and cellulose flocks. Similarly, global warming potential of materials from synthetic fibers or petrochemical source is considerably higher than compared environmentally responsible alternatives, some of them present values very close to zero (Desarnauld, Constanzo, Carvalho & Arlaud, 2005).

Thermal and acoustic insulation is a necessity to improve building performance and to reduce energy consumption. The most important parameters about insulation material selection are still performance characteristics and cost. The environmental performance of materials is often disregarded during the selection process. In the last years, materials continue to dominate the market haven't change partly because of the wide range of production networks and effective industry investments. However, environmentally responsible alternatives from bio-fibers and renewable sources

present compatible performance characteristics with much lower environmental impacts which make them an increasingly popular area of research and development.

2.2.1. Thermal Properties of Some Insulation Materials

The fundamental aim of thermal insulation systems and materials is reducing the transmission of heat flow (Asdrubali *et al*., 2015). The thermal insulation performance of a material is evaluated depending on some essential thermal properties for both steady-state and unsteady state. The thermal conductivity, the thermal transmittance, the thermal diffusivity, the thermal effusivity, and the specific heat capacity are significant parameters that express the thermal performance.

The most determinant steady-state property of thermal insulation materials is the thermal conductivity, where the overall goal is to obtain the lowest possible conductivity values (Jelle, 2011). The thermal conductivity (λ) is defined as the steady-state heat flow passes through a unit area of 1 m thick homogenous material induced by a temperature gradient equal to 1 K at the faces, it is expressed in W/mK (Asdrubali *et al*., 2015; Schiavoni *et al.*, 2016). Lower thermal conductivity values mean higher thermal resistance and lower thermal transmittance. Materials with thermal conductivity values below 0.07 W/mK are usually recognized as thermal insulators (Asdrubali *et al*., 2015).

The thermal transmittance is (*U*-Value) is defined as the steady-state heat flow passes through a unit area of a heterogeneous material or complex component induced by a temperature gradient equal to 1 K at the faces, it is expressed in W/m^2K (Schiavoni *et al*., 2016). The thickness of the material and the heat flow due to convection and radiation are also considered in the U-Value measurements (Asdrubali *et al*., 2015). Thermal resistance, *R*-value, is the inverse of thermal transmittance.

The specific heat capacity (c) is the thermal energy required by 1 kg of material to increase its temperature 1 K, and it is expressed in kJ/kgK. The specific heat capacity is a material's ability to store thermal energy. Higher specific heat capacity value is an

indicator of the better capacity of heat storage before the actual temperature increase of the material starts.

The most determinant unsteady state property of thermal insulation materials is the thermal diffusivity which expresses the propagation of thermal waves inside the media (Schiavoni *et al*., 2016). The thermal diffusivity (*D*) reveals a material's ability to conduct and store thermal energy over time (Asdrubali *et al*., 2015). In other words, it is a measure of how fast the temperature of the material adapts to the temperature around it. The thermal diffusivity (*D*) is a material's thermal conductivity (λ) divided by density, and specific heat capacity (c) and it is expressed in m^2/s.

The thermal effusivity (*e*) is a parameter that reveals a material's heat transition behavior with an adjacent object or its surroundings. The thermal effusivity is the square root of the multiplication of the material's thermal conductivity, density, and specific heat capacity.

Schiavoni *et al.* (2016) report density, thermal conductivity and specific heat values of some common conventional and alternative insulation materials as well as fire classifications. Thermal diffusivity results are calculated following published numbers. **Table 2.1** presents the distinctive thermal characteristics of selected thermal insulation products currently available in the market. Cross interpretation of the table reveals that alternative insulation materials from renewable sources or bio-fibers exhibit compatible thermal behaviors with low conductivity, low diffusivity, and high specific heat values. Products are available in the market with variable dimension and density values. Considering this diversity, PUR foam exhibits the lowest conductivity values among conventional materials, while the kenaf board has the lowest conductivity among alternative materials. Specific heat and diffusivity values of alternative materials are generally higher than selected conventional ones.

Table 2.1. Thermal characteristics of the conventional and alternative building insulation materials (Schiavoni *et al*., 2016).

Description	Density, ρ (kg/m³)	Thermal Conductivity, λ (W/mK)	Specific Heat, c (kJ/kg K)	Fire class	Thermal Diffusivity, D (m²/s)
Conventional Materials					
Rock Wool	40-200	0.033-0.040	0.8-1.0	A1-A2	$1.25E^{-6}$ - $2.00E^{-7}$
Glass Wool	15-75	0.031-0.037	0.9-1.0	A1-A2	$2.30E^{-6}$ - $4.93E^{-7}$
Polyurethane Foam	15-45	0.022-0.040	1.3-1.5	E	$1.13E^{-6}$ - $5.93E^{-7}$
EPS Foam	15-35	0.031-0.037	1.3	E	$1.59E^{-6}$ - $8.13E^{-7}$
XPS Foam	32-40	0.032-0.037	1.5-1.7	E	$6.67E^{-7}$ - $5.44E^{-7}$
Alternative Materials					
Cellulose Insulation	30-80	0.037-0.042	1.3-1.6	B-C-E	$9.49E^{-7}$ - $3.28E^{-7}$
Cork Board	110-170	0.037-0.050	1.5-1.7	E	$2.24E^{-7}$ - $1.73E^{-7}$
Wood Fiber Insulation	50-270	0.038-0.050	1.9-2.1	E	$4.00E^{-7}$ - $8.82E^{-8}$
Hemp Mat	20-90	0.038-0.060	1.6-1.7	E	$1.19E^{-6}$ - $3.92E^{-7}$
Kenaf Boards	30-180	0.034-0.043	1.6-1.7	D	$7.08E^{-7}$ - $1.41E^{-7}$
Flax Mat	20-100	0.038-0.075	1.4-1.6	E	$1.36E^{-6}$ - $4.69\ E^{-7}$
Sheep Wool Mat	10-25	0.038-0.054	1.3-1.7	E	$2.92E^{-6}$ - $1.27\ E^{-6}$

2.2.2. Sound Absorption Properties of Some Insulation Materials

When soundwaves interact with the material, the energy of incident soundwave is reflected from the surface, transmitted through the material and absorbed within the material (Long, 2006). The law of conservation of energy states that energy cannot be created or destroyed, but it can change into other forms. The basic principle behind the sound absorption behavior of materials depends on that rule. Part of the initial energy of incident soundwave is lost due to the vibration of air molecules on the surface and within the pores of the material. By using absorbers, sound can be converted into the form of heat energy. Sound absorption is defined dissipation of acoustic energy inside a material because of friction, thermal loss or resonance phenomena (Schiavoni *et al*., 2016).

Building materials can be classified regarding their ability to reflect, absorb or transmit sound waves. Open porosity is fundamental for sound absorption. Open pores ensure an uninterrupted channel of communication with the outer surface of the material, which allows better sound absorption properties (Berardi & Iannace, 2015). Porous materials can be grouped as cellular, fibrous, or granular with respect to their microstructure (Arenas & Asdrubali, 2018).

Granular materials consist of many distinct macroscopic bodies in contact. Granular materials are highly heterogenous and exhibit a discrete nature. Cellular materials are formed by periodic inner structures who repeatedly tessellates to occupy the space. Fibrous materials are collections of large numbers of continues fibers or randomly elongated filaments and series of tunnel-like openings (Berardi & Iannace, 2015). Fibers can be from natural or artificial origin. The ability of sound absorption depends on thickness, density, porosity, fiber size, fiber orientation, tortuosity and airflow resistivity. (Antonio, 2011; Arenas & Asdrubali, 2018; Berardi & Iannace, 2015; Errman, 2015). Porous sound absorption materials are usually recognized as favorable thermal insulation characteristics (Schiavoni *et al.*, 2016).

The absorption characteristic of a material is directly linked with the thickness at lower frequencies (Antonio, 2011). Increasing the sample thickness improves the sound absorption coefficient at lower frequency ranges. For fibrous materials, absorption increases with the specific surface area of the fiber (Antonio, 2011). Microstructure and type of pores are closely related to the sound absorption mechanism. Since fibrous materials are usually anisotropic, airflow resistivity changes in between different directions. Tortuosity is the shape factor of the structure that deals with irregularity and non-uniform distribution of pores of the material (Antonio, 2011). The tortuosity increases the path length of the sound waves and viscous losses. As a result, it creates a resistivity in favor of sound absorption.

The sound absorption coefficient (α) is designated as the most determining parameter for sound absorption characteristics of materials. The sound absorption coefficient is defined as the ratio of the sum of absorbed and transmitted sound energy by the overall incident sound energy on the surface, ranging from 0 (reflective) to 1 (absorptive)

(Antonio, 2011). Since sound absorption is frequency-dependent, acoustic performance properties are usually expressed as a spectrum within a selected frequency range. Single number indexes are also present, which could be misleading for interpretation of the overall absorption behavior of materials. Absorption coefficient values of porous absorbers generally increase with frequency and they can perform within wide frequency ranges (Errman, 2015). Sound absorbers can be used to control the sound fields in performance spaces, to increase sound absorption characteristics of building partitions and to control reverberation or excess noise for acoustical comfort and speech comprehension.

Sound insulation is very often mistaken with sound absorption. Sound insulation needs the sound transferred through the structure to be reduced. Sound insulation property of materials or systems is assessed by transmission loss (TL). Noise reduction coefficient (NRC) is the mean value of the sound absorption coefficients at 250, 500, 1000 and 2000 Hertz. NRC is used to express the sound absorption behavior as a single number. However, since it is a simplification, NRC value cannot be a determinant parameter on overall sound absorption characteristics. **Table 2.2** shows the sound absorption coefficient and NRC values of selected conventional and alternative materials with respect to the thickness and density parameters.

The sound absorption coefficient and NRC of EPS and XPS exhibit lower results than the other conventional insulation materials due to closed porosity. Comparison based on NRC values reveals that cellulose and flax insulation mats have the best results among all materials under study. For higher frequencies (1000 Hz and 2000 Hz), wood fiber insulation materials have compatible characteristics with rock wool, glass wool, and polyurethane foam. The overall interpretation of the presented results proves that natural fibers have great potential to be used for sound absorption applications.

Table 2.2. Sound absorption coefficients of the conventional and alternative building insulation materials (Pedroso *et al*., 2017; Euchora, 2003; Heraklith, 2015).

Description	Thickness (mm)	Density, ρ (kg/m³)	Sound Absorption Coefficient, α				NRC
			Frequency				
			250 Hz	500 Hz	1000 Hz	2000 Hz	
Conventional Materials							
Rock Wool	50	80	0.30	0.50	0.80	0.90	0.64
Glass Wool	50	50	0.50	0.50	0.80	0.90	0.68
Polyurethane Foam	50	30	0.30	0.70	0.90	0.80	0.67
EPS Foam	50	28	0.20	0.40	0.80	0.65	0.5
XPS Foam	50	25	0.15	0.25	0.40	0.50	0.33
Alternative Materials							
Cellulose Mat	50	28	0.60	0.90	0.75	0.55	0.70
Cork Board	50	105	0.15	0.40	0.60	0.40	0.41
Wood Fiber Insulation	25	n.a.	0.15	0.30	0.75	0.95	0.55
Hemp Mat	40	40	0.60	0.60	0.55	0.50	0.57
Kenaf Boards	50	20	0.39	0.52	0.58	0.62	0.53
Flax Mat	35	43	0.65	0.84	0.80	0.55	0.71
Sheep Wool Mat	60	25	0.21	0.40	0.65	0.82	0.52

2.2.3. Basic Physical and Mechanical Properties of Some Building Insulation Materials

In addition to environmental impact, specific thermal behavior and sound absorption characteristics, there are certain other performance parameters for the comprehensive evaluation of a building insulation material. Density, water vapor diffusion resistance, compressive strength, tensile strength, and service temperature range are among critical performance criteria. **Table 2.3** presents some basic physical and mechanical characteristics of common conventional and alternative building insulation materials.

Density (ρ) is the mass of a unit volume of a material that has a direct influence on many building material performance parameters. Thermal conductivity, thermal transmittance, thermal resistance, thermal diffusivity, and thermal effusivity, as well as sound insulation characteristics of materials, exhibit density-dependent behavior.

Water vapor diffusion resistance factor (μ-value) is a unitless parameter for the water vapor permeability evaluation of building materials compared to the unit value assigned to air. Water vapor permeability is inversely proportional to μ-value. Materials with high water vapor permeability allow a passage of moisture to prevent condensation. Moisture content affects material performance, occupant comfort, and energy efficiency of building envelopes since it has a primary influence on heating and cooling loads.

Compressive strength is the maximum stress that material or structure can resist before rupture. Results for materials that do not fracture are calculated as the compressive stress at specific deformation of the material's original height. Tensile strength is the ultimate stress that material or structure can resist during elongation before fracture. A relative strength could be required from insulation materials depending on their intended use locations and installation procedures.

Service temperature range is an interval in which a material can function without compromising the original behavior. Within the maximum and minimum operating temperatures, the material is expected to perform efficiently.

Table 2.3. Basic physical and mechanical properties of the conventional and alternative building insulation materials (Schiavoni *et al.,* 2016; Moretti *et al.,* 2016; Pfundstein *et al.,* 2007; Euchora, 2003; Heraklith, 2015; Corklink, 2012; Thermonature, 2015).

Description	Typical Thickness (mm)	Density, ρ (kg/m³)	Water Vapor Diffusion Resistance Factor, μ	Compression Stress at 10% Deformation (kPa)	Tensile Strength (kPa)	Temperature Service Range (ºC)
Conventional Materials						
Rock Wool	90 - 150	30 - 200	1.0-1.3	70	>10	from -100 ºC to 750 ºC
Glass Wool	40 - 100	15 - 100	1.0-1.1	25	>10	from -100 ºC to 500 ºC
Polyurethane Foam	60 - 85	15 - 50	30-170	>130	>50	from -50 ºC to 120 ºC
EPS Foam	20 - 200	15 - 50	20-70	80 - 200	<150	from -80 ºC to 80 ºC
XPS Foam	30 - 160	30 - 55	80-150	300	<150	from -60 ºC to 75 ºC
Alternative Materials						
Cellulose Insulation Boards	25-180	30 - 80	1.7-3.0	2.5	n.a.	up to 60 ºC
Cork Board	10 -300	65 - 200	5.0-30.0	85	30 - 200	from -80 ºC to 140 ºC
Wood Fiber Insulation	15 - 120	50-270	1.0-5.0	50 - 200	2.5 - 50	up to 110 ºC
Hemp Mat	30 - 220	20-90	1.0-2.0	*not resistant to compression	> 2 x net weight	up to 120 ºC
Kenaf Boards	8 - 100	30-180	1.2-2.3	1.65 - 2.97	3.7 - 9.6	up to 250 ºC
Flax Mat	50 - 100	20-100	1.0-2.0	n.a.	n.a.	n.a.
Sheep Wool Mat	40-180	10-25	1.0-3.0	n.a.	> 2 x net weight	up to 150 ºC

Alternative insulation materials from bio-fiber or recycled content exhibit competitive thermal, acoustic, physical, and mechanical performance characteristics compared with conventional insulation products. Cellulose, cork, wood fiber, hemp, kenaf, flax, and sheep wool-based insulation products are already commercialized and available in the market. Performance-wise, mentioned alternative materials have the capability to replace conventional insulation materials. Bio-fiber based building insulation materials are valid alternatives to synthetic products.

2.3. Thermal and Acoustic Characteristics of Bio-Fibers

The development of sustainable building insulation materials from bio-fibers is currently a significant area of research. Natural fibers have considerably high-grade sound absorption and thermal insulation properties and are available in large quantities as a by-product of other production cycles (Berardi & Iannace, 2015). Natural fibers are characterized by their low density, suitable mechanical properties, simple processing, high stability, non-abrasive nature and fair price (Berardi & Iannace, 2015). Furthermore, natural fibers have a positive impact on environmental sustainability and occupational health benefits.

Natural fibers can be of plant, animal or mineral origins. Plant fibers can be categorized into stalk or wood fiber (e.g. wheat straw, rice, softwood), bast or skin fiber (e.g. hemp, flax, kenaf), leaf fiber (e.g. sisal, palm), seed fiber (e.g. cotton), and fruit fiber (e.g. coconut) (Berardi & Iannace, 2015).

The use of bio-fibers decreases the need for synthetic fibers. Fibers locally available should be preferred, since locality and availability are essential factors for sustainable development. The main disadvantages of natural fibers are their limited resistivity on biologic attacks and insufficient fire behavior in comparison with some artificial products. In order to overcome the mentioned negative aspects, bio-fibers are often treated with certain chemicals that lessen their level of sustainability.

Less treated natural fibers would perform better in terms of energy-savings and sustainability (Asdrubali *et al.,* 2012). The fiber diameter is another critical microstructural parameter since it is directly related to the sound absorption characteristics of fibrous materials (Arenas & Asdrubali, 2018).

Thermal and acoustic characterization of bio-fibers that are already in use as building materials within variable composites and other bio-fibers that are considered as prospective building material substances have been studied by different researchers.

Due to their inherited thermal conductivity and sound absorption characteristics, bio-fibers are valid alternatives to synthetic ones. **Table 2.4** reveals that high-frequency sound absorption coefficient values and lower thermal conductivity performances of bio-fibers are significant. Depending on the density and thickness, the mentioned performances may subject to improvements.

Table 2.4. Thermal conductivity and sound absorption coefficient values of unprocessed plant-based natural fibers at specific density and thicknesses (Berardi & Iannace, 2015; Alemdar & Sain, 2017; Arenas & Asdrubali, 2018; Weidong & Yan, 2012; Iannace, 2017).

Description	Fiber Diameter (μm)	Thickness (mm)	Density, ρ (kg/m³)	Thermal Conductivity λ (W/mK)	Sound Absorption Coefficient, α			
					Frequency			
					250 Hz	500 Hz	1000 Hz	2000 Hz
Cork	- cellular-	30	100	0.039	0.20	0.10	0.30	0.86
Wood	16-38	40	100	n.a.	0.40	0.50	0.65	0.91
Hemp	5-94	30	50	0.050	0.15	0.25	0.51	0.70
Kenaf	21-78	60	100	0.440	0.30	0.61	0.99	0.95
Flax	3-22	40	30	0.040	0.31	0.55	0.82	0.81
Wheat Straw	10-80	60	30 (for α) 50 (for λ)	0.067	0.11	0.20	0.49	0.60

The use of plant-based bio-fibers as building materials has a very long history; they were used for various construction purposes since the beginning of agricultural societies. However, that is a nearly forgotten tradition whereafter the introduction of synthetic fibers. Awareness of the environmental impacts of commonly-used conventional building materials has risen interest in natural fibers again. Even though some of these fibers are already commercialized as building products, their market share is quite low. Several other fibers are currently under research and development to reveal their characteristics as sources for building materials.

2.3.1. Wheat Straw as a Promising Bio-Fiber Ingredient in Thermal and Sound Insulation Materials

Straw is one of the oldest plants used for various building applications such as bales for load-bearing walls in low-rise structures, as bio-aggregate for lime and earth plasters, as roof covering, and as loose floor covering. Wheat straw (Triticum aestivum L.) is frequently preferred in Europe for straw-bale building constructions as it is easily accessible, widely available, and affordable; however, it has fewer other usages with higher value-added (Nunes, 2017).

Different from other plant-based materials used in the building industry such as hemp and kenaf, wheat straw is a by-product of preexisting fundamental food production, abundant all over the world (Nunes, 2017). Every year, tons of unused wheat straw residues are generated; however, only a small fraction is used in applications such as feedstock or energy production (Alemdar & Sain, 2007). The implementation of agricultural residues in building materials would create an alternative industrial field for unused renewable by-products.

Straw is composed of cellulose, hemicellulose, lignin, components soluble in water, and inorganic minerals including silica. Various plant species are capable of absorbing soluble silica from the soil and then translocating and depositing it in the form of $SiO_2.nH_2O$ in different parts of the plant (Cheng, Kim & Lin, 1992). The insoluble silica in the plants has an amorphous structure and often referred to as biogenic opals (Cheng *et al.,* 1992). The silica content increases the straw's durability (Nunes, 2017).

Figure 2.1 shows cross section images of different wheat straw fibers. From outside to inside, wheat straw fibers compose of a complex structure of very dense exterior structure with variable thickness and a very porous interior structure with random pore size distribution (Bouasker, Belayachi, Hoxha & Al-Mukhtar, 2014).

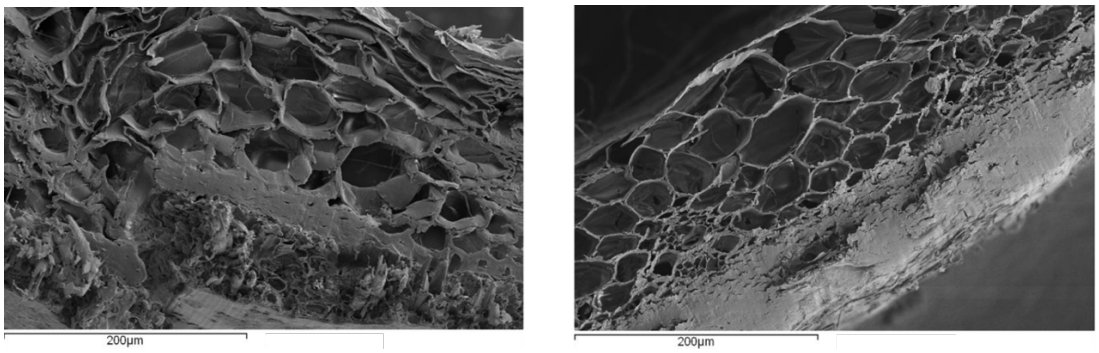


Figure 2.1. Cross section images of wheat straw fibers (Bouasker, *et al.,* 2014).

Thermal insulation behavior of straw fibers is one of the predominant advantages that is widely appreciated. For 60 kg/m^3 dense straw sample, thermal conductivity is 0.07 W/mK, thermal diffusivity is 18.2 x 10^{-7} m^2/s, and specific heat capacity is 0.6 kJ/kgK (Asdrubali *et al*., 2015). The thermal conductivity of straw is directly related to moisture content. Wheat straw also responds to the shifts in relative humidity like many other bio-based building materials. The isotherm response is the temperature-dependent reaction of materials on rising and declining relative humidity levels (Nunes, 2017). Flow resistivity of water reduces with the temperature rise, which improves the diffusion of the water into fibers. The water absorption coefficient of straw fibers varies from 290% to 400% after 60 minutes of water immersion at 20 °C (Bouasker, *et al.,* 2014). The sorption-desorption isotherms reveal that hygroscopic characteristics of wheat straw fibers improve hygrothermal comfort of building occupants (Bouasker, *et al.,* 2014).

Sain and Panthapulakkal (2006), determined tensile strength and modulus of elasticity of wheat straw fibers prepared by mechanical processing; results are reported as 58.7±51 MPa and 3.7±2.6 GPa respectively. NRC value of 50 mm thick and 80 kg/m^3 dense binderless straw boards compacted through heat and pressure is reported as 0.70 (Pedroso *et al.,* 2017).

Since plants consume CO_2 during their lifetime, straw fibers usage as a building element has a positive influence on sustainable development since it is a renewable source. Wheat straw fibers are traditional reinforcing agents with their specific properties appropriate for construction materials. Although there are certain

disadvantages such as inefficient compressive strength of straw, openness to biologic attacks and high levels of flammability as many other bio-fibers, mentioned characteristics would be engineered with chemical treatments. Wheat straw fibers have a potential to be used inside material compositions for building sector.

2.4. Lime Mortars Throughout History

Limestone, $Ca(CO)_3$, is a naturally occurring sedimentary rock. Limestone is an abundant mineral in the earth's crust that can be found in different forms and is categorized according to its origin, structure, chemical composition, and geological formation (Oates, 1998). For various industrial productions, it is a significant raw material. Quicklime (CaO), is produced through the calcination of limestone ($CaCO_3$) at temperatures ranging from 700 °C to 900 °C. Slaked lime, $Ca(OH)_2$, is obtained by mixing quicklime (CaO) with water (H_2O) in a process called slaking. Slaked lime is commonly named non-hydraulic lime.

When exposed to air, non-hydraulic lime reacts with atmospheric CO_2 to re-establish calcium carbonate in a process called carbonation. The mentioned series of chemical reactions is commonly known as the lime cycle. Hydrated lime is defined as the dry and powdered calcium hydroxide product. Natural hydraulic lime is produced from certain types of limestone, containing natural impurities such as silica, alumina, and iron, which sets through both carbonation and hydration reactions (Oates, 1998).

Non-hydraulic lime mortar is characterized by low drying shrinkage, good water vapor permeability, low mechanical strength, slow setting times, and poor water resistance (Zhang *et al.,* 2018). Hydraulic lime exhibits moderate mechanical strength, faster setting times and good water resistance (Zhang *et al.,* 2018).

Major consumer of limestone is the construction sector; it is the primary raw material of cement production, and it is used as a binder or aggregate in many building applications (Oates, 1998). Lime-based mortars were used in construction since the antiquity, one of the earliest evidence of the use of lime dates back almost 10.000 years ago, by Çatalhöyük, Turkey (7400 BC. - 6200 BC.) where lime plaster floors are

discovered (Kingery, Vandiver & Prickett, 1988; Arizzi & Cultrone, 2013). By around 1000 BC., quicklime and hydrated lime were known and widely used by many civilizations, including Romans, Greeks, Egyptians, Incas, Mayans, and Chinese (Oates, 1998). Lime as a building material with various application techniques and purposes is present in a significant portion of the world architectural heritage, especially in Europe, America, North Africa, and West Asia (Arizzi & Cultrone, 2013).

There are various compositions, additives, nature, and quality of the historic lime mortars that have survived to this day (Veiga, 2017). To cope up with well-known incontinences of non-hydraulic lime-based mortars, various additives, admixtures, and fibers were used within mortar compositions. Historical lime-based mortar examples prove that protein-based organic materials such as plant fibers, blood, hair, milk, and eggs were used to improve mortar performance characteristics (Arizzi & Cultrone, 2012). Natural fibers, mainly straw and wood chips, were used as reinforcing agents to improve fracture behavior of lime mortars via forming a net into the binder with no specific order (Stefanidou, Papachristoforou & Kesikidou, 2016). Stefanidou *et al.* (2016) state that the function of natural fibers was to transfer loads and to prevent the propagation of cracks by bridging the openings. Organic and artificial pozzolans, mineral fillers, ceramic powder, or crushed bricks were used as additives to the lime binder to particularly improve mechanical performance of mortars (Arizzi & Cultrone, 2012). Specific organic admixtures with air-entraining or water-entraining capabilities, such as linseed oil, were used to permanently engineer mortar characteristics (Nunes & Slizkova, 2014).

Natural hydraulic lime mortars and lime mortars with pozzolanic additives were commonly used empirically until the reason behind the setting process in hydraulic binders is accurately discovered (Silva, Ferreira-Pinto & Gomes, 2014). At the beginning of the 19th century, it is proved that a binder's hydraulicity results from the clay content in the limestones or the simultaneous calcination of limestone and clay (Silva *et al.,* 2014). Scientific knowledge about hydraulic reactions encouraged the industrial production of hydraulic lime and eventually Portland cement (Veiga, 2017).

Due to the development and implementation of Portland cement in the 19th century, lime-based building materials are gradually superseded by cement-based mortars. Superior mechanical strength and shorter setting and hardening times of the Portland cement were induced the lime-based mortars' fall into disuse (Barbero-Barrera *et al.,* 2013). The widespread application of cement led to the disappearance of the traditional techniques related to lime mortars (Veiga, 2017). However, the material performance characteristics of cement, especially higher mechanical strength, lower water vapor permeability, and the transfer of soluble salts to the supports were not compatible with the old masonries (Barbero-Barrera *et al.,* 2013).

In addition to incompatible material characteristics with historical structures, cement production has a massive harmful environmental impact on global warming due to the high level of CO_2 emissions. The industry itself is responsible for 5-8% of the global CO_2 emissions caused only by cement manufacturing (Jelle, 2011; Rashad, 2013). Moreover, cement production releases other environmentally harmful gasses such as SO_3 and NO_x, which have high acidification potential (Rashad, 2013). On the other hand, lime-based mortars absorb a high amount of CO_2 during the setting phase, which can account for 62% of the emissions from the combustion process (Bribian *et al.,* 2011).

Starting from the '90s, realizing the incompatibility of cement mortars on the fabric of traditional and historic constructions facilitated a return to lime mortars in restoration and renovation works (Barbero-Barrera *et al.,* 2013). In the last four decades, many scientific studies on lime and lime-based mortars have been conducted to compensate for the lost artisanal knowledge of the past, including the analysis of old mortars (Veiga, 2017).

The binder: aggregate ratio is a very significant factor that directly affects the mortar characteristics and performance properties. Researches reveal that volumetric proportions of the binder: aggregate are usually in the range of 1: 1 to 1: 2,5 in historical lime-based mortars (Veiga, 2017). Lime putties are often visible possibly due to non-hydrated quicklime, poorly mixed hydrated powder or re-precipitation of calcium carbonate (Veiga, 2017). The physicomechanical, chemical and

microstructural investigations on historical lime mortars have widely proved the presence of various pozzolanic admixtures in the mortar matrix (Matias, Faria & Torres, 2014). Lime production methods and hydration processes are also under consideration by many investigations. The existence and preservation of various historical buildings or their fractions up to this point verify the durability of the structures and selected materials. Increased interest in lime as a building material is promoted several studies about the historical materials and new lime-based products.

2.4.1. Pozzolanic Admixtures

Pozzolan is defined as "a siliceous and aluminous material which, in itself, possesses little or no cementitious value but which will, in finely divided form in the presence of moisture, react chemically with calcium hydroxide at ordinary temperature to form compounds possessing cementitious properties" (ASTM, 2019, p. 6). Pozzolans are classified as natural and artificial. Pozzolans obtained from naturally occurring minerals are generally from volcanic origin. Artificial pozzolans are either industrial by-products such as silica fume, fly ash and ceramic powder or obtained via calcination of clays. Once calcined at elevated temperatures, agricultural wastes like rice husk ash or wheat straw ash possess pozzolanic characteristics as well (Frias, Villar-Cocina, Sanchez de Rojas & Valencia-Moralez, 2005).

Various physicochemical characteristics, including the content of the glassy compounds, the cumulative and active silica content, the grain size distribution, and the specific surface area, influence the reactivity of a pozzolan (Moropoulou, Bakolas & Aggelakopoulou, 2004). Pozzolans containing particles with finer grain sizes as well as comparatively higher specific surfaces, and high percentages of amorphous silico-aluminates are highly reactive (Cabrera & Rojas, 2001). Moreover, the clay quality and the calcination temperature are significant parameters about the reactivity of artificial pozzolans (Moropoulou *et al.,* 2004).

The use of pozzolans as additives promotes hydraulic characteristics, elevates mechanical strength, and contributes higher durability to severe climate and moisture conditions of lime-based mortars (Moropoulou *et al.,* 2004). Various historic

structures show evidence for the use of pozzolans as cementitious admixtures within lime-based mortars. Lime-based mortars with calcined clays obtained from milled by-products as pozzolanic additives were accepted as quite durable and reliable and used for long centuries until the introduction of first hydraulic binders (Matias *et al.,* 2014). Two competitive chemical reactions occur within lime-pozzolan mixtures, which are pozzolanic reaction and carbonation reaction.

2.4.2. Pozzolanic Reaction

Pozzolanic activity is a material's ability to react with portlandite ($Ca(OH)_2$) in the presence of water (Bakolas *et al*., 2006). A pozzolan's reactivity predominantly depends on its mineralogical and chemical structure, the amorphous phase content, the dehydroxylation degree, the specific surface area, the portlandite content in the composition, the existence of various admixtures, and the water to binder ratio in the mixture (Bakolas *et al*., 2006). The response rate, the reaction rate, and the total portlandite consumption rate are the main parameters to assess the pozzolanic activity of a pozzolan (Grist, Paine, Heath, Norman & Pinder, 2013).

Certain compounds having cementitious characteristics occur due to the pozzolanic reaction (Frias & Cabrera, 2001). As a result of the reaction between Ca^{2+} ions and simple silicate and aluminate ions, calcium silicate hydrates (CSH) and tetracalcium aluminate hydrate (C_4AH_{13}) are formed (Cerny *et al.,* 2006). There are 30 different phases of CSH gels that are known by this time, usually with a low crystallinity degree under normal atmospheric conditions (Matias *et al.*, 2014). Depending on predominant phases, calcium silicate hydrates may be classified as Type I (i.e. honeycomb formation), which is the most common phase, and Type II (i.e. fibrous formation) (Matias *et al*, 2014). Pozzolanic reaction rates directly linked with temperature and relative humidity. High temperature and saturated relative humidity promote pozzolanic reaction (Fortes-Revilla *et al.,* 2006).

2.4.3. Carbonation Reaction

The carbonation is defined as the reaction between $Ca(OH)_2$ and diffused CO_2, which leads to the formation of $CaCO_3$ i.e. calcium carbonate (Çizer, Van Balen, Elsen & Van Gemert, 2012). The carbonation reaction is controlled by two main processes; the diffusion of CO_2 into the pore structure of $Ca(OH)_2$ is followed by the chemical reaction between dissolved CO_2 and $Ca(OH)_2$ (Çizer *et al*., 2012). The openness of the pore structure and the presence of water inside the pores are essential to ensure the diffusivity of carbon dioxide into the matrix (Van Balen, 2005). The carbonation reaction rate is directly influenced by temperature and relative humidity (Fortes-Revilla, 2006). CO_2 diffusivity depends on the pore system, drying rate, capillary transport regime and capillary condensation (Çizer *et al*., 2012).

Lime hardening due to carbonation is responsible for increasing mortar strength (Van Balen, 2005). Due to the morphology of the portlandite crystals, the carbonation of slaked lime is faster than the carbonation of lime hydrate (Çizer *et al*., 2012). Traditionally, lime mortars are wetted and dried repeatedly to enhance carbonation which can be explained by the fact that the carbonation process ends before all lime is carbonated; the mentioned technique detaches the outer carbonated layer from inner uncarbonated one as portlandite is more soluble than calcite (Van Balen, 2005).

2.4.4. Metakaolin

Metakaolin is a highly active pozzolanic material obtained via the dehydroxylation of the kaolinitic clays at temperatures around 700 °C – 800 °C (Bakolas, Aggelakopoulou, Moropoulou & Anagnostopoulou, 2006). The main constituent of kaolin is kaolinite mineral ($2H_2O.Al_2O_3.2SiO_2$), which is a hydrous aluminosilicate (Rashad, 2013). The transformation from the crystalline to the amorphous phase accompanies the dehydroxylation process of kaolinite, and this transition is affected by the calcination conditions (Shvarzman, Kovler, Grader & Shter, 2003).
Kaolin typically contains 46% SiO_2, 40% Al_2O_3, and 14% H_2O (Rashad, 2013). In the ambient atmosphere, the weight loss of pure kaolin is almost 14% after dehydroxylation (Shvarzman *et al.,* 2003; Rashad, 2013).

Metakaolin is an amorphous material that has a high capacity to rapidly react with $Ca(OH)_2$ due to the large specific surface area of its grains and high acidic oxide content ($Al_2O_3 + SiO_2 > 90\%$) (Fortes-Revilla, Martinez-Ramirez & Blanco-Varela, 2006). The main constituent of metakaolin is the metakaolinite ($Al_2Si_2O_7$) whose reactive components are silica (SiO_2) and alumina (Al_2O_3) (Pavlik & Uzakova, 2016). Pozzolanic activity of metakaolinite is strongly linked with the crystallinity of the kaolinite (Shvarzman *et al.,* 2003). Metakaolin is used within high-performance concrete, precast concrete, fiber reinforced concrete, and lime-based mortar compositions (Siddique & Klaus, 2009). Metakaolin usage increases mechanical strength, resistance to chemical attacks, and durability, which also enhances the workability and appearance of compositions (Siddique & Klaus, 2009).

The main pozzolanic reaction products that are determined in the lime-metakaolin mixtures are CSH, tetracalcium aluminate hydrate (C_4AH_{13}) and stratlingite (C_2ASH_8) (Moropoulou *et al.,* 2004; Pavlik & Uzakova, 2016). On the other hand, Bakolas *et al.* (2006) state that no C_4AH_{13} formation is detected up to 270 days of curing; instead, monocarboaluminate (C_4ACH_{11}) is formed during the pozzolanic reaction. The obtained results reveal that the tetracalcium aluminate hydrate (C_4AH_{13}) phase is unstable with aging (Gameiro, Santos-Silva, Veiga & Velosa, 2012). Depending on the curing temperatures, C_3AH_6 (hydrogarnet) formation is also observed which is associated with higher temperatures (Bakolas *et al.,* 2006). Hydrogarnet is said to have negative impacts on the mechanical strength and durability of metakaolin-lime mortars (Gameiro *et al.,* 2012). Stratlingite and calcium hydroxide are identified as incompatible phases at normal temperatures; stratlingite occurs when the metakaolin amount is enough to consume most or all $Ca(OH)_2$ content in the mixture (Pavlik & Uzakova, 2016). Stratlingite doesn't occur at metakaolin/lime pastes with low metakaolin content (Gameiro *et al.,* 2012). The reduction of metakaolin content in lime-metakaolin mortars results in a decrease in the formation of hydraulic crystalline phases (Gameiro *et al.,* 2012).

The total open porosity and cumulative volume decrease as the metakaolin-lime ratio increases (Bakolas *et al.,* 2006). The mechanical strength of lime-metakaolin mortars is higher than slaked lime mortars (Fortes-Revilla *et al.,* 2006). The ratio of the

cumulative weight of lime and metakaolin over the weight of the used aggregate is a fundamental parameter that directly affects the porosity and the mechanical strength of the mortar mixture (Fortes-Revilla *et al.,* 2006). Pozzolanic reaction decreases the shrinkage behavior of lime-metakaolin mortars (Pavlik & Uzakova, 2016).

2.5. Lime-Based Pozzolanic Mortars Used in Anatolia

Historically, lime-based mortars with pozzolanic additives such as crushed ceramics and volcanic tuff were used in Anatolia since the antiquity (Degryse, Elsen & Waelkens, 2002). Various aggregates and admixtures have been used to improve the performance characteristics of lime mortars. Performance characteristics of historical lime-based mortar samples from the Turkish context were revealed by various studies (Tavukçuoğlu, Caner-Saltık & Erol, 2018; İpekoğlu, Böke & Çizer, 2007; Tunçoku & Caner-Saltık, 2006; Böke, Akkurt, İpekoğlu & Uğurlu, 2006; Degryse *et al.,* 2002; Güleç & Tulun, 1997).

Crushed bricks or fired clays were extensively used as aggregates for lime-based mortars to enhance hydraulic characteristics since ancient times (Böke *et al.,* 2006). Mortars consist of lime as a binder and brick pieces and brick dust as an aggregate are commonly called as "horasan mortar" in Anatolia (İpekoğlu *et al.,* 2007). Mineralogical analysis of historical lime mortar samples revealed the existence of CSH gels and calcium aluminate hydrate formations, which is the clear indication of pozzolanic activity between the binder and the aggregate (İpekoğlu *et al.,* 2007; Tunçoku & Caner-Saltık, 2006). Moreover, plant fibers, especially straw fibers, traditionally have been used as bio-aggregate within lime mortars to enhance flexural strength and to control shrinkage phenomena (Stefanidou *et al.,* 2016).

Degryse *et al.* (2002) studied ancient lime-mortar samples collected from the Roman city of Sagalassos (southwest Turkey) dating from the 6th to the early 7th century. Three different types of aggregates were identified within lime-based mortar samples; limestone, crushed ceramics, and volcanic tuff (Degryse *et al.*, 2002). While crushed ceramic aggregates were used in mortars related to enhancing the hydraulic

performance of water-bearing constructions, volcanic materials were used to improve mechanical properties (Degryse *et al.*, 2002).

Tunçoku and Caner-Saltık (2006) studied ancient stone and brick masonry mortars from historical monuments situated central Anatolia dated to the 12th and 13th centuries. The research revealed that the mortars contained a high percentage of lime as a binder, which is common in historic mortars (Tunçoku & Caner-Saltık, 2006). The density and porosity values of studied samples are in the range of 1.43 – 1.76 g/cm^3 and 33 - 43%, respectively (Tunçoku & Caner-Saltık, 2006). A considerable amount of Opal-A was detected inside fine aggregates that has high pozzolanic activity and is responsible for cementitious compounds' formation (Tunçoku & Caner-Saltık, 2006).

Böke *et al.* (2006) studied lime mortars with brick aggregates from the 14th and 15th centuries used within bath buildings. The density and porosity values of studied samples were nearly 1.7 g/cm^3 and 38% by volume, respectively (Böke *et al.*, 2016). The ratio of binder over aggregate was around 1/3 by weight, and mineralogical analysis revealed that the pozzolanic reaction between the lime binder and brick aggregates mainly derived from amorphous clay mineral dissociation products (Böke *et al.*, 2016).

İpekoğlu *et al.* (2007) studied lime-based mortar samples collected from three different madrasah buildings located at western Anatolia dating back to the 16th and the 17th centuries. The ratio of binder over aggregate was around 1/2 by weight in brick masonry mortars and 1/3 by weight in stone masonry mortars (İpekoğlu *et al.,* 2007). The density and porosity values of studied samples were in the range of 1.6 – 1.8 g/cm^3 and 30-40% by volume, respectively (İpekoğlu *et al.,* 2007). Crushed bricks were used as aggregates, which exhibited pozzolanic behavior (İpekoğlu *et al.,* 2007).

Tavukçuoğlu *et al.* (2018) studied performance characteristics and local construction techniques of mortar samples collected from traditional dwellings from the southwest of Turkey, Salihli-Manisa region. The analysis revealed that there is a diversity among interior and exterior mortar compositions; exterior stone masonry mortars are found to

be composed of slaked lime, straw fibers, and pozzolanic additives; which are still durable (Tavukçuoğlu *et al.,* 2018). The density and porosity values of studied stone masonry slaked lime-pozzolan mortar samples are 1.80 g/cm^3 and 31% by volume, respectively (Tavukçuoğlu *et al.,* 2018). Moreover, water vapor diffusion resistance factor (μ-value) of the lime-pozzolan mortar sample is 10.7, which exhibits medium water vapor permeability (Tavukçuoğlu *et al.,* 2018). The ratio of binder over aggregate was in the range of 1/2,5 and 1/3 by weight in stone masonry mortars (Tavukçuoğlu *et al.,* 2018). It is concluded that calcined natural clay that composes of kaolin and illite was used as a pozzolanic additive within mortar mixtures (Tavukçuoğlu *et al.,* 2018).

The historical materials techniques and the knowledge achieved on those technologies show that by using natural resources, it is possible to produce long-term durable and ecological building materials with particular performances. For instance, the analyses show that the multi-layered historic masonry dome belonging to the Şengül Hammam, which is a 15th century Turkish bath located in Ankara, can function as an energy-efficient superstructure due to its low thermal transmittance value below 0.50 W/m^{2}K, which is the accepted threshold level given in TS 825:2013 standard for Ankara region (Tavukçuoğlu, Çiçek & Grinzato, 2008; TSI, 2013). Also, the interior plaster layers with the sound absorption coefficient at frequency 1000 Hz of 0.27 in the damp state (being in equilibrium at 85% RH) and the sound absorption coefficient at frequency 1000 Hz of 0.29 in dry state functions 7 times sound absorptive than cement-based plasters (Aydın, Tavukçuoğlu & Çalışkan, 2008). Furthermore, all layers of historic dome structure are highly-breathable materials that allow continuity through the overall dome composition, therefore eliminate the risk of condensation (Tavukçuoğlu *et al.,* 2008). On the other hand, some exterior and interior plaster layers still provide water impermeability to protect the dome structure from water intake and some interior plaster layers and the porous dome masonry composed of historic solid brick and lime-mortar still perform as high thermal resistive layers (Tavukçuoğlu *et al.,* 2008).

Studies focused on different periods from antiquity till the last century and different building typologies including archeological sites and historical monuments as well as traditional dwellings proved the widespread usage of lime-based mortars with

pozzolanic additives in Anatolia. The studies on raw material characteristics and performance properties of historical mortars and plasters revealed that the use of natural and artificial pozzolans and organic materials as pozzolanic additives improves performance characteristics of lime-based historic mortars and ensure their long-term durability. Due to the pozzolanic nature of the lime-based mixtures, the historical mortars and plasters have potential to have self-healing properties as well. Joint interpretation of results shows that basic physical and mineralogical characteristics of lime-based mortars with pozzolanic additives exhibit similar characteristics relating density, porosity, and the ratio of binder over aggregate values as well as material compositions. This is a clear indication of the transfer of knowledge about traditional lime-based mortar techniques that continued interruptedly for centuries. Still, the knowledge about traditional techniques and practices about lime-based mortars have almost lost due to the widespread usage of cement. Recently, awareness about the performance characteristics, environmental sustainability and the overall compatibility of materials with existing traditional building stock revive the interest of lime-based mortars with pozzolanic additives and bio-aggregates. Their particular performance properties related with their compositional properties were found to be inspiring for the production of new porous building materials with high thermal resistivity and sound absorption properties.

CHAPTER 3

MATERIAL AND METHOD

In this chapter, sample preparation methods and the laboratory analyses conducted on those samples are explained in detail. Sample preparation was done both for;

— a specific type of traditional exterior plaster which was the inspiring sample due to its long-term durability, its composition involving natural resources of the region, and very porous nature,

— new mortar samples produced in reference to the compositional properties of the traditional plaster.

The performance and compositional properties of the traditional sample were examined in terms of basic physical and physicomechanical characteristics, binder-aggregate ratio, and particle size distribution. Its microstructure and raw material characteristics were examined employing XRD, pozzolanic activity, and optical microscopy image analyses. The performance properties of newly-produced mortar samples were examined in terms of basic physical, physicomechanical and mechanical properties including thermal and acoustical properties. The mineralogical composition of the mortar products and their microstructure were examined by means of XRD analyses and cross-section image analyses. The pozzolanic activity of the straw used as aggregate and the metakaolin used as a pozzolanic additive in the mixture of new mortar samples were examined utilizing XRD and pozzolanic activity analyses. Sample preparation and the procedures of laboratory tests were explained under respective subheadings.

3.1. Sample Preparation

Here, the preparation of traditional exterior plaster sample and new mortar samples, produced in reference to the compositional properties of the studied traditional plaster, for several laboratory analyses are explained. Moreover, the nomenclature of the samples is described.

3.1.1. Traditional Exterior Plaster Sample as an Inspiring Material

In Anatolia, the lime-based mortars with pozzolanic additives and bio-fibers are the mixtures commonly-used for traditional mortar and plasters. Such compositions are observed to have used in many traditional houses of Kemer Village in Manisa-Salihli as exterior and interior plasters applied on timber-framed wall and stone masonry wall components. At some stone walls, lime-based straw-mixed exterior plasters are applied in two layers while lime-based straw mixed interior plasters are applied on mud plaster as a finish coat. At some timber-framed walls, lime-based straw-mixed exterior and interior plasters are applied on mud plaster as finish coats. On the other hand, one of the original exterior plaster applied on the timber-framed wall of a traditional house more than 200 years old differs from the other straw-mixed plaster samples. That sample was visually-observed that its mixture involves a considerably-higher amount of straw fiber, is still sound, and functions still being in contact with timber lath. The average thickness of the questioned mortar layer is in the range of 2 cm to 3 cm. There is a necessity to discover the compositional properties of such an extraordinary and durable exterior plaster since such compositions can be inspiring for achieving a construction material with particular thermal and sound insulation performances. From this point of view, that specific type of traditional exterior plaster sample was selected to examine its compositional properties to be inspiring for the preparation of innovative mortars. The traditional sample (coded as SK.Pe.6) within its authentic composition is shown in **Figure 3.1**.

Several analyses were conducted to learn the original raw material characteristics, mineralogical and microstructural features, basic physical and physicomechanical properties of the sample. Type of binder and aggregates, the ratio of binder over aggregate, particle size distribution, pozzolanic activity, density, porosity, water vapor permeability, and ultrasonic pulse velocity of the sample are investigated. Obtained data formed a foundation to learn about traditional construction techniques employed in this specific area and to characterize new material mixtures because the investigated mortar mixture is still durable and keeps functioning which is an evidence of the composition's efficiency.

Investigations on the traditional material and construction technology that achieved to survive to this time are essential to generate appropriate intervention scenarios for cultural and architectural heritage. Uncovered knowledge about traditional techniques is expected to be guiding for the new material productions.



Figure 3.1. Original lime mortar samples collected from the traditional Kemer Village house

3.1.2. Lime-Pozzolan Mortars with Straw Aggregate

The compositional properties and performance properties of traditionally used lime-based mortars become an inspiration for the production of new porous lime-based straw-mixed mortar compositions with or without pozzolanic admixtures. Investigations on the reference historic sample (SK.Pe.6) showed that pure lime was used as a binder and a high amount of straw is used as bio-aggregate. Reference sample has a very porous matrix and still present high pozzolanic activity with sufficient mechanical strength.

Pozzolanic reaction products that are discovered during mineralogical analysis are associated with two possible sources. The first one is the usage of a pozzolanic admixture within the material composition, a common technique to enhance hydraulic and mechanical performances of lime-based mortars.

The second possible explanation is that wheat straw fibers would have acted as a silica source for the pozzolanic reaction; since wheat straw, like most of the plant fibers, contains high amounts of amorphous silica in its natural composition. Examination of wheat straw fibers as possible pozzolanic admixtures to lime-based mortars is one of the research objectives of this study. Therefore, several mixtures mainly composed of lime, wheat straw fibers with or without metakaolin were prepared in the various binder: pozzolanic additive: straw ratios. In the mixtures, the individual and combined impact of straw fiber and metakaolin additive to the physical, thermal, acoustical, and mechanical performances of the new mortar products were investigated.

All mixtures were prepared with hydrated and powdered $Ca(OH)_2$, produced by Sigma-Aldrich (Spain) with a minimum 96% of purity, while the relevant percentage of $CaCO_3$ is about 3%. Since the water content in slaked lime may vary substantially, the dry hydrated lime powder was preferred to have more precision in the weight proportions. $Ca(OH)_2$ was mixed with a known amount of distilled water and waited at least 1 week before sampling. Metakaolin was produced by the calcination of kaolin at 700 °C for 2 hours in the oven. Kaolin produced by Sigma-Aldrich (Spain) was used as a raw material source. Calcined kaolin was waited 24 hours to cool. The formation of the metakaolin product from kaolin was confirmed via FTIR analysis.

Sun-dried wheat straw was obtained from the Ankara region. Wheat straws were separated from wheat kernels, woody stems, and earth manually. Remaining wheat straws are trimmed up to 3 cm in length and 3 mm in width by hand to obtain straw fibers. **Figure 3.2** shows the wheat straw fibers and kaolin calcination procedure. Each process is repeated following the needs of sample preparations.



a) **b)**

Figure 3.2. Raw materials preparation **a)** wheat straw fibers **b)** metakaolin

Ten different material compositions are formulated to reveal the impacts of metakaolin and wheat straw on lime-based mixtures. Lime: metakaolin: wheat straw ratios as fractions by weight are presented in **Table 3.1**. For the mixture preparations, weight proportions were used to prevent measuring inaccuracies on the mixing process. In the sample codes, the first number indicates the overall binder fracture by weight, whereas the second number denotes the aggregate fracture by weight. Before the first number, letters were used to define the binder content. Letters L, M, and W indicate the presence of lime, metakaolin, and wheat straw fibers, respectively. Samples can be grouped regarding their compositions. The first group is composed of lime and wheat straw with various binder: aggregate ratios.

In the second group, $Ca(OH)_2$ and metakaolin were mixed in the ratio of 1:1 by weight together with wheat straw fibers, which means the substitution of lime by metakaolin compared with the first group. The wheat straw ratios are the same as the first group. The reference mortar of the first group, L1W0, was prepared without any pozzolanic additions or straw fibers. The reference mortar of the second group, LM1W0, was prepared with lime: pozzolan ratio 1:1 and without straw fibers.

Water content within the mixtures was determined regarding the desired flow consistency, which corresponds to the appropriate workability of approximately 15±1 cm. The flow table consistency was determined according to the Turkish Standard TS EN 1015-3 (TSI, 2000). The standard test procedure begins with the placement of the mold with the standard shape and size in the center of the flow table and filling it with prepared fresh mortar mixture. Then, the mold is removed within 15 seconds, and the table is jolted 15 times at constant frequency, approximately once per second. The flow diameter of the fresh mortar mixture is determined by measuring the width of the spread mortar sample in two directions at right angles and taking the average of the measured values. The procedure was repeated each time after water addition until the flow diameter reaches to desired consistency.

Several mortar mixtures, corresponding to each of the ten combinations, were prepared with different lime: metakaolin: straw fiber ratios, as shown in **Table 3.1**. The distilled water blended $Ca(OH)_2$ was prepared in laboratory conditions at least one week before the material preparation with a known amount of powdered $Ca(OH)_2$ and distilled water. The overall weight of $Ca(OH)_2$ and water were calculated and recorded separately for sampling. Weight fractions, presented in **Table 3.1**, are based on the weight of dry powdered $Ca(OH)_2$.

The mixing procedure was the same for all mortar samples. First, the total amount of water-blended $Ca(OH)_2$ was mixed with the total amount of metakaolin and distilled water, and the paste was mixed manually for 10 minutes to obtain homogeneity. Then, straw fibers were added gradually, and the paste was stirred another 10 minutes. The consistency of fresh mortar paste was controlled with the flow table test, and the fresh mortar was cast into the wooden molds for initial curing. The interior sections of molds were coated with acetate paper to ensure the demolding.

Table 3.1. Lime: metakaolin: wheat straw proportions in the mixtures and flow diameters, fractions by weight

Sample Code	$Ca(OH)_2$	Metakaolin	Straw	Flow Diameter (cm)
Lime: Straw Compositions				
L1W0	1	-	-	14 ± 1
L9W1	9	-	1	15 ± 1
L7W1	7	-	1	15 ± 1
L5W1	5	-	1	15 ± 1
L3W1	3	-	1	15 ± 1
Lime: Metakaolin: Straw Compositions				
LM1W0	1	1	-	15 ± 1
LM9W1	4.5	4.5	1	15 ± 1
LM7W1	3.5	3.5	1	15 ± 1
LM5W1	2.5	2.5	1	15 ± 1
LM3W1	1.5	1.5	1	15 ± 1

The fresh mortar samples were stored in sealed climatic chambers at approximately 90% relative humidity (RH) and temperature of 21±3 °C. Carbon dioxide concentration within climate chambers was increased through an additional CO_2 gas source that was supplied by the chemical reaction between oxalic acid ($C_2H_2O_4$) and sodium bicarbonate ($NaHCO_3$) **(Equation 3.1).**

$$C_2H_2O_4 + 2NaHCO_3 \rightarrow C_2O_4Na_2 + 2CO_2 + 2H_2O \quad \textbf{(3.1)}$$

A carbon dioxide concentration of almost 2000 ppm in the climate chambers, each are approximately 200 liters, was provided by mixing 4 g oxalic acid, 6.8 g sodium bicarbonate, and 50 ml distilled water in a glass beaker to enhance carbonation. CO_2 gas source was renewed every day during the curing period. The change of RH, temperature, and CO_2 concentrations were monitored and recorded by TESTO 480 indoor air quality measuring device. These curing conditions were selected to enhance pozzolanic reaction as well as carbonation reaction. **Figure 3.3.** shows the standard curing setup.



Figure 3.3. Curing conditions and setup inside climate chambers

The samples were demolded after 7 days and left to cure over grid-lined shelves in the same curing conditions for an additional 21 days. After a total of 28 days of curing, samples were taken out from the climate chambers and stored in ambient laboratory conditions (T=21±2 °C and RH= 32%) for 5 days. Subsequently, all the samples were transferred to the desiccators filled with solid $CaCl_2$ granules to stop hydration. Dehydrating with high temperatures wasn't preferred because of the existence of straw fibers. RH and temperature levels of desiccators were monitored with data loggers. The samples were weighed each day to observe drying behaviors. Climate chambers and desiccators are presented in **Figure 3.4**.



a) **b)**

Figure 3.4. Curing and dehydration spaces **a)** climate chambers **b)** desiccators

Several standards report specific sample dimensions for certain procedures. Dimensions and sections of samples were determined according to the standards relating to performed experiments. For this reason, standards for sound absorption coefficient, compressive and flexural strength, and thermal conductivity tests were determinative in sampling dimensions. Samples of four geometrical shapes were prepared as follows;

- cylindrical test specimens with 100 mm in diameter and 30 mm in height for low-frequency sound absorption coefficient measurement procedure, 2 parallel samples for each composition, 20 samples in total **(Figure 3.5)**,
- cylindrical test specimens with 28 mm in diameter and 30 mm in height for high-frequency sound absorption coefficient measurement procedure, 2 parallel samples for each composition, 20 samples in total **(Figure 3.5)**,
- prisms with the size 40 x 40 x 160 mm for the determination of compressive and flexural strength, 3 parallel samples for each composition, 30 samples in total **(Figure 3.6)**,
- prisms with the size 300 x 300 x 30 mm for the determination of thermal conductivity, 10 samples in total **(Figure 3.7)**.

Overall, 80 material samples were produced for 10 different material composition; **Figure 3.5**, **Figure 3.6**, and **Figure 3.7** shows test specimens. Thicknesses of the material samples reduced with drying due to gravitational forces during the curing period. Except for samples produced for thermal conductivity tests, each test specimen has at least one parallel sample. As can be seen from the figures, some samples couldn't be produced properly or broken during or after the curing period. L1W0-1 was broken after sound absorption coefficient measurements. LM1W0 specimens for mechanical tests couldn't be demolded as one piece. L1W0-5 sample produced for thermal conductivity test was broken at the very end of the curing procedure, probably due to high drying shrinkage. **Table 3.2** reports conducted material performance analysis and followed standards. Material samples or fragments of the test specimens were used to conduct analyses who do not specify absolute dimensions. The experimentation period was started with non-destructive test methods.

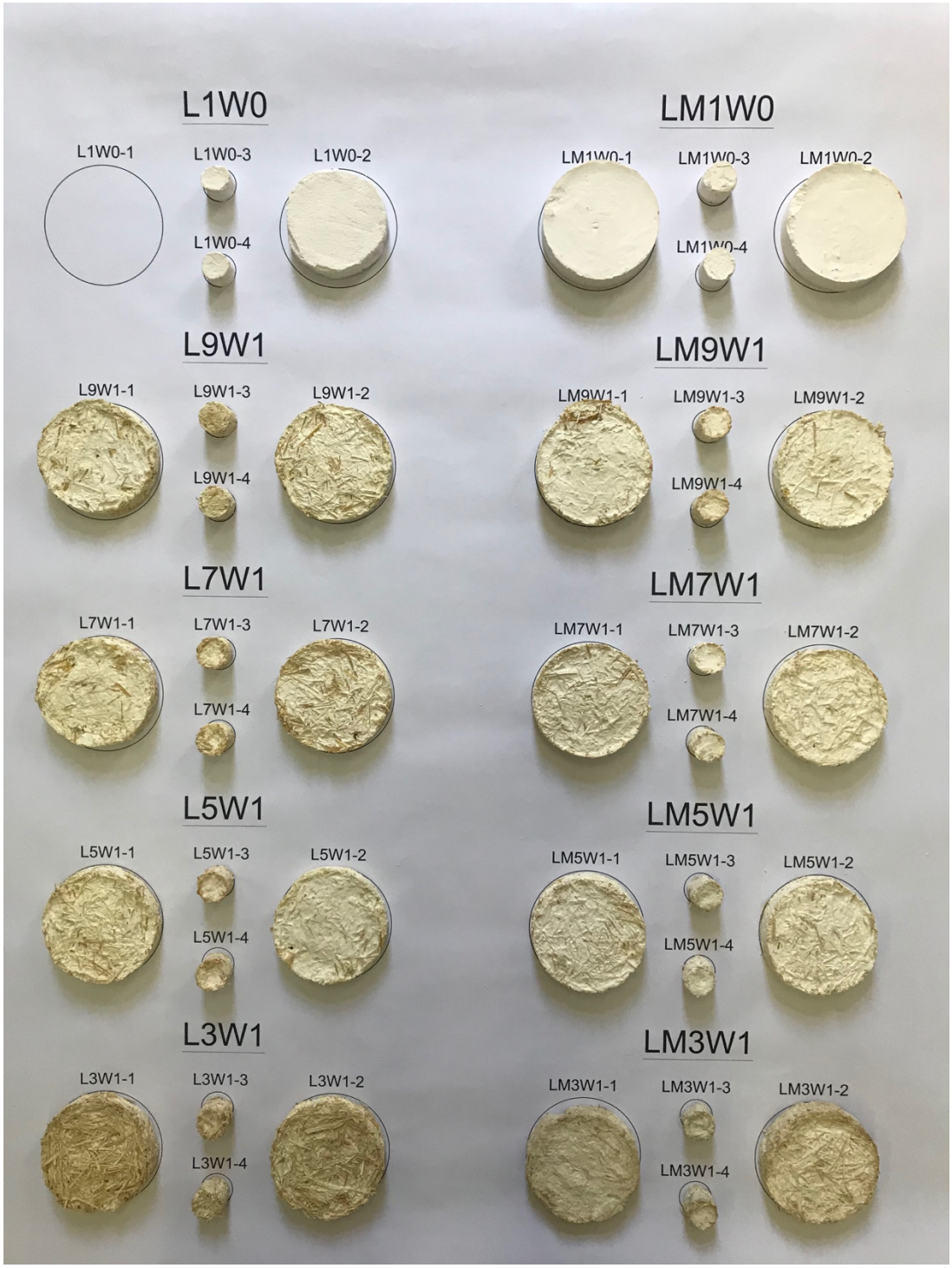


Figure 3.5. Samples produced for sound absorption coefficient measurements according to ISO 10534-2:1998

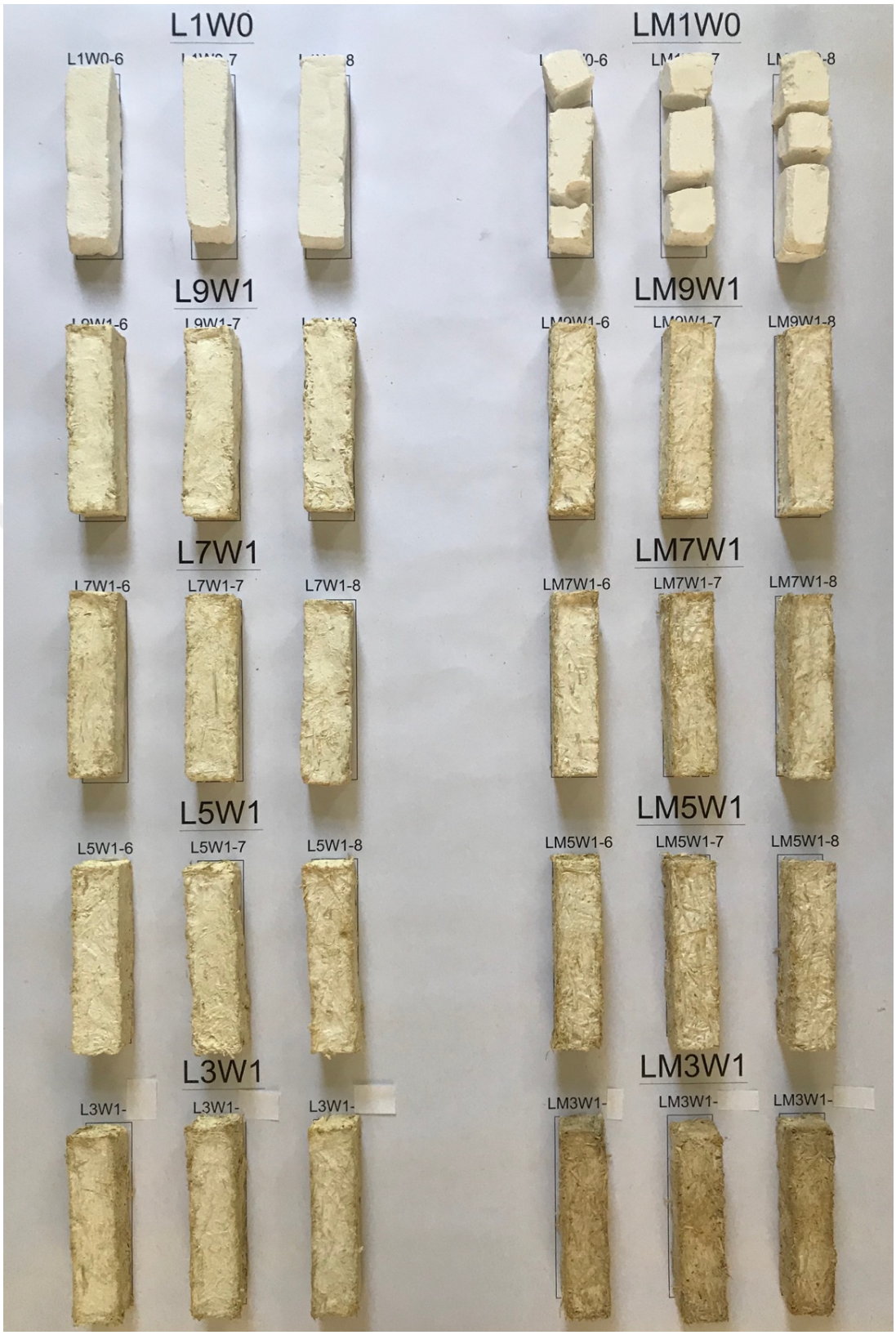


Figure 3.6. Samples produced for compressive and flexural strength measurements according to TS EN 1015-11:2000



Figure 3.7. Samples produced for thermal conductivity measurements

Table 3.2. Material properties, performed experiments and followed analyses methods

Material Property	**Analysis Method**
Compositional Properties	
Binder/aggregate ratio, % by weight	Teutonico, 1988; TS EN 1015-1:2000
Particle size distribution, % by weight	
Physical Properties	
Bulk Density - (ρ), g/cm³	Teutonico, 1998; TS EN 1015-10:2001
Effective Porosity - (φ), % by volume	
Water Absorption Coefficient - *(θ)*, % by weight	
Equivalent air thickness of water vapor permeability - (*SD*), m	Teutonico, 1988; ASTM E96/E96M-16; TS EN 1015-19:2000-10; ISO 12572:2016
Water vapor diffusion resistance index - *(μ-value)*, unitless	
Water vapor transmission rate - (*RT*), g/hm^2	
Physicomechanical Properties	
Ultrasonic Pulse Velocity - (*UPV*), m/s	ASTM C597-16; TS EN 12504-4:2012
Modulus of Elasticity - (*MoE*), MPa	
Mechanical Properties	
Flexural Strength- (σ_f), kPa	TS EN 1015-11:2000
Compressive Strength- (σ_c), kPa	
Acoustical Properties	
Sound Absorption Coefficient - *(α)*, unitless	ISO 10534-2:1998
Noise Reduction Coefficient- (*NRC*), unitless	
Weighted Sound Absorption Coefficient - *(αw)*, unitless	TS EN ISO 11654:2002
Thermal Properties	
Thermal Conductivity - (λ), W/m.K	ASTM C518-17; TS EN 12667:2003
Thermal Diffusivity - (*D*), m²/s	
Thermal Effusivity - (*e*), J/m²K$\sqrt{s}$	
Specific Heat Capacity - (*c*), J/kg.K	TS 4048:1984; ASTM C351-92b
Active Infrared Thermography	ISO 10880:2017
Pozzolanic Activity	
Saturated Lime Method	EDTA titration
Conductivity Measurement Method	Luxan *et al.*, 1989
Mineralogical and Microstructural Properties	
Cross Section Analysis	Stereo Optic Microscope
X-Ray Diffraction Analysis (XRD)	X-Ray Diffractometer

3.2. Determination of Basic Physical Properties

The laboratory analyses were conducted on the traditional sample collected from the Kemer Village (Salihli-Manisa) and the new mortar samples produced in laboratory conditions to determine basic physical properties which are bulk density (ρ), effective porosity (φ), water absorption capacity (θ), equivalent air thickness of water vapor permeability (*SD*), water vapor diffusion resistance index (μ-*value*), and water vapor transmission rate (*RT*). The methods for the laboratory analyses, terminologies, and equations are further explained. Discussion of the mentioned basic physical properties reveals the pore structure and hygroscopic behavior of studied materials.

For the bulk density, effective porosity, and water absorption capacity analysis, cylindrical samples, 28 mm in diameter and 30 mm in height, were used. Experimentations were performed according to TS EN 1015-10:2001 standards and methods proposed by Teutonico *et al.* (1988). First, the samples were immersed into distilled water in ambient laboratory conditions, and after 24 hours, weights of the saturated samples were recorded ($m_{24HOURS}$). Then, the samples were again submerged into distilled water, and placed in a vacuum chamber at 0,132 atm (100 torr) pressure to get rid of air trapped inside pores. After 2 hours, the samples were transferred underwater to the basket in the immersion bath to determine their saturated and submerged Archimedes weights (m_{ARCH}). Next, samples were removed from the immersion bath and surface-dried carefully in order to remove surface moisture and were weighed to determine their saturated weight (m_{SAT}). Samples were dried to constant weight at 40 ºC in the oven for 48 hours, and their weight was recorded as the dry weight of the samples (m_{DRY}). Dry weights of the samples were recorded before the saturation procedure as well; however, these values weren't valid since certain disintegrations were observed during saturation processes. The weighting procedures were repeated for 20 material samples from 10 different compositions. Each composition was represented by two parallel samples to have more accurate results. **Figure 3.8-a** shows the samples used in the determination of bulk density, porosity, and water absorption capacity values.



a) **b)**

Figure 3.8. a) Water-immersed samples prepared for the determination of bulk density, effective porosity, and water absorption capacity **b)** Samples prepared for the determination of equivalent air thickness of water vapor permeability and water vapor diffusion resistance index

Bulk density (ρ), also called apparent density, is the ratio of the mass to the apparent volume of the sample, including the pore space (Teutonico *et al.,* 1988). It is expressed in g/cm^3 and calculated by the formula presented in **Equation 3.2** (Teutonico *et al.,* 1988; TS EN 1015-10:2001).

$$\boldsymbol{\rho = \frac{m_{DRY}}{m_{SAT} - m_{ARCH}}, g/cm^3} \qquad \textbf{(3.2)}$$

Effective porosity (φ) is the ratio of the total volume of voids in a solid mass over the total volume. (Teutonico *et al.,* 1988). It is expressed as the percentage of volume and calculated by the formula presented in **Equation 3.3** (Teutonico *et al.,* 1988).

$$\boldsymbol{\varphi = \frac{m_{SAT} - m_{DRY}}{m_{SAT} - m_{ARCH}} x\ 100, \%\ \text{by volume}} \qquad \textbf{(3.3)}$$

Water absorption coefficient (θ) is defined as the maximum amount of water absorbed by a porous material submerged in distilled water at room temperature and pressure (Teutonico *et al.,* 1988). It is expressed as the percentage of the dry mass of the sample and calculated by the formula presented in **Equation 3.4** (Teutonico *et al.,* 1988).

$$\boldsymbol{\theta = \frac{m_{SAT} - m_{DRY}}{m_{DRY}} x\ 100, \%\ \text{by weight}} \qquad \textbf{(3.4)}$$

For the equivalent air thickness of water vapor permeability (*SD*), water vapor diffusion resistance index (*μ-value*), and water vapor transmission rate (*RT*) analyses, test specimens were prepared from the samples specifically produced for mechanical experimentations. The rectangular prisms with varying thickness, ranging between 2 cm to 4 cm, were obtained from larger samples. Experimentations were performed according to TS EN 1015-19:2000-10 and ASTM E96/E96 M-16 standards, and methods proposed by Teutonico *et al.* (1988).

Two parallel samples were prepared for each composition. The thickness of each sample was measured on four sides, and the mean thickness values were recorded (*So*). The circular test cups were filled with distilled water till 2 cm air gap between the top of the container and the water surface. The samples were placed among wet cups. All air-exposed surfaces, except for the top surface, were sealed with at least 3 layers of stretch film and taped to prevent water vapor transmission from anywhere but upper surface. Cups were labeled, and their weights were recorded as initial values.

Wet cups were placed inside desiccators filled with $CaCl_2$ to ensure standard relative humidity levels. The temperature and RH levels were controlled with data loggers. **Figure 3.8-b** represents standard experimentation setup. 40% mean RH value was obtained inside the curing chambers. Each wet cup was weighed at appropriate time intervals to record the weight loss caused by evaporation until weight loss per unit time became constant.

Water vapor permeability is defined as "the time rate of water vapor transmission through unit area of flat material of unit thickness induced by unit vapor pressure difference between two specific surfaces, under specified temperature and humidity conditions" (ASTM Standard E96/E96 M-16). Water vapor permeability properties of materials are discussed as equivalent air thickness of water vapor permeability *(SD)* which is calculated by **Equation 3.5**. Water vapor permeability (SD^{-1}) is calculated by dividing the *SD* value to 1. The water vapor diffusion resistance index (*μ-value*) is determined by diving *SD* value with the thickness of the relevant material sample as shown in **Equation 3.5**.

$$SD = \mu \times So = \left(\frac{\psi L \times A \times (P_1 - P_2)}{I}\right) - SL \text{ , m} \quad (3.5)$$

SD: Equivalent air thickness of water vapor permeability, (m)

SD^{-1}*:* Water vapor permeability value, (m^{-1})

μ*:* Water vapor diffusion resistance index, unitless

So: Mean thickness of the sample, (m)

ψL*:* Constant, 6.89 x 10^{-6} (kg/m^2)

A: Area of the sample through which water vapor is evaporated, (m^2)

P_1, P_2*:* Partial vapor pressures on two sides of the sample, difference between 100% RH and 40% RH (kg/m^2)

I: Weight change in unit time, (kg/h)

SL: Thickness of the air beneath the sample, (m)

Water vapor transmission rate (*RT*) is defined as "the steady water vapor flow in unit time through unit area of a body, normal to specific parallel surfaces, under specific conditions of temperature and humidity at each surface" (ASTM Standard E96/E96 M-16). Water vapor transmission rate (RT) is expressed in g/hm^2 and calculated by the formula presented in **Equation 3.6**.

$$RT = \frac{G}{t \times A}, \; g/hm^2 \quad (3.6)$$

RT: Water vapor transmission rate, (g/hm^2)

G: Change in mass, (g)

t: Time, (h)

A: Area of the sample through which water vapor is evaporated, (m^2)

Water vapor permeability classes are defined by TS EN ISO 7783:2012 standard according to the equivalent air thickness of water vapor permeability *(SD)* and water vapor transmission rate (*RT*) values of building materials which are presented in **Table 3.3**. Standard designates the building materials with SD values smaller than 0.14 as high permeability, SD values between 0.14 and 1.4 as medium permeability, and SD values higher than 1.4 as low permeability.

Table 3.3. Water vapor permeability classes for building materials according to *SD* and *RT* values (TSI, 2012)

Permeability Class	***SD* (m)**	***RT* (g/hm^2)**
High Permeability	$SD < 0.14$	$RT > 6.0$
Medium Permeability	$0.14 < SD < 1.4$	$0.6 < RT < 6.0$
Low Permeability	$SD > 1.4$	$RT < 0.6$

3.3. Determination of Physicomechanical Properties

The laboratory analyses were conducted on the traditional sample and the newly-produced mortar samples to determine physicomechanical properties, which are ultrasonic pulse velocity (UPV) and modulus of elasticity (MoE). The methods for the laboratory analyses, terminologies, and equations are further explained. For UPV procedure, circular material samples, which are 10 cm in diameter and have different thickness values varying between 1.6 cm and 2.6 cm, were used.

The ultrasonic pulse velocity (UPV) is a non-destructive method that uses ultrasonic waves to estimate the strength of the material by determining internal cracks, defects or changes caused by deterioration (Naik, Malhotra & Popovics, 2004). UPV procedure is mainly the propagation velocity of a pulse of sound waves from one point to another where the distance between two points is known. Standard testing equipment consists of a pulse generator, a transmitter, a receiver, and a recorder. UPV value *(V)* is calculated by dividing the path length between two points *(L)*, where probes are placed, into the transit time *(t)*. Pulse velocity is expressed in m/s and calculated by the formula presented in **Equation 3.7** (ASTM C597-16, TS EN 12504-4:2012).

$$\boldsymbol{V = \frac{L}{t}} \ , m/s \qquad \textbf{(3.7)}$$

Pulse velocity can be measured in 3 different configurations regarding the transducer's arrangement that are the direct transmission, semidirect transmission, and indirect transmission (Naik *et al.,* 2004). The direct transmission method is designated as the most satisfactory arrangement since it is the most efficient placement to transmit and receive the maximum energy of the pulse (Naik *et al.,* 2004).

Direct UPV measurements were performed on material samples using PUNDIT*plus* with transmitter and receiver probes of 54 kHz. The thicknesses in which the test was performed and the obtained time data were recorded. Probes having a frequency of 54 kHz are known to be very sensitive to pressure level employed by the operator and generally used with a proper couplant.

Generally, material samples have irregular surfaces and higher porosity levels due to the usage of straw aggregate. Therefore, measurement with normal pressure and without a couplant gave no results. For this reason, two different techniques were performed for pulse velocity measurements, and their results were recorded separately. The first one was UPV measurement with a mastic couplant usage and with a normal pressure application. The second one was the UPV measurement without couplant usage and with a slightly higher-pressure application.

The modulus of elasticity is the ratio of stress to strain, which reveals the deformation capacity of material under external forces. The comparison of obtained values with standard values gives an idea about the decay of materials. The dynamic modulus of elasticity (MoE_{dyn}) is calculated indirectly using the bulk density and UPV data together with Poisson's ratio. It is expressed in MPa and calculated by the formula presented in **Equation 3.8** (ASTM C597-16, TS EN 12504-4:2012).

$$\boldsymbol{MoE_{dyn} = \rho \times V^2 \times \frac{(1+\nu_{dyn})\times(1-2\nu_{dyn})}{\nu_{dyn}}}\textbf{, MPa} \qquad \textbf{(3.8)}$$

MoE_{dyn}: Dynamic modulus of elasticity, (MPa)
ρ: Bulk density of material, (kg/m^3)
V: Ultrasonic pulse velocity, (m/s)
ν_{dyn} : Poisson's ratio, (unitless)

Poisson's ratio (ν_{dyn}) is the ratio of lateral strain to the axial strain of the material under stress, which varies in the range of 0.0 – 0.5. For dynamic modulus of elasticity calculations of studied material samples, Poisson's ratio is accepted as 0.18, depending on the literature findings.

3.4. Determination of Mechanical Properties

The laboratory analyses were conducted on the straw-mixed lime-based mortars (LW) and straw-mixed lime-pozzolan mortars (LMW) to determine compressive strength (σ_c) and flexural strength (σ_f) values. The methods for the laboratory analyses, terminologies, and equations are further explained. The flexural strength test has a standard sample dimension of 4x4x16 cm, and 3 parallel material samples are required. Compressive strength was determined on the broken halves of the samples obtained after flexural strength tests. The flexural and compressive strength tests were conducted with UTEST universal testing machine equipped with 50 kN capacity load cells.

Flexural strength (σ_f) is the maximum flexural stress at the moment of yield. The Flexural strength values of test specimens were determined via the three-point bending test. Width and height of the samples were recorded concerning placement configurations. Samples were placed horizontally onto two supporting rollers in which the distance (L) is 100 mm. The third roller is the loading roller, which is located above the test specimen and midway between supporting rollers. Flexural strength is expressed in kPa and calculated by the formula presented in **Equation 3.9** (TS EN 1015-11:2000). **Figure 3.9-a** represents the flexural strength measurement procedure.

$$\boldsymbol{\sigma_f = 1.5 \times \frac{F \times L}{b \times d^2} \times 1000 \text{ , kPa}} \qquad \textbf{(3.9)}$$

σ_f = Flexural strength, (kPa)
F = The maximum load applied to sample, (N)
L = Distance between the supports, 100 mm, (mm)
b = Width of the sample, (mm)
d = Thickness of the sample, (mm)

Compressive strength (σ_c) is the maximum amount of compressive load before fracturing, divided by the material's cross-section area. Samples with known cross-sections were loaded uniformly in the longitudinal direction. The ultimate force data (F) were obtained from the testing machine as an output of the test.

Compressive strength is expressed in kPa and calculated by the formula presented in **Equation 3.10** (TS EN 1015-11:2000). **Figure 3.9-b** represents the compressive strength measurement procedure.

$$\sigma_c = \frac{F}{a \times b} \times 1000 \text{ , } kPa \qquad (3.10)$$

σ_c = Compressive strength, (kPa)

F= The maximum load applied to sample, (N)

a= Width of the sample, (mm)

b= Depth of the sample, 40 mm, (mm)



a) **b)**

Figure 3.9. a) Flexural strength test setup **b)** Compressive strength test setup

3.5. Determination of Acoustical Properties

The laboratory analyses were performed on the newly-produced mortar specimens to determine certain acoustical properties, which are sound absorption coefficient (α), noise reduction coefficient (NRC), and weighted sound absorption coefficient (αw). The methods for the laboratory analyses, terminologies, and equations are further explained.

Sound absorption coefficient values were determined by the standing wave method using the impedance tube, also called a standing wave tube or Kundt's tube. Two-microphone transfer-function technique is used for impedance tube measurements, as reported by ISO 10534-2:1998 (Oldham, Egan & Cookson, 2011). The measurements were performed using Brüel & Kjær Impedance Tube Kit with the sample holders of 100 and 28 mm in diameter, and with a noise generator unit which generates sinusoidal sound signals. The larger impedance tube kit is used for frequencies between 50 Hz to 1600 Hz. The smaller impedance tube kit is for higher frequencies ranging from 1000 Hz to 5000 Hz. The material sample is placed in the sample holder, and an adjustable rigid plunger is placed behind the material sample to provide a reflecting surface. For data processing, SCS80FA software together with dBFA suit software was used.

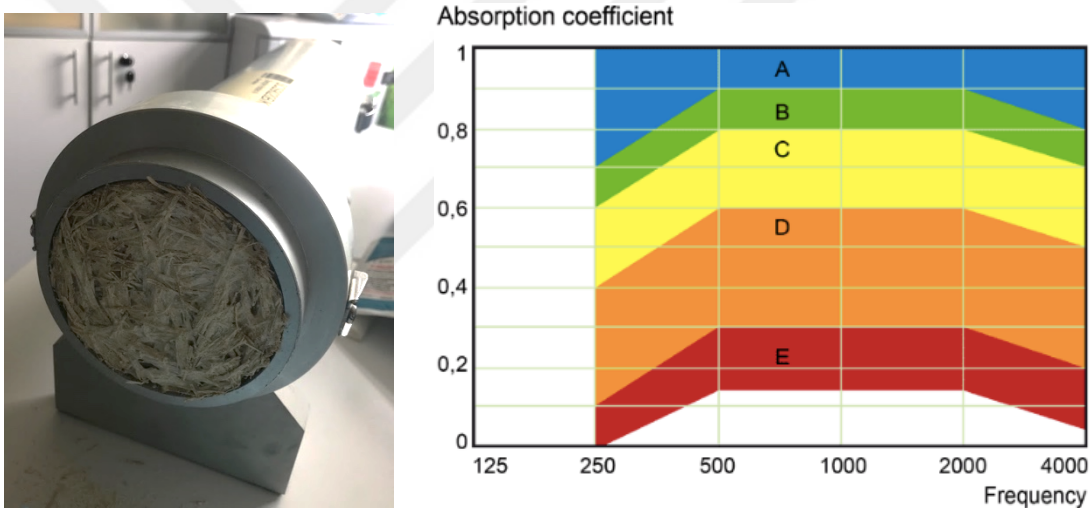
The technique requires cylindrical specimens with proper diameters depending on the studied frequency range. The average thicknesses of the material samples are in the range of 2 cm to 3 cm. To prevent measurement inaccuracies, air gaps between the sample and the tube walls were closed with modeling clay. Two parallel samples for each composition were tested, and measurements were repeated 3 times for all test specimens. Noise reduction coefficients and weighted sound absorption coefficients were calculated depending on the data obtained from the sound absorption coefficient measurements. **Figure 3.10-a** test specimen placement into the sample holder.

Frequency-dependent sound absorption coefficient values (α) were presented in 1/3 octave bandwidth by SCS80FA software. The obtained data were adjusted to the studied central frequencies of 1/1 octave band, which are 63 Hz, 125 Hz, 250 Hz, 500 Hz, 1000 Hz, 2000 Hz, and 4000 Hz. For each material composition, the average of 6 measurements from 2 parallel specimens was calculated and presented as sound absorption coefficient value.

Noise reduction coefficient (NRC) is the average sound absorption coefficients over the speech frequencies, 250 Hz, 500 Hz, 1000 Hz and 2000 Hz. NRC is a single-number index and often used to characterize porous absorbers (Long, 2006). It is a unitless performance property and calculated by the formula presented in **Equation 3.11** (ISO 10534-2:1998).

$$NRC = \frac{\alpha_{250}+\alpha_{500}+\alpha_{1000}+\alpha_{2000}}{4}, \textit{ unitless} \quad \textbf{(3.11)}$$

Weighted sound absorption coefficient (αw) is calculated by the comparison between sound absorption coefficient values of material samples for 250 Hz - 4000 Hz in 1/1 octave bands and the standard curve proposed by TS EN ISO 11654:2000. The standard curve is shifted against the measured sound absorption coefficient values (α) until unfavorable deviations are less than or equal to 0.10 (Adams, 2016). An unfavorable deviation occurs when the measured value is lower than the curve value at a particular frequency (Adams, 2016). The weighted sound absorption coefficient (αw) is the value of the relocated reference curve at 500 Hz. It is a unitless performance property. **Figure 3.10-b** shows the standard curve (TS EN ISO 11654:2000).



a) **b)**

Figure 3.10. a) Material sample inside impedance tube sample holder **b)** Standard curve and classes defined by TS EN ISO 11654:2000

3.6. Determination of Thermal Properties

The laboratory analyses were conducted on the new mortar samples to determine certain thermal properties, which are thermal conductivity *(λ),* thermal diffusivity *(D),* thermal effusivity *(e),* and specific heat capacity *(c)*. Additionally, active infrared thermography was performed on the straw-mixed lime-based mortars (LW) and straw-mixed lime-pozzolan mortars (LMW) together with some common building materials.

The ability of a material to transfer or conduct heat is called thermal conductivity. Thermal conductivity *(λ)* measurements were performed with the FOX 314 heat flow meter, according to TS EN 12667:2003 and ASTM C518-17 standards. The heat flow meter utilizes a steady-state one-dimensional heat flux through a material sample between two parallel plates at constant but different temperatures (ASTM, 2017). Fourier's law of heat conduction method is employed to calculate thermal conductivity (Kreith & Black, 1980).

The width and depth of the material samples are per test apparatus' standards, which is 30 cm by 30 cm. The thickness values (L) are in the range of 2 cm to 3 cm. The sample thicknesses of the test specimens are confirmed by the embedded optical encoders within the heat flow meter since the thickness value is critical.

The desired measurement temperature was selected as 25 ºC. The pre-defined temperature difference ($\Delta \boldsymbol{T}$) across the test specimen was 20 ºC. The resulting heat flux (Q/A) is measured by heat flux transducers on both of the plates. Thermal conductivity is expressed in W/mK and calculated by the formula presented in **Equation 3.12.**

$$\boldsymbol{\lambda = \frac{Q \times L}{A \times \Delta T}}\ \boldsymbol{, W/mK} \qquad \textbf{(3.12)}$$

λ= Thermal conductivity, (W/mK)
Q= Energy, (W)
A= Area, (m^2)
L= Thickness, (m)
ΔT= Temperature difference, (K)

Thermal diffusivity (D) is the rate of heat transfer through the material at constant pressure. Thermal diffusivity is a non-steady state material property to reveal the material's response rate to heat changes. It is expressed in m^2/s and calculated by the formula presented in **Equation 3.13**.

$$\boldsymbol{D = \frac{\lambda}{\rho \times c}}\text{, m}^2\text{/s} \quad \textbf{(3.13)}$$

D= Thermal diffusivity, (m^2/s)

λ= Thermal conductivity, (W/mK)

ρ= Density, (kg/m^3)

c= Specific heat capacity, (J/kgK)

Thermal effusivity (e) is the ability of a material to store or dissipate thermal energy with its surroundings. Thermal effusivity is related to the material's behavior of acceleration to reach thermal equilibrium. It is expressed in $J/s^{1/2}m^2K$ and calculated by the formula presented in **Equation 3.14**.

$$\boldsymbol{e = \sqrt{\lambda \times \rho \times c}}\text{, J/s}^{1/2}\text{m}^2\text{K} \quad \textbf{(3.14)}$$

e= Thermal effusivity, ($J/s^{1/2}m^2K$)

λ= Thermal conductivity, (W/mK)

ρ= Density, (kg/m^3)

c= Specific heat capacity, (J/kgK)

The specific heat capacity (c) is the thermal energy required by 1 kg of material to raise its temperature 1 K. The specific heat capacity values of the new mortar samples were measured according to the basic principle of conservation of energy. Heat energy transfers due to temperature differences. Material samples were heated up to 50 ºC in the oven for 24 hours. To have an adequate level of temperature difference, distilled water of 10 ºC was used. Heat transfer was measured between the material sample and distilled water in calorimetry until thermal equilibrium was reached. The quantity of heat energy gained by water equals the quantity of energy lost by the material sample. The specific heat capacity is expressed in J/kgK and calculated by the formulas presented in **Equation 3.15** and **Equation 3.16** (TS 4048:1984, ASTM C351-92b).

$$\mathbf{Q_{gained} = Q_{lost}} \quad \textbf{(3.15)}$$

$$\boldsymbol{Q = m \times c \times \Delta T} \textbf{ , J/kgK} \quad \textbf{(3.16)}$$

Q= Heat energy, *(J)*

m= mass of the sample, *(kg)*

c= specific heat capacity, *(J/kgK)*

ΔT= Temperature difference, *(K)*

Infrared thermography (IRT) is a methodology used to determine the surface temperature profile of the studied frame. Thermal energy emitted from the objects in the infrared band is detected by thermal cameras. IRT can be used to determine certain thermophysical properties, defects, and inhomogeneities of building materials nondestructively (Hain, Bartl & Jacko, 2009).

Infrared thermography measurements were performed to compare the thermal performance of the new mortar samples of this study with common building material samples including thermal insulation materials; which are rock wool, glass wool, EPS, AAC insulation block, marble and beech wood samples. Active infrared thermography methodology, which requires an external thermal excitement, was employed for the measurements. Two halogen lamps were used as heating sources to create a thermal gradient on the material samples which were remotely controlled. The thermographic camera was replaced in the center of the test setup.

The main principle of active IRT is the measurement of surface temperature differences with respect to time, which occurs because of different thermal diffusivity characteristics of test specimens (Hain *et al*., 2009). Measurement was started with the thermal equilibrium state of material samples. After a pre-defined time interval, halogen lamps were opened, and samples were heated for around 220 seconds. Measurement was concluded when test specimens turned into their equilibrium state with the surrounding environment. **Figure 3.11** shows the experimental setup and materials used.



Figure 3.11. Active infrared thermography measurement setup and material samples

3.7. Determination of Compositional Properties

Binder/aggregate ratio and particle size distribution analyses were performed according to the method proposed by Teutonico *et al.* (1988) to reveal the compositional properties of the traditional lime-based exterior plaster sample. Two parallel samples taken from the traditional mortar were collected and dried at 60 ºC in the oven until they reach the constant weight. Dry weights (W_1) of the samples were recorded. Samples were treated with dilute hydrochloric acid (HCl) solution to dissolve the binder content, and they were kept into the solution until the reaction ended. Filter paper, whose weight was recorded earlier (W_2), was used to extract acid-insoluble parts of the samples within the HCl solution. The acid-insoluble parts, together with filter paper, were washed with distilled water and dried at 60 ºC in the oven. After drying, acid-insoluble sections together with filter paper were weighed (W_3). The weight of filter paper (W_2) was subtracted from the measured cumulative value (W_3), and the weight of the acid-insoluble aggregates was revealed (W_4). The binder weight was calculated by the subtraction of acid-insoluble aggregate weight (W_4) from the original sample weight (W_1). The ratio of binder over aggregate was reported as percentage by weight. Teutonico *et al.* (1988) point out the limitations of the procedure regarding the acid dissolution behavior of calcareous aggregates, which can be misleading.

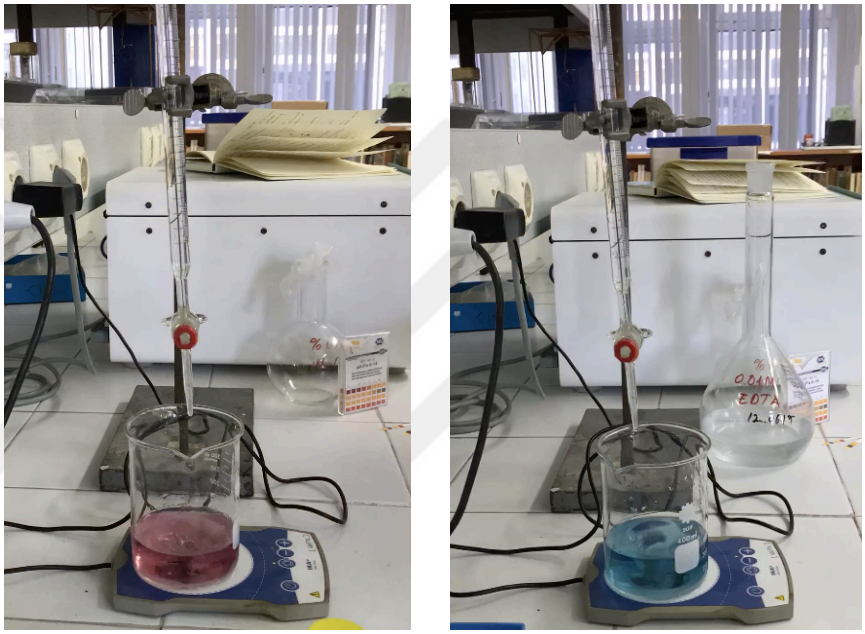
Acid-insoluble aggregates, obtained from the previous procedure, were sieved in a standard sieve set with specific sizes of 16 mm, 8 mm, 4 mm, 2 mm, 1 mm, 0.500 mm, 0.250 mm, 0.125 mm, and 0.063 mm to determine the particle size distribution (TS EN 1015-1:2000). First, each empty sieve was weighted, and the value was recorded. The aggregates were placed in the sieve set from the coarser opening sieve, and the set was agitated for approximately 2 minutes. Then, the weight of each sieve together with the remaining aggregates was recorded. Finally, the weight of each sieve was deducted from the recorded cumulative values. The aggregates, whose size was smaller than 0.125 mm, were separated to be used in the pozzolanic activity tests.

3.8. Determination of Pozzolanic Activity

The laboratory analyses were conducted on the traditional material sample and raw materials, wheat straw and metakaolin, used in the sampling to determine pozzolanic activity characteristics. Two different techniques were employed, which are the saturated lime method and the electrical conductivity measurement method proposed by Luxan, Madruga, and Saavedra (1989).

The saturated lime method is a direct measurement technique in which the powdered material sample is mixed with the saturated lime solution. The amount of pozzolanic reaction is determined by measuring residual $Ca(OH)_2$ by chemical titration. The saturated lime method was used to assess the pozzolanic activity of the traditional lime-mortar sample collected from Kemer Village, wheat straw, and metakaolin. For each specimen, 2 samples were prepared. 0.2 g of powdered material samples with particle size smaller than 0.125 mm were mixed with 30 ml of saturated $Ca(OH)_2$ solution and covered tightly. For the traditional sample, prepared solutions were kept for 7 days. For wheat straw, measurements were conducted on both 7 days and 14 days after preparation to observe the effect of duration. For the metakaolin samples, the pozzolanic activity test was conducted after 7 days. For each test period, a dummy sample, which consists of 30 ml $Ca(OH)_2$ without any material powder, was prepared.

During the measurement, 10 ml of sample solution was mixed with 90 ml distilled water, approximately 5 ml of 10% NaOH solution, and calcon indicator. The analysis depends on the visual observation of color change since at first, the color of the solution is pink due to the calcon addition as presented in **Figure 3.12-a**. The solution was titrated with 0.01 M EDTA (ethylenediaminetetraacetic acid) solution. The procedure was stopped when the solution color turns into turquoise (**Figure 3.12-b**). The amount of EDTA used to consume residual Ca^{++} inside the solutions was compared with the test results of the standard blank specimen.



a) **b)**

Figure 3.12. Pozzolanic activity test with saturated lime method **a)** before chemical titration with EDTA **b)** after chemical titration with EDTA

The electrical conductivity measurement method proposed by Luxan *et al.* (1989) is an indirect technique to determine pozzolanic behavior. First, the initial conductivity value of 200 ml of saturated $Ca(OH)_2$ solution was recorded. Then, 5 g of sample powder with particle size smaller than 0.125 mm was mixed with 200 ml of saturated lime solution. The solution was kept under constant stirring. After 120 seconds, the electrical conductivity of the solution was tested. The difference between the initial and final conductivity value was used to evaluate pozzolanic activity by classification proposed by Luxan *et al.* (1989) and presented in **Table 3.4**.

The conductivity measurements were performed with Metrohm AG Herisau conductometer. The electrical conductivity is expressed in mmho.cm^{-1} and calculated by the formula presented in **Equation 3.17** (Black, 1965).

$$EC = \frac{0.0014118 \times R_{std}}{R_{ext}} \times 1000 \text{ , mmho.cm}^{-1} \qquad (3.17)$$

EC: Electrical conductivity, (mmho.cm^{-1})

R_{std}*:* The cell resistance with standard solution of 0.01 N KCl, (kΩ)

R_{sext}*:* The cell resistance with extract solution, (kΩ)

Table 3.4. Evaluation of pozzolanic activity by conductivity measurement (Luxan *et al.,*1989)

Classification of material	**Variation in conductivity (mS/cm)**
Non pozzolanic	Less than 0.4
Variable pozzolanicity	Between 0.4 and 1.2
Good pozzolanicity	Greater than 1.2

3.9. Determination of Mineralogical and Microstructural Properties

The laboratory analyses were conducted on the traditional sample collected from the Kemer Village (Salihli-Manisa) and the new mortar samples produced in laboratory conditions to determine mineralogical and microstructural properties via X-ray diffraction (XRD) analysis and image analysis of cross-sections. The methods for the laboratory analysis and terminologies are further explained.

For XRD analyses, sample powders with particle sizes smaller than 0.125 mm were prepared. For newly-produced mortar compositions, both inner and outer powder samples were prepared to investigate mineralogical differences that would be caused by favored chemical reactions depending on the water and CO_2 content. X-ray diffraction analysis was conducted on the traditional sample to reveal its mineralogical content. XRD analyses were performed on the new mortar samples to observe pozzolanic reaction and carbonation reaction products particularly.

Bruker X-ray powder diffractometer D8 instrument and DiffracSuite software were used for measurements. Analyses were performed with CuKα radiation adjusted to 40 kV. The XRD traces were studied in the 5º - 70 º 2θ range. Obtained diffraction patterns were evaluated with EVA software regarding peak location and intensity values.

Image analyses of cross-sections of traditional sample and new mortar samples were performed to determine the microstructural properties of test specimens by using the Leica stereo optic microscope with 7x, 12.5x, and 25x magnification. For the cross-section preparation of the traditional material sample, a test specimen with an adequate size was impregnated with epoxy resin. After 24 hours, hardened samples were cut into slices. Cross-sections of the material samples were prepared by cutting prismatic samples properly with a band saw machine. Since the samples are highly porous, epoxy resin infusion was avoided for clear observation of the textures.

CHAPTER 4

RESULTS

In this section, the results of laboratory analyses on the traditional lime-based mortar sample obtained from Kemer Village and the newly-produced mortar samples are presented in detail. The overall performance properties of the traditional sample, raw materials used in the production of the new materials, and the new lime-based mortars are distinguished under the related subheadings.

4.1. Performance and Compositional Properties of the Traditional Exterior Plaster Sample

The compositional and raw material characteristics of the traditional exterior plaster sample obtained from Kemer Village (SK.Pe.6) are presented in **Table 4.1**, **Figure 4.1**, **Figure 4.2, Figure 4.3** and **Figure 4.4**. The obtained data are summarized below;

- The aggregate content within mortar composition is almost 9% by weight, and the ratio of binder over aggregate is approximately 10 to 1 by weight (**Table 4.1**).
- The percentage of very fine aggregate content (particle size < 0.125 mm) is almost 3%, where the fine aggregate (0.125 mm< particle size < 0.250 mm) is around 2% by weight (**Figure 4.1**). Straw is dominantly used as a bio-aggregate in the mortar mixture. It is observed that aggregate types with smaller sizes also exist in the mortar texture to a lesser extent (**Figure 4.2**). The aggregates above 2 mm and below 4 mm have the largest ratio with 34%. **Figure 4.3** presents the aggregate content of the traditional mortar sample.
- Calcite, quartz, and tobermorite minerals are detected via XRD analysis **(Figure 4.4)**. The existence of calcite proves the usage of lime ($Ca(OH)_2$) as the binder within the traditional mortar mixture. Tobermorite (CSH) traces indicate the pozzolanic reaction between $Ca(OH)_2$ and the pozzolanic additive.
- The low intensity of quartz peaks confirms the grain size distribution findings and visual observations in which the fine aggregate ratio is particularly low.

- Interpretation of obtained results shows that the traditional sample (SK.Pe.6) is a lime-based straw-mixed mortar blended with pozzolanic additive.

Table 4.1. The aggregate content by weight (%) and binder/aggregate ratio of the historical mortar sample (SK.Pe.6)

Sample	Aggregate content, % by weight	Binder/Aggregate Ratio
SK.Pe.6	8,9%	10,2

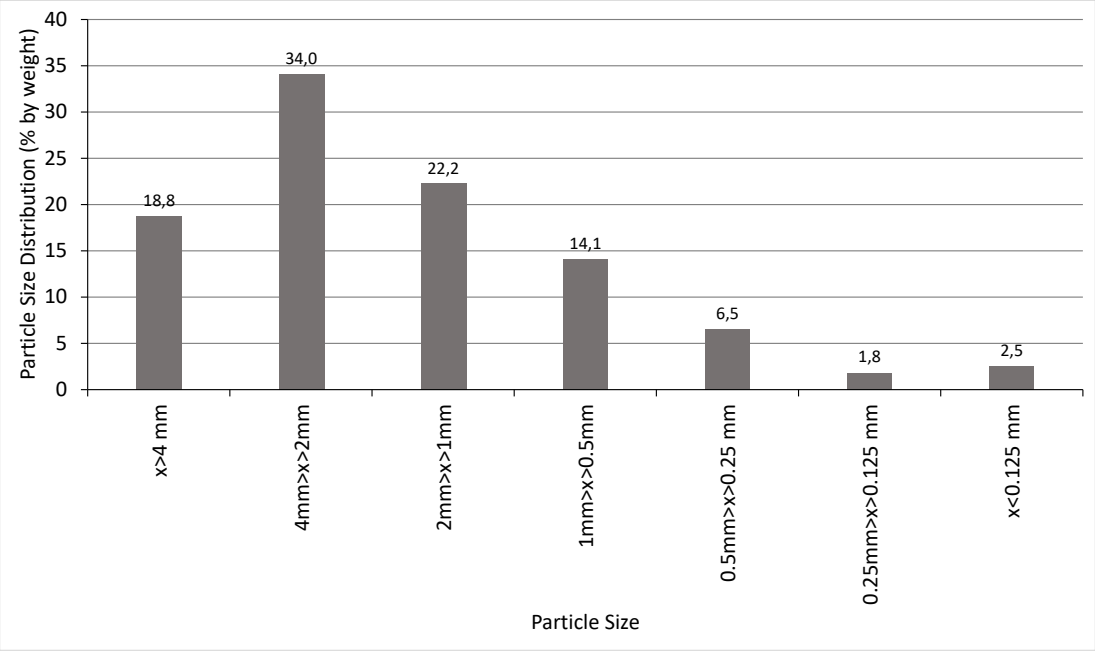


Figure 4.1. The particle size distribution of aggregates of the traditional exterior plaster sample by weight

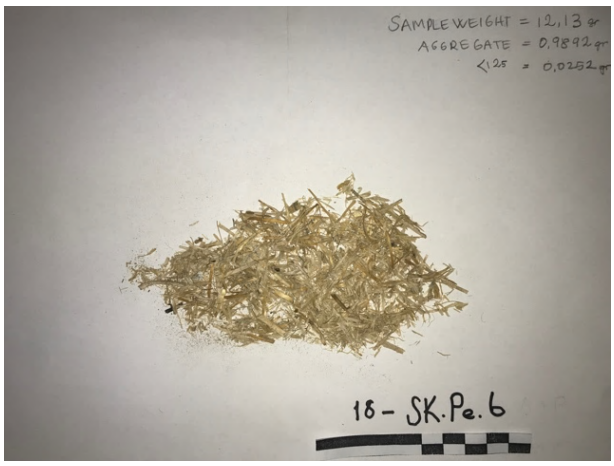


Figure 4.2. The aggregate content of the traditional lime-based straw-mixed mortar (SK.Pe.6)

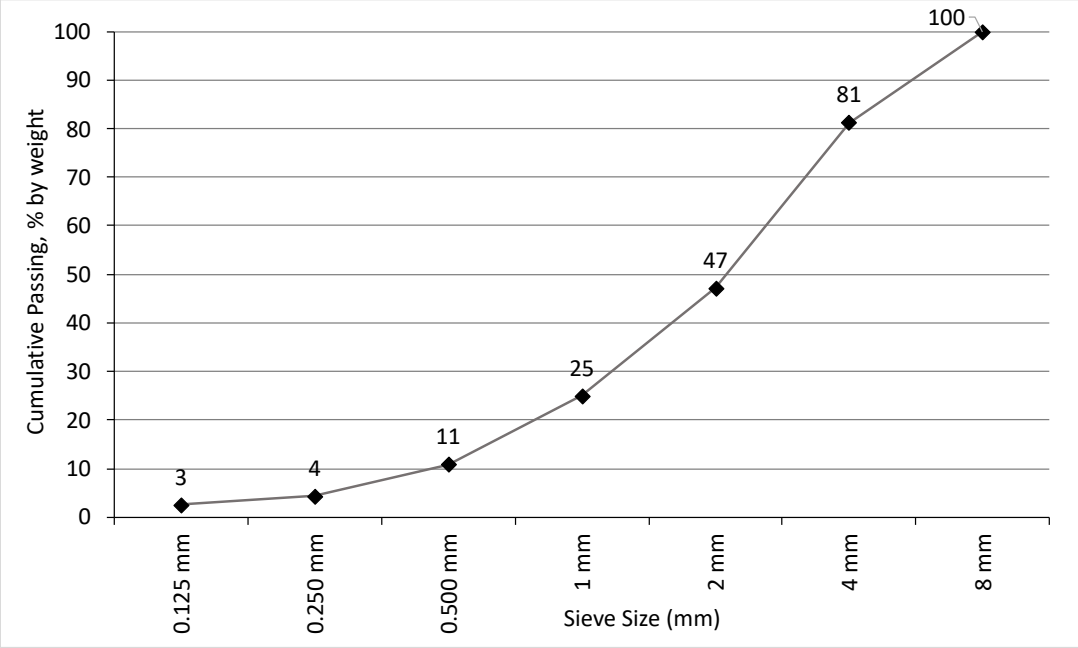


Figure 4.3. The cumulative passing percentage of grains of SK.Pe.6

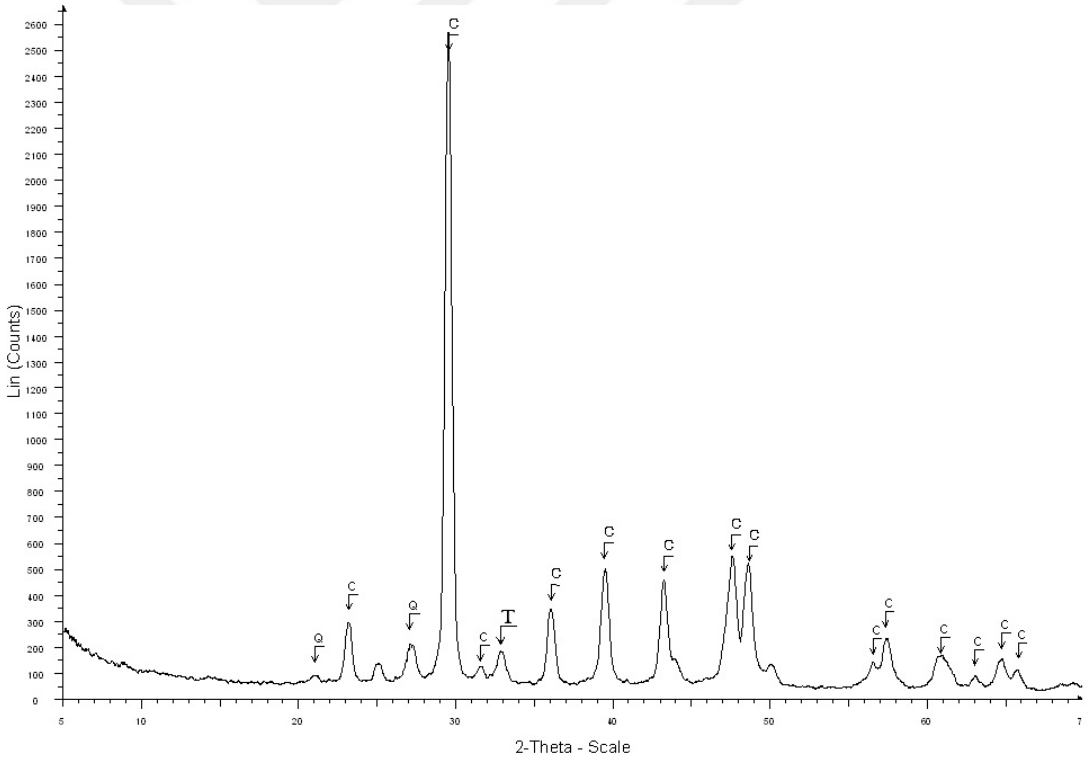


Figure 4.4. XRD traces of SK.Pe.6 (Q: quartz, C: calcite, T: tobermorite (CSH))

Figure 4.5 represents the microstructural properties of the studied traditional lime-based mortar sample with various scales. Cross-section images obtained via stereo optic microscope reveals the existence of straw fibers, which are various in different sizes, and quartz traces. Microcracks around straw fibers and the porous inner structure of the historical lime-based sample are visible. The distribution of the aggregates is random.

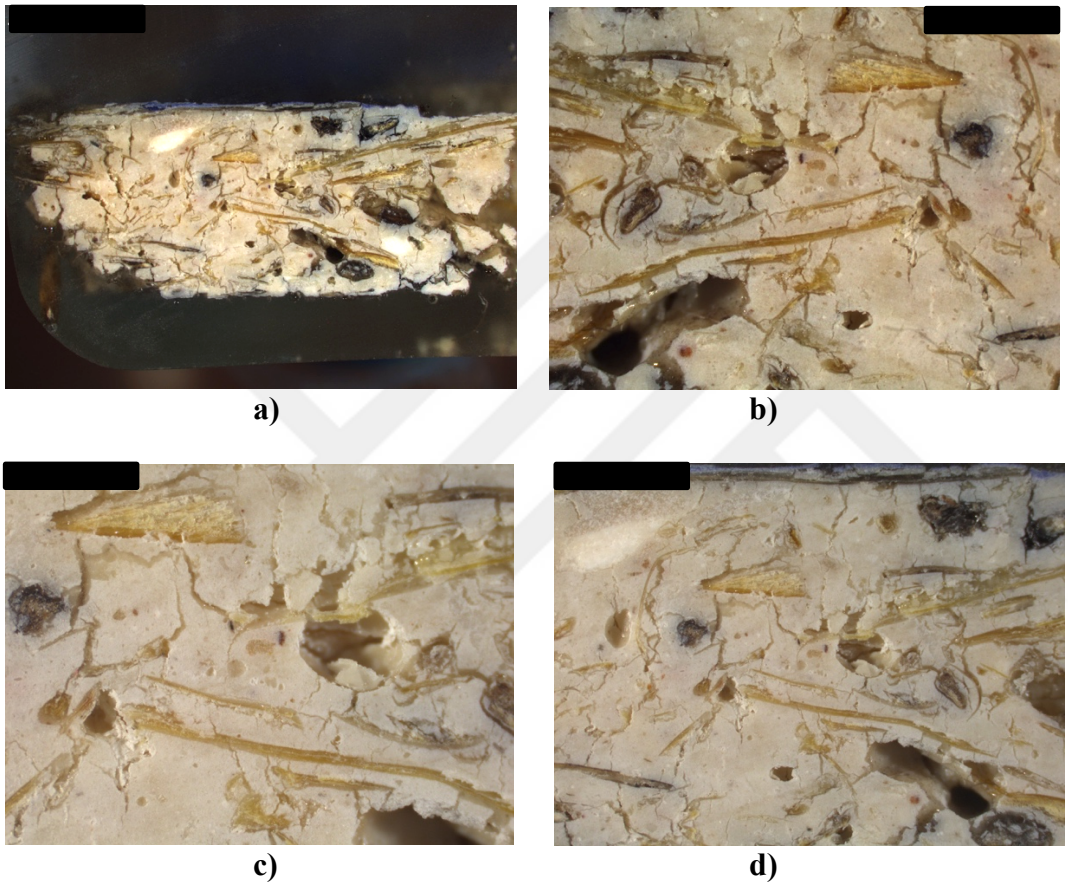


Figure 4.5. Cross-section images of SK.Pe.6 with various scales

The basic physical, physicochemical, mechanical and pozzolanic activity properties of the traditional exterior plaster sample are summarized in **Table 4.2** and descried as follows;

- The average bulk density and effective porosity values of SK.Pe.6 are 0.7 g/cm^3 and 69.5% by volume, respectively.
- The equivalent thickness of water vapor permeability (SD) value is 0,05 for the studied sample of 1.4 cm in thickness. Water vapor diffusion index (μ-value) value is 3.85.

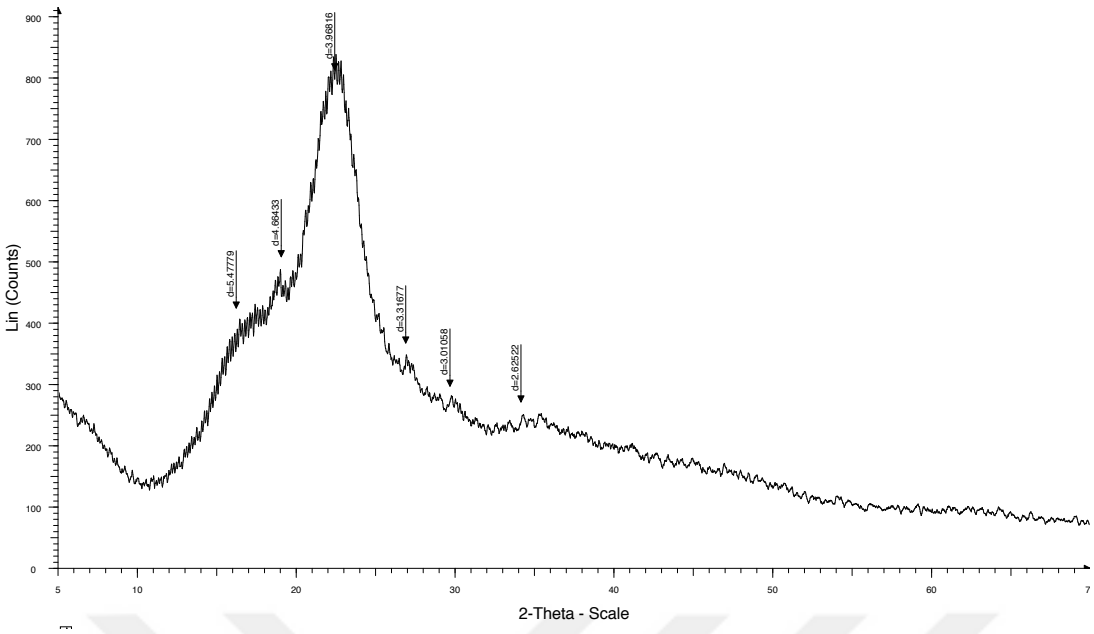
- The ultrasonic pulse velocity (UPV) value of the historical mortar of 1.1 cm in thickness is 557.7 m/s, and the modulus of the elasticity of the same sample is approximately 200 MPa.
- The pozzolanic activity test was conducted with the saturated lime method for aggregates with smaller than 0.125 mm grain sizes. Pozzolanic activity test was performed with 0.0242 g material sample rather than the standard weight of 0.2 g, since the fine aggregate content of the SK.Pe.6 is very low, as it is presented in **Figure 4.2** and **Figure 4.3**. The result of the pozzolanic activity test is presented as the weight of the $Ca(OH)_2$ in grams fixed by the 1 g of pozzolan, which is 266 mg for the studied sample.

Table 4.2. Physical, physicomechanical properties, water vapor permeability and pozzolanic activity characteristics of historical mortar sample

Sample	Bulk Density – ρ, g/cm³	Effective Porosity - φ, % by volume	SD, m	μ-value, unitless	UPV, m/s	MoE, MPa	$Ca(OH)_2$ / 1 g Pozzolan (mg)
SK.Pe.6	0,7	69,5	0,05	3,85	557,7	200,3	266

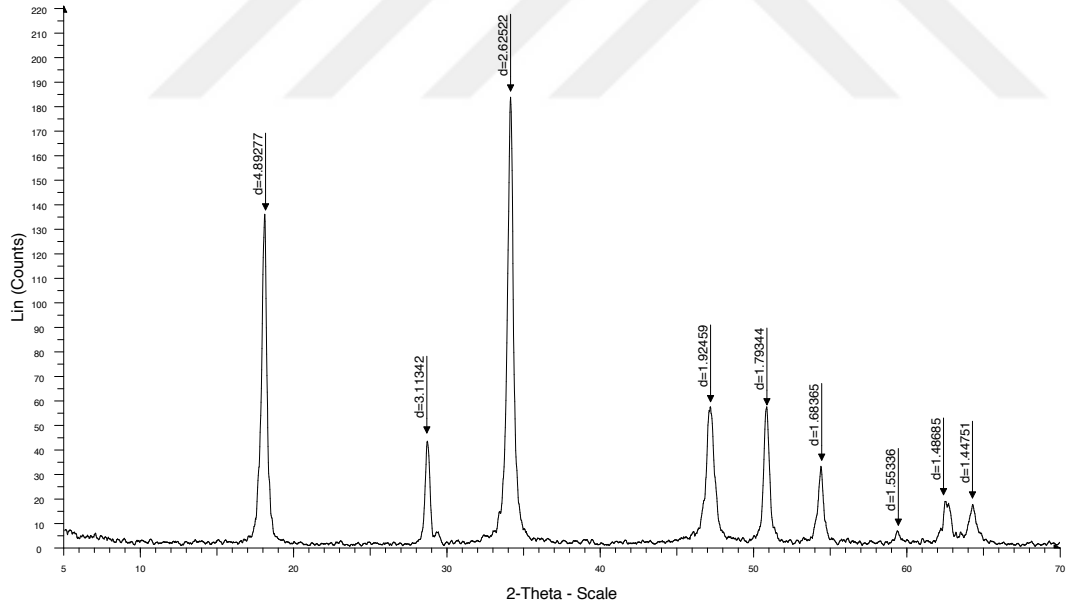
4.2. Some Raw Material Characteristics of Straw Aggregate, Metakaolin Additive and Lime Binder Used in the Mixture of Newly-Produced Mortars

For the production of the straw-mixed lime-based mortar samples and straw-mixed lime-pozzolan mortar samples, raw materials to be used were investigated. Metakaolin, used as a pozzolanic additive, is a well-known pozzolan produced from the calcination of kaolin clay. Wheat straw is a natural silica source as of most of the plants. The pozzolanic activity measurements were conducted on wheat straw and metakaolin samples smaller than 0.125 mm in grain size with the saturated lime method and the conductivity measurement method proposed by Luxan *et al.* (1989). Tests with the saturated lime method were conducted on the 7^{th} and 14^{th} day after the reaction starts. XRD analyses were performed on the powdered wheat straw, $Ca(OH)_2$, kaolin, and metakaolin samples and results are shown in **Figure 4.6, 4.7, 4.8**, and **4.49.** The pozzolanic activity measurement results are shown in **Table 4.3** and **Table 4.4**.



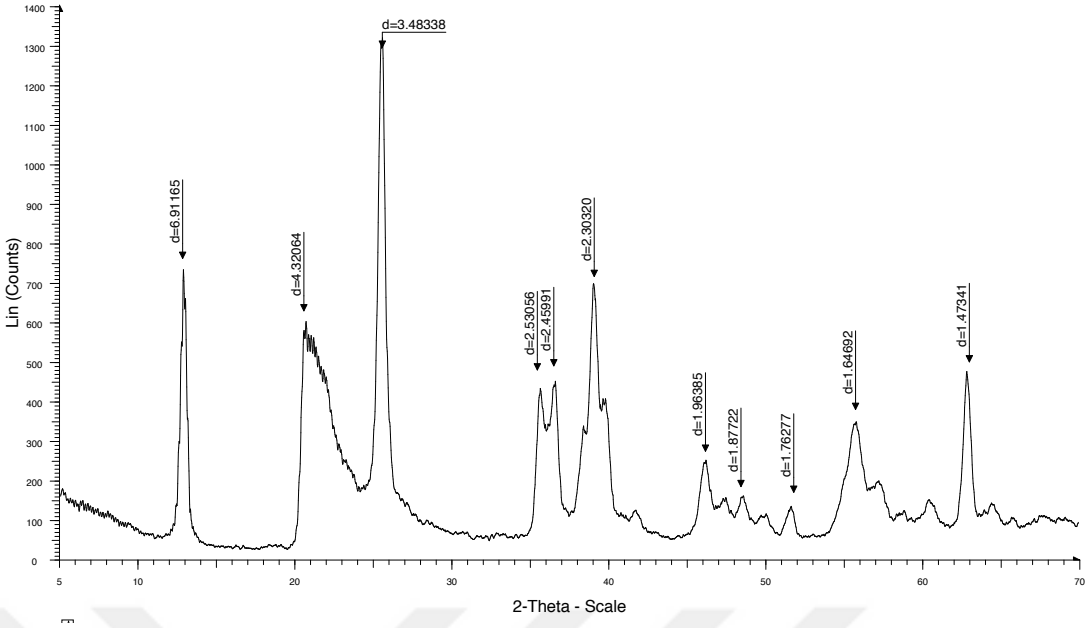
2θ° Cu Kα

Figure 4.6. XRD traces of wheat straw (<0.125 mm in grain size)



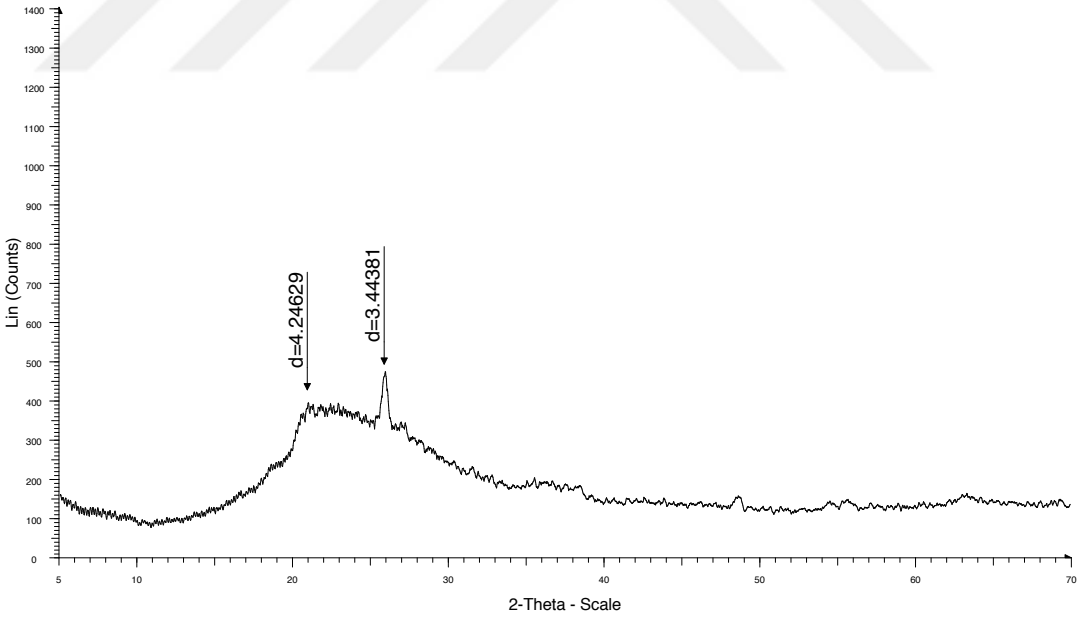
2θ° Cu Kα

Figure 4.7. XRD traces of $Ca(OH)_2$ (<0.125 mm in grain size)



2θ° Cu Kα

Figure 4.8. XRD traces of kaolin (<0.125 mm in grain size)



2θ° Cu Kα

Figure 4.9. XRD traces of metakaolin (<0.125 mm in grain size)

Pozzolanic activity of wheat straw particles smaller than 0.125 mm is 14.7±6.2 mg $Ca(OH)_2$ / g pozzolan 7 days after the pozzolanic reaction starts. Pozzolanic activity of wheat straw particles smaller than 0.125 mm increased to 38.8±1.2 mg $Ca(OH)_2$ / g pozzolan 14 days after the pozzolanic reaction starts (**Table 4.3**). Metakaolin exhibits considerably higher pozzolanic activity than straw, 102.90±7.41 mg $Ca(OH)_2$ / g pozzolan 7 days after the pozzolanic reaction starts. Pozzolanic activity measurements conducted with the saturated lime method show that the pozzolanic activity of straw enhances with time. Pozzolanic activity measurement results conducted with the electrical conductivity method are presented in **Table 4.4**. According to the classification made by Luxan *et al.* (1989), straw has good pozzolanicity. On the other hand, metakaolin exhibits variable pozzolanicity. Cross-interpretation of the results of conducted analyses shows that the speed of pozzolanic reaction is higher in straw, however, overall pozzolanic characteristic of metakaolin is considerably higher than straw.

Table 4.3. Pozzolanic activity measurements of wheat straw and metakaolin with saturated lime method

Sample	**$Ca(OH)_2$/1 g Pozzolan (mg)**
Straw / 7 days after the reaction starts	14.7 ± 6.2
Straw / 14 days after the reaction starts	38.8 ± 1.2
Metakaolin / 7 days after the reaction starts	102.90 ± 7.41

Table 4.4. Pozzolanic activity measurements of wheat straw and metakaolin with electrical conductivity method

Sample	**Electrical Conductivity (mS/cm)**
Straw	1.97
Metakaolin	0.80

4.3. Basic Physical Properties of New Mortar Samples

The bulk density, effective porosity, and water absorption capacity of the straw-mixed lime-based (LW) and straw mixed lime-pozzolan (LMW) mortar samples are presented in **Table 4.5** and **Figure 4.10**. The basic physical properties of those samples are summarized below:

— All straw-mixed lime-based (LW) and straw mixed lime-pozzolan (LMW) samples are lightweight and highly-porous materials that have very high water absorption capacity.
— Among the straw-mixed lime-based (LW) mortars, the bulk density, effective porosity and water absorption capacity of the Sample L1W0, which is the reference sample without straw aggregate, are 1.13 g/cm^3, 52% by volume, and 46% by weight, respectively. The other ones with straw aggregate in various ratios (L9W1, L7W1, L5W1, and L3W1) are less dense and more porous mortars. Their bulk density and effective porosity values vary in the range of 0.49–0.68 g/cm^3 and 70–77%, with water absorption capacities in the range of 103–158%.
— In lime-based mortars, the straw aggregate added in various ratios decreases the density of the reference sample to the half while 1.5 times in average increases its effective porosity and 2.7 times in average its water absorption capacity.
— Among the straw-mixed lime-pozzolan (LMW) mortars, the bulk density, effective porosity and water absorption capacity of the sample LM1W0, which is the reference sample without straw aggregate, are 0.79 g/cm^3, 61% by volume, and 77% by weight, respectively. The other ones with straw aggregate in various ratios (LM9W1, LM7W1, LM5W1, and LM3W1) are less dense and more porous mortars. Their bulk density and effective porosity values vary in the range of 0.42–0.63 g/cm^3 and 73–80%, with water absorption capacities in the range of 116–191%.
— In lime-pozzolan based mortars, the straw aggregate added in various ratios decreases the density of reference sample about two-third while 1.2 times in average increases its effective porosity and 1.9 times in average its water absorption capacity.
— When two reference samples, lime-based and lime-pozzolan mortars without straw aggregate (L1W0 and LM1W0) are compared, the lime-based one is denser and less porous than the lime mortars with metakaolin additive.
— Straw-mixed lime-based and lime-pozzolan mortars have similar density and effective porosity values while lime-pozzolan mortars are slightly less dense and slightly more porous than lime-based ones.

Table 4.5. The bulk density, effective porosity and water absorption capacity values of the straw-mixed lime-based (LW) and straw-mixed lime-pozzolan (LMW) samples

Sample	Bulk Density - ρ, g/cm³	Porosity - φ, % by volume	Water Absorption Coefficient - θ, % by weight
L1W0	1.13 ± 0.01	51.60 ± 1.47	45.57 ± 1.66
L9W1	0.68 ± 0.01	69.56 ± 0.07	103.05 ± 2.14
L7W1	0.62 ± 0.01	70.92 ± 0.06	113.50 ± 2.27
L5W1	0.63 ± 0.03	72.03 ± 1.43	114.13 ± 7.08
L3W1	0.49 ± 0.03	77.09 ± 1.19	158.34 ± 11.33
LM1W0	0.79 ± 0.04	60.71 ± 3.83	77.13 ± 8.34
LM9W1	0.55 ± 0.00	74.71 ± 0.78	135.22 ± 2.59
LM7W1	0.63 ± 0.01	72.72 ± 0.46	115.92 ± 2.60
LM5W1	0.53 ± 0.02	75.77 ± 0.12	144.14 ± 4.86
LM3W1	0.42 ± 0.01	80.02 ± 1.06	190.80 ± 2.88

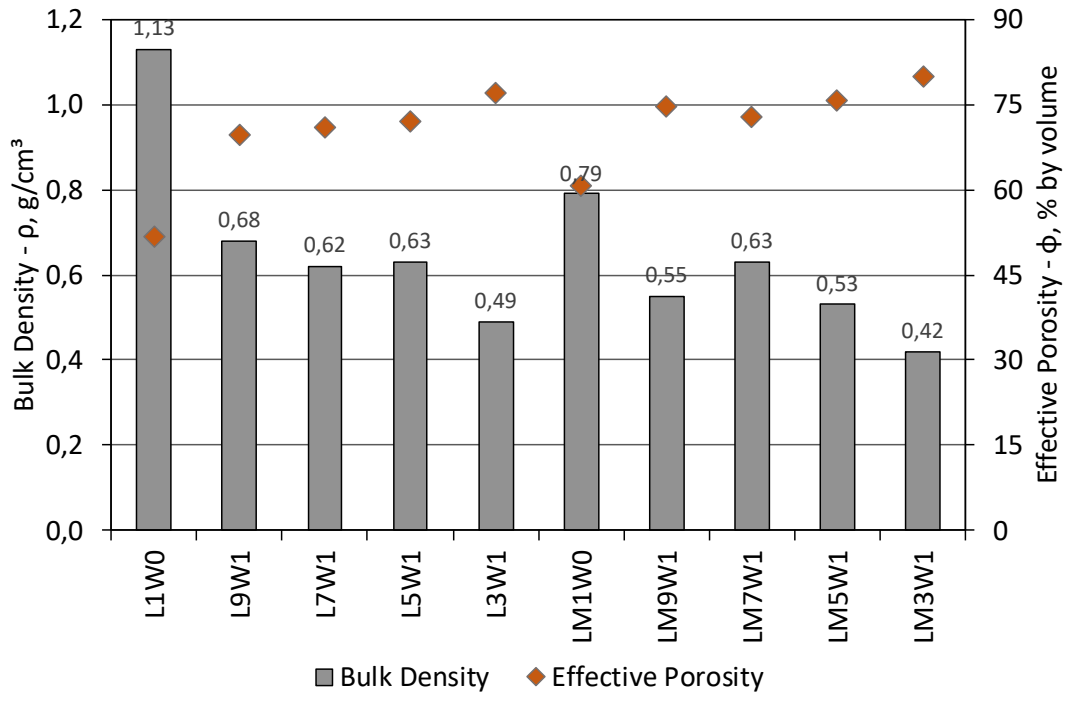


Figure 4.10. The graph showing the bulk density (g/m³) and effective porosity (% by volume) values of the straw-mixed lime-based (LW) and straw mixed lime-pozzolan (LMW) samples.

The equivalent air layer thickness of water vapor diffusion (SD, m), water vapor diffusion resistance index (μ, unitless), and water vapor transmission rate (RT, g/hm^2) values of the straw-mixed lime-based (LW) and straw mixed lime-pozzolan (LMW) are presented in **Table 4.6** and **Figure 4.11**. Their water vapor permeability characteristics are summarized below:

- All lime-based (LW) and straw mixed lime-pozzolan (LMW) samples with and without straw content are highly water vapor permeable mortars. Their μ values are in the range of 1.2–3.5, RT values of 2 cm-thick samples are in the range of 6.6–15.8 g/hm^2, and SD values for 3 cm-thick samples are in the range of 0.04–0.10 m. The SD values lower than 0.14 m and RT values higher than 6.0 g/hm^2 are classified as high-water vapor permeable in the standard TS EN ISO 7783:2012. Therefore, all newly-produced mortars are highly water vapor permeable materials. Among all samples, LM3W1 has the lowest μ-value and highest RT value with 1.23 and 15.81 g/hm^2, respectively.
- The samples L1W0 and LM1W0, which are the reference samples without straw aggregate, have μ values of 3 and 4, respectively.
- The μ values of all the other mortar samples with straw aggregate in various ratios (L9W1, L7W1, L5W1, L3W1 and LM9W1, LM7W1, LM5W1, LM3W1) are similar and in the range of 1 and 2.
- When new mortars mixed with and without straw aggregate are compared, the straw-mixed mortars are slightly more water vapor permeable than the ones without straw aggregate.

Table 4.6. The equivalent air layer thickness of water vapor diffusion (SD, m), water vapor diffusion resistance index (μ, unitless), and water vapor transmission rate (RT, g/hm^2) values of the straw-mixed lime-based (LW) and straw mixed lime-pozzolan (LMW) samples.

Sample	$SD_{3\ cm}$ (m)*	μ-value (unitless)	RT (g/hm^2)	Water Vapor Permeability Class**
L1W0	0.08 ± 0.01	2.79 ± 0.18	10.98 ± 2.73	Highly Permeable
L9W1	0.04 ± 0.00	1.39 ± 0.02	15.69 ± 0.91	Highly Permeable
L7W1	0.05 ± 0.00	1.67 ± 0.02	14.01 ± 0.65	Highly Permeable
L5W1	0.05 ± 0.00	1.63 ± 0.00	13.47 ± 0.98	Highly Permeable
L3W1	0.05 ± 0.00	1.51 ± 0.05	13.88 ± 0.63	Highly Permeable
LM1W0	0.10 ± 0.00	3.50 ± 0.08	6.58 ± 0.73	Highly Permeable
LM9W1	0.04 ± 0.00	1.33 ± 0.09	14.49 ± 1.05	Highly Permeable
LM7W1	0.04 ± 0.00	1.40 ± 0.05	14.43 ± 0.86	Highly Permeable
LM5W1	0.04 ± 0.00	1.39 ± 0.15	14.65 ± 0.86	Highly Permeable
LM3W1	0.04 ± 0.00	1.23 ± 0.02	15.81 ± 0.69	Highly Permeable

* SD values are calculated for material thickness of 3,00 cm.
** Water vapor permeability classes are determined according to TS EN ISO 7783:2012.

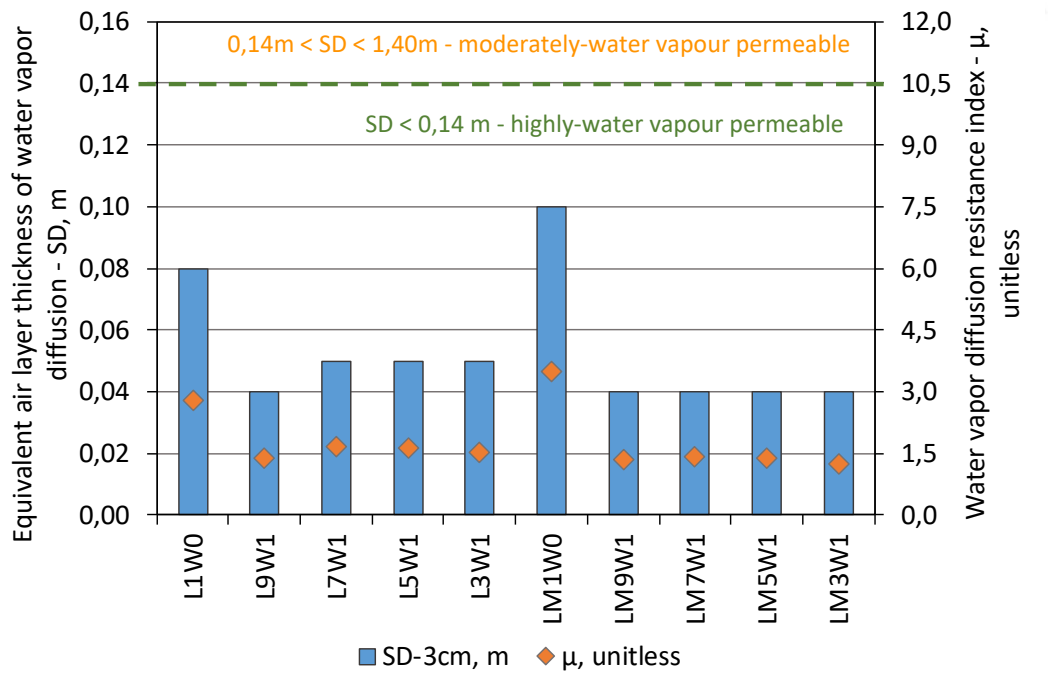


Figure 4.11. The graph showing the equivalent air layer thickness of water vapor diffusion ($SD_{3\ cm}$, m) and water vapor diffusion resistance index (μ, unitless) values of the straw-mixed lime-based (LW) and straw mixed lime-pozzolan (LMW) samples.

4.4. Physicomechanical Properties of New Mortar Samples

The ultrasonic pulse velocities (UPV, m/s) and the modulus of elasticity values (MoE, MPa), calculated with the bulk density and UPV data, obtained from the straw-mixed lime-based (LW) mortars and straw mixed lime-pozzolan (LMW) mortars are presented in **Table 4.7**, **Figure 4.12,** and **Figure 4.13**. Those properties are summarized below:

— The samples L1W0 and LM1W0, which are the reference samples without straw aggregate, have higher physicomechanical characteristics than the others with straw aggregate (**Figure 4.13**). The UPV values of the samples L1W0 and LM1W0 are 1470±193 m/s and 1380±93 m/s, respectively. The MoE values of those samples are 2294±624 MPa and 1417±128 MPa, accordingly.

— The ultrasonic pulse velocity data obtained from the straw-mixed mortars show that newly-produced mortars with straw aggregate have poor physicomechanical properties and present a heterogeneous nature. Mainly two ranges of UPV data, namely an upper range and a lower range, for the straw-mixed samples are observed during UPV transit time measurements (**Figure 4.12**). The upper range of the UPV data varies between 381–510 m/s with an average of 437±49 m/s, corresponding to the MoE values of 106±37 MPa. The lower range of the UPV data obtained from the same samples varies between 189–246 m/s with an average of 224±17 m/s, corresponding to the MoE values of 28±7 MPa.

— On the other hand, constant transit time readings are available with a slight pressure application when taking measurements. As a UPV measurement technique, applying a very slight pressure during measurements is recommended for such very fibrous mortar samples until constant transit time readings are achieved. Therefore, for the evaluation of physicomechanical performance of newly-produced mortar samples the $UPV_{W/PRESS}$ and $MoE_{W/PRESS}$ values were used.

— The $UPV_{W/PRESS}$ and $MoE_{W/PRESS}$ achieved for the straw-mixed mortar samples are 565±60 m/s and 174±59 MPa, respectively (**Figure 4.10**). The lime-based mortars with metakaolin (LMW samples) are observed to have slightly lower MoE than the lime-based mortars without metakaolin (LW samples).

— The transit time data could not be measured from the lime-based mortar sample L3W1 which has the highest amount of straw in its mixture.

Table 4.7. The ultrasonic pulse velocity (UPV, m/s) and corresponding modulus of elasticity (MoE, MPa) values of the new mortar samples

Sample	$UPV_{w/PRESS}$	$UPV_{UP-RANGE}$	$UPV_{LOW-RANGE}$	$MoE_{w/PRESS}$	$MoE_{UP-RANGE}$	$MoE_{LOW-RANGE}$
	m/s	m/s	m/s	MPa	MPa	MPa
L1W0	1470 ± 193	1470 ± 193	1470 ± 193	2294 ± 624	2294 ± 624	2294 ± 624
L9W1	663 ± 54	510 ± 51	226 ± 33	275 ± 47	163 ± 34	32 ± 9
L7W1	593 ± 53	487 ± 53	246 ± 60	204 ± 35	138 ± 29	37 ± 19
L5W1	609 ± 78	457 ± 45	225 ± 43	206 ± 46	123 ± 25	31 ± 12
L3W1	N.A.	N.A.	N.A.	N.A.	N.A.	N.A.
LM1W0	1380 ± 93	1380 ± 93	1380 ± 93	1417 ± 128	1418 ± 128	1419 ± 128
LM9W1	553 ± 64	414 ± 25	231 ± 53	147 ± 36	88 ± 10	29 ± 14
LM7W1	528 ± 38	419 ± 18	222 ± 36	161 ± 57	101 ± 8	29 ± 10
LM5W1	522 ± 31	393 ± 45	227 ± 47	132 ± 18	75 ± 17	26 ± 11
LM3W1	490 ± 51	381 ± 40	189 ± 47	94 ± 20	57 ± 12	15 ± 8

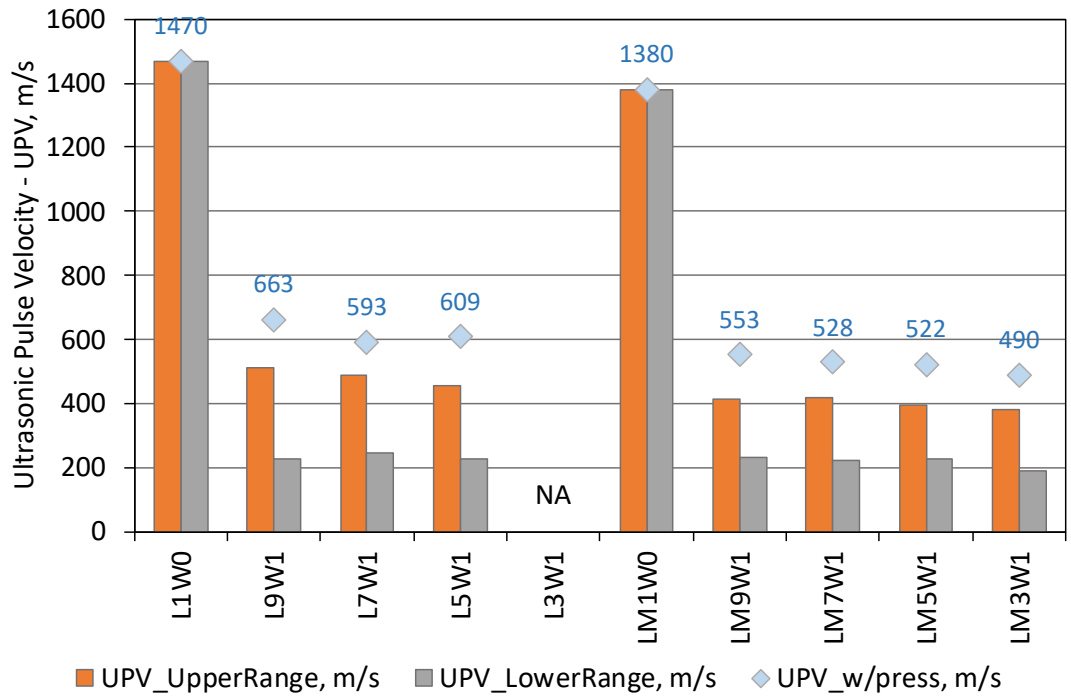


Figure 4.12. The graph showing the upper range and lower range of ultrasonic pulse velocity values ($UPV_{LOW-RANGE}$, $UPV_{UP-RANGE}$) of the new mortar samples and their UPV values obtained with a slight pressure ($UPV_{w/PRESS}$).

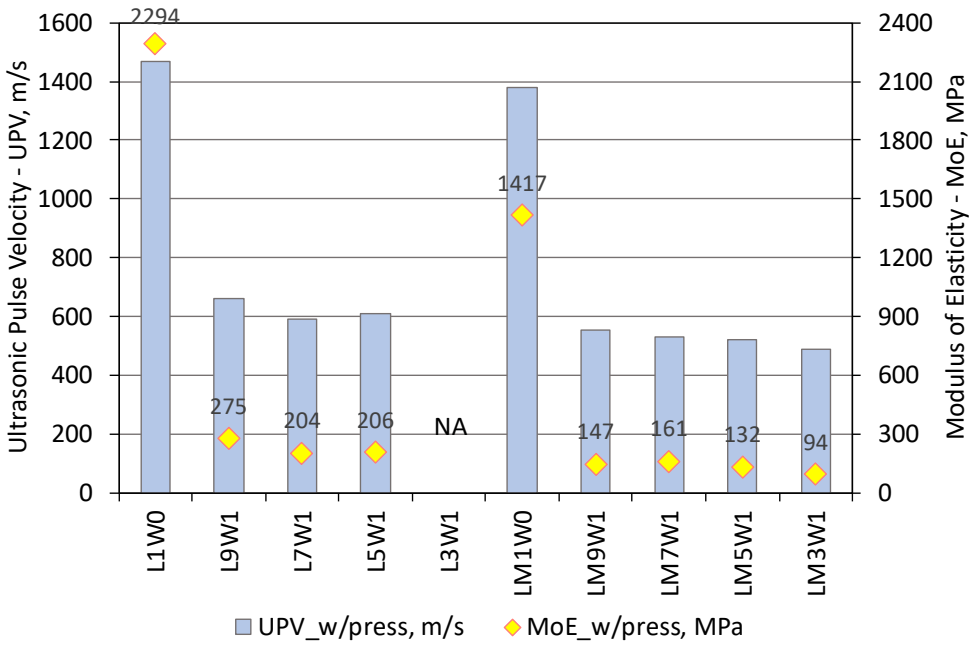


Figure 4.13. The graph showing the UPV values obtained with a slight pressure ($UPV_{w/PRESS}$) and corresponding modulus of elasticity values belonging to the new mortar samples.

4.5. Mechanical Properties of New Mortar Samples

The flexural strength and compressive strength values of the straw-mixed lime-based (LW) mortars and straw mixed lime-pozzolan (LMW) mortars are presented in **Table 4.8** and **Figure 4.14**. For the sample LM1W0, no results were obtained from the flexural strength measurement due to the unavailability of the appropriate test specimen. The data achieved is summarized below:

— The samples L1W0 and LM1W0, which are the reference samples without straw aggregate, have higher mechanical characteristics than the others with straw aggregate. The flexural strength of the sample L1W0 is 1383 kPa while the compressive strength of the samples L1W0 and LM1W0 are 2204 kPa and 5326 kPa, respectively. The lime-pozzolan mortar LM1W0 in which metakaolin is used as pozzolan additive has compressive strength two times more than lime-based one L1W0 although it (LM1W0) has lime binder half in amount.

— The flexural and compressive strength of the straw-mixed mortars show that new mortars with straw aggregate have poor mechanical properties with the average values of 387±81 kPa and 357±92 kPa, respectively. The data show that the straw content in the mixture with binder: straw ratios of 9:1 to 3:1 reduces the mechanical properties of mortars noticeably.

— Similar and low values achieved in flexural and compressive strength of straw-mixed lime-based and lime-pozzolan mortars while there is not a gradual reduction in their strength with the increase in straw aggregate in their mixtures.

Table 4.8. The flexural strength and compressive strength values of the straw-mixed lime-based (LW) and straw mixed lime-pozzolan (LMW) samples

Sample	Bulk Density ρ, g/cm³	Flexural Strength σf, kPa	Compressive Strength σc, kPa
L1W0	1.13	1383 ± 23	2204 ± 187
L9W1	0.68	281 ± 36	341 ± 30
L7W1	0.62	405 ± 71	404 ± 60
L5W1	0.63	354 ± 0	295 ± 36
L3W1	0.49	547 ± 189	472 ± 96
LM1W0	0.79	N.A.	5326 ± 619
LM9W1	0.55	313 ± 15	257 ± 58
LM7W1	0.63	416 ± 132	491 ± 62
LM5W1	0.53	409 ± 24	343 ± 70
LM3W1	0.42	368 ± 19	252 ± 19

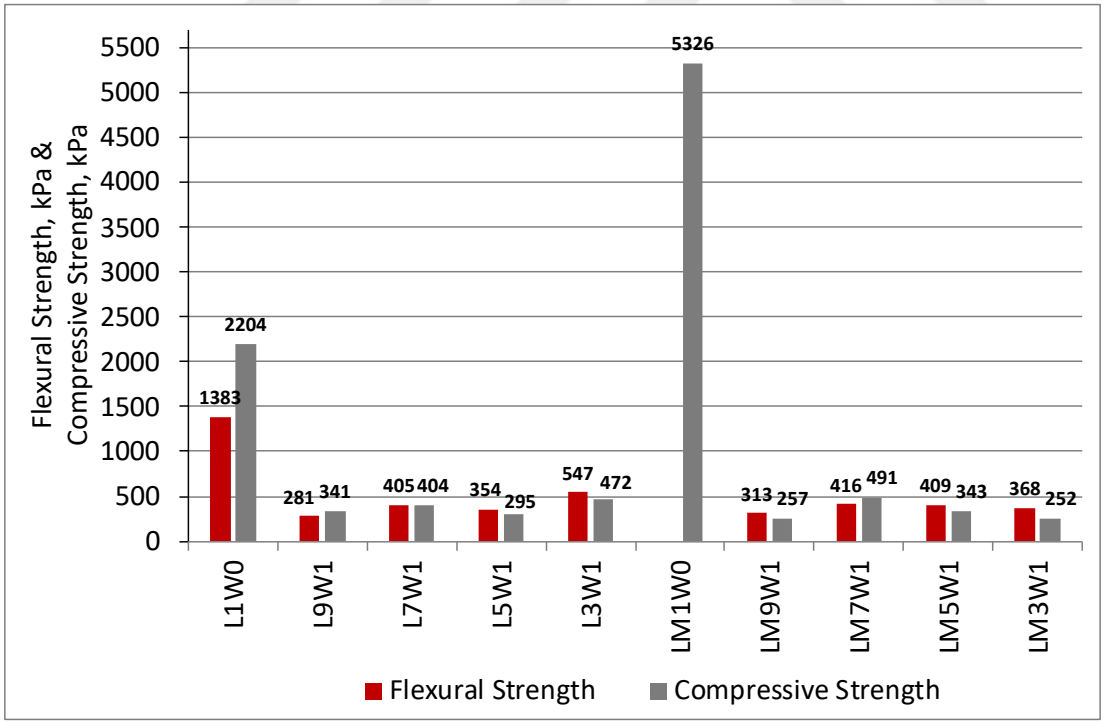


Figure 4.14. The graph showing the flexural strength (kPa) and compressive strength (kPa) values of the straw-mixed lime-based (LW) and straw mixed lime-pozzolan (LMW) samples.

4.6. Acoustical Properties of New Mortar Samples

The sound absorption coefficient (α), the noise reduction coefficient (NRC), and the weighted sound absorption coefficient (αw**)** data of the straw-mixed lime-based (LW) and straw mixed lime-pozzolan (LMW) mortar samples are presented in **Table 4.9, Table 4.10, Figure 4.15**, **Figure 4.16**, and **Figure 4.17**. Sound absorption coefficient values lower than 0.1 were marked to point out the reflectivity of the material at that specific frequencies. The obtained data are summarized below;

- The sound absorption coefficients (α) of L1W0 are in the range of 0.02 and 0.31 between 63 Hz and 4000 Hz. The maximum α value is at 1000 Hz. The noise reduction coefficient (NRC) value of the same sample is 0.17, where the weighted sound absorption coefficient value is 0.22.
- The sound absorption coefficients (α) of L9W1 are in the range of 0.01 and 0.33 between 63 Hz and 4000 Hz. The maximum α value is at 1000 Hz. NRC value of the same sample is 0.22, where αw value is 0.29.
- The sound absorption coefficients (α) of L7W1 are in the range of 0.02 and 0.42 between 63 Hz and 4000 Hz. The maximum α value is at 1000 Hz. NRC value of the same sample is 0.28, where αw value is 0.33.
- The sound absorption coefficients (α) of L5W1 are in the range of 0.02 and 0.41 between 63 Hz and 4000 Hz. The maximum α value is at 1000 Hz. NRC value of the same sample is 0.28, where αw value is 0.34.
- The sound absorption coefficients (α) of L3W1 are in the range of 0.01 and 0.76 between 63 Hz and 4000 Hz. The maximum α value is at 1000 Hz. NRC value of the same sample is 0.46, where αw value is 0.40.
- The sound absorption coefficients (α) of LM1W0 are in the range of 0.01 and 0.20 between 63 Hz and 4000 Hz. The maximum α value is at 2000 Hz. NRC value of the same sample is 0.11, where αw value is 0.16.
- The sound absorption coefficients (α) of LM9W1 are in the range of 0.02 and 0.28 between 63 Hz and 4000 Hz. The maximum α value is at 1000 Hz. NRC value of the same sample is 0.16, where αw value is 0.18.
- The sound absorption coefficients (α) of LM7W1 are in the range of 0.03 and 0.22 between 63 Hz and 4000 Hz. The maximum α value is at 500 Hz. NRC value of the same sample is 0.16, where αw value is 0.22.

- The sound absorption coefficients (α) of LM5W1 are in the range of 0.03 and 0.36 between 63 Hz and 4000 Hz. The maximum α value is at 1000 Hz. NRC value of the same sample is 0.24, where αw value is 0.28.
- The sound absorption coefficients (α) of LM3W1 are in the range of 0.03 and 0.28 between 63 Hz and 4000 Hz. The maximum α value is at 1000 Hz. NRC value of the same sample is 0.20, where αw value is 0.25.

Table 4.9. Sound absorption coefficient (α) values of the newly-produced mortar samples in octave band central frequencies (Hz)

Sample	Bulk Density ρ, g/cm³	Octave Band Central Frequencies (Hz)						
		63 Hz	125 Hz	250 Hz	500 Hz	1000 Hz	2000 Hz	4000 Hz
L1W0	1.13	0.02	0.02	0.04	0.17	0.31	0.17	0.12
L9W1	0.68	0.01	0.04	0.11	0.19	0.33	0.26	0.19
L7W1	0.62	0.02	0.04	0.12	0.28	0.42	0.30	0.22
L5W1	0.63	0.02	0.04	0.12	0.28	0.41	0.32	0.26
L3W1	0.49	0.01	0.02	0.10	0.39	0.76	0.60	0.51
LM1W0	0.79	0.01	0.02	0.02	0.06	0.15	0.20	0.14
LM9W1	0.55	0.02	0.05	0.08	0.14	0.28	0.12	0.12
LM7W1	0.63	0.03	0.06	0.11	0.22	0.20	0.13	0.14
LM5W1	0.53	0.02	0.08	0.15	0.20	0.36	0.25	0.20
LM3W1	0.42	0.03	0.07	0.13	0.15	0.28	0.24	0.22

Table 4.10. Noise reduction coefficient (NRC) and weighted sound absorption coefficient (αw) values of the newly-produced mortar samples

Sample	Bulk Density ρ, g/cm³	Noise Reduction Coefficient NRC, unitless	Weighted Sound Absorption Coefficient αw, unitless
L1W0	1.13	0.17	0.22
L9W1	0.68	0.22	0.29
L7W1	0.62	0.28	0.33
L5W1	0.63	0.28	0.34
L3W1	0.49	0.46	0.40
LM1W0	0.79	0.11	0.16
LM9W1	0.55	0.16	0.18
LM7W1	0.63	0.16	0.22
LM5W1	0.53	0.24	0.28
LM3W1	0.42	0.20	0.25

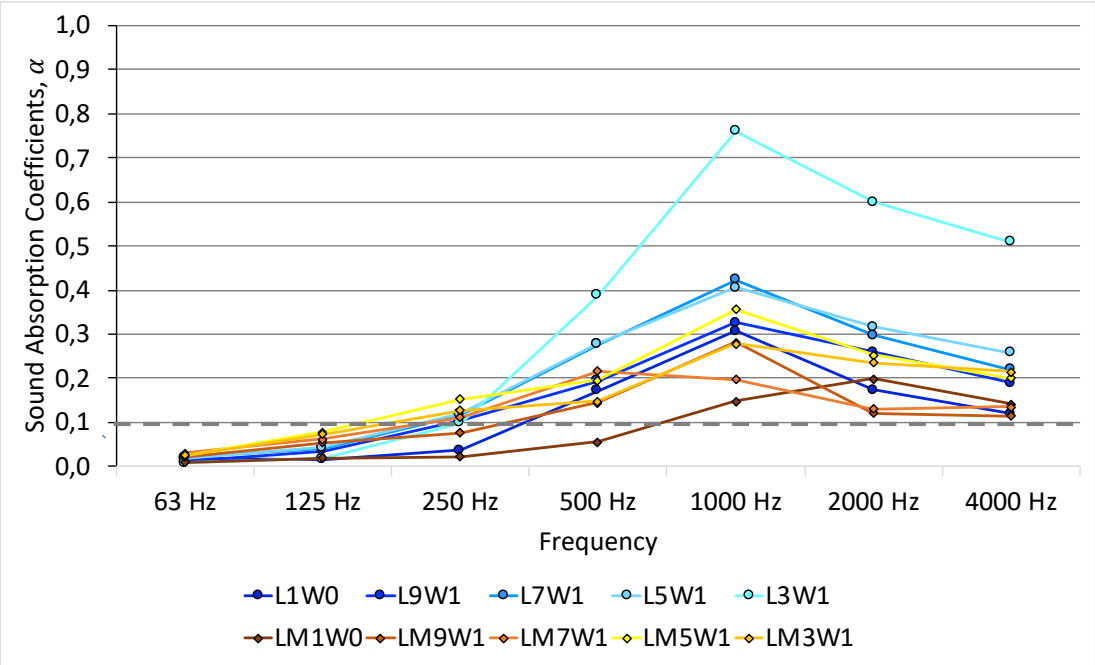


Figure 4.15. Sound absorption coefficients of the new mortar samples

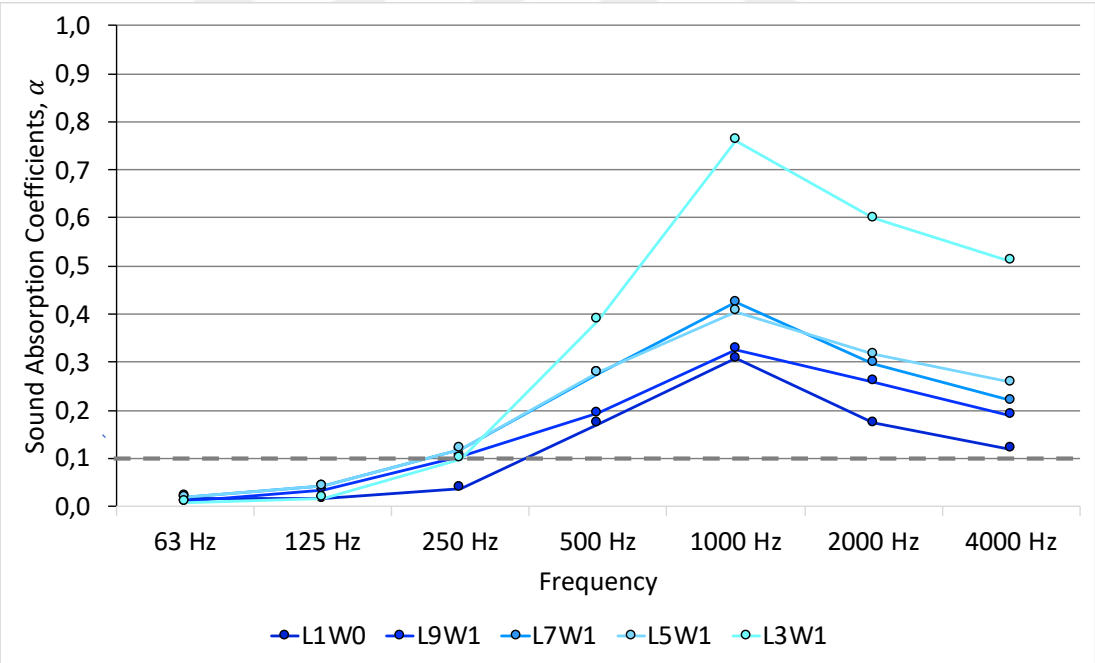


Figure 4.16. Sound absorption coefficients of the straw-mixed lime-based (LW) mortar samples

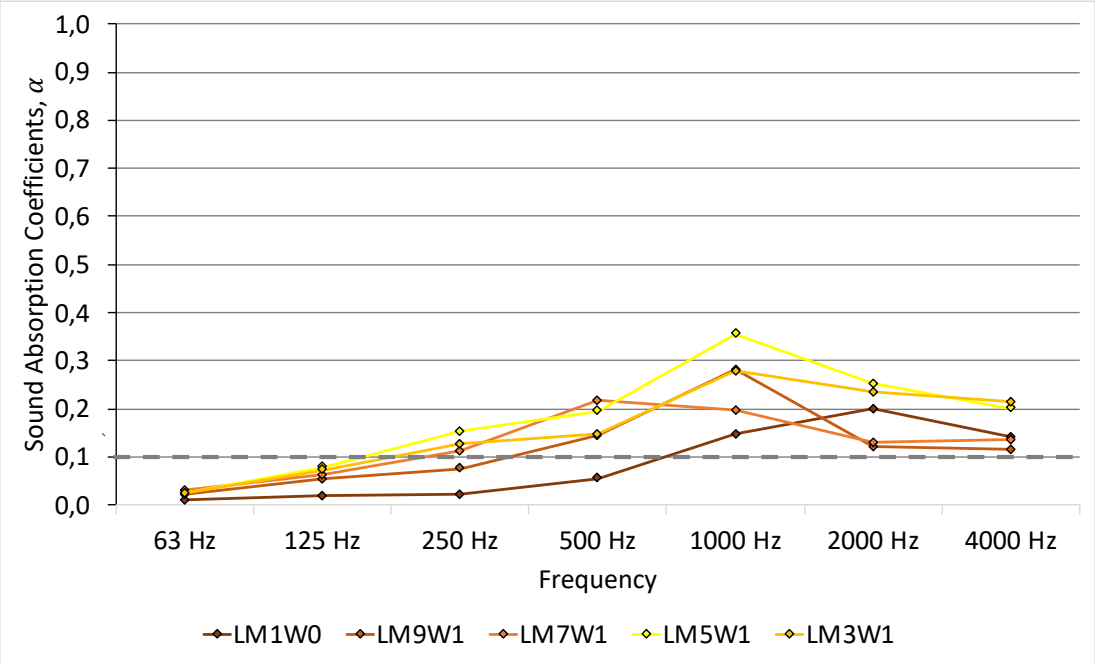


Figure 4.17. Sound absorption coefficients of the straw mixed lime-pozzolan (LMW) mortar samples

4.7. Thermal Properties of New Mortar Samples

The thermal conductivity (λ), specific heat capacity (c), thermal diffusivity (D), and thermal effusivity (e) data of the new mortar samples are presented in **Table 4.11** and **Figure 4.18**. Bulk density, thermal conductivity, and specific heat properties were determined by laboratory analysis in the study. These properties were used to estimate thermal diffusivity and thermal effusivity. The obtained data are summarized below;

- Thermal conductivity values of the new mortar samples are ranging from 0.0608 W/mK to 0.1202 W/mK.
- The thermal conductivity value of LM1W0 is 0.1773 W/mK, which is the highest among all samples.
- Thermal conductivity values of lime-based straw mixed samples without pozzolanic additive (L9W1, L7W1, L5W1, L3W1) are in the range of 0.0810 and 0.1202.
- Thermal conductivity values of lime-based straw mixed samples with pozzolanic additive (LM9W1, LM7W1, LM5W1, LM3W1) are in the range of 0.0608 and 0.0796.
- Mortar samples with pozzolanic additive have lower thermal conductivity values.
- Specific heat values of the new mortar samples are ranging from 3.06 kJ/kgK to 20.27 kJ/kgK.

- Specific heat values of lime-based straw mixed samples without pozzolanic additive (L9W1, L7W1, L5W1, L3W1) are in the range of 5.34 kJ/kgK and 12.82 kJ/kgK.
- Specific heat values of lime-based straw mixed samples with pozzolanic additive (LM9W1, LM7W1, LM5W1, LM3W1) are in the range of 5.97 kJ/kgK and 20.27 kJ/kgK.
- Specific heat value of LM3W1 is 20.27 kJ/kgK, which is the highest among all samples. Thermal diffusivity value of the same sample is 7.14 E^{-9} m^2/s, which is the lowest among studied new mortar samples.
- Thermal diffusivity values of the new mortar samples are ranging from 9.78E^{-9} m^2/s to 4.35E^{-8} m^2/s.
- Thermal effusivity values of the new mortar samples are ranging from 404.05 $J/s^{1/2}m^2K$ to 1072.39 $J/s^{1/2}m^2K$.

Table 4.11. Thermal conductivity, specific heat, thermal diffusivity, and thermal effusivity values of new mortar samples in relation to density and thickness values

Sample	Thickness *d*, cm	Bulk Density ρ, g/cm^3	Thermal Conductivity λ, W/mK	Specific Heat *c*, kJ/kgK	Thermal Diffusivity *D*, m^2/s	Thermal Effusivity *e*, J/s$^{1/2}$m^{2}K
L1W0	N.A.	1.13	N.A.	5.16±0.03	N.A.	N.A.
L9W1	2	0.68	0.1202	5.34± 0.97	3.33E^{-8}	658.03
L7W1	2.1	0.62	0.1097	6.70± 0.44	2.62E^{-8}	677.52
L5W1	2.5	0.63	0.0843	3.06± 0.04	4.35E^{-8}	404.05
L3W1	2.3	0.49	0.0810	12.82± 0.27	1.29E^{-8}	711.75
LM1W0	3	0.79	0.1773	8.22± 0.06	2.73E^{-8}	1072.39
LM9W1	3	0.55	0.0796	5.97± 1.13	2.41E^{-8}	512.35
LM7W1	2.6	0.63	0.0738	12.02± 0.14	9.78E^{-9}	746.11
LM5W1	2.5	0.53	0.0730	14.92± 0.01	9.30E^{-9}	756.95
LM3W1	2.1	0.42	0.0608	20.27± 2.60	7.14E^{-9}	719.06

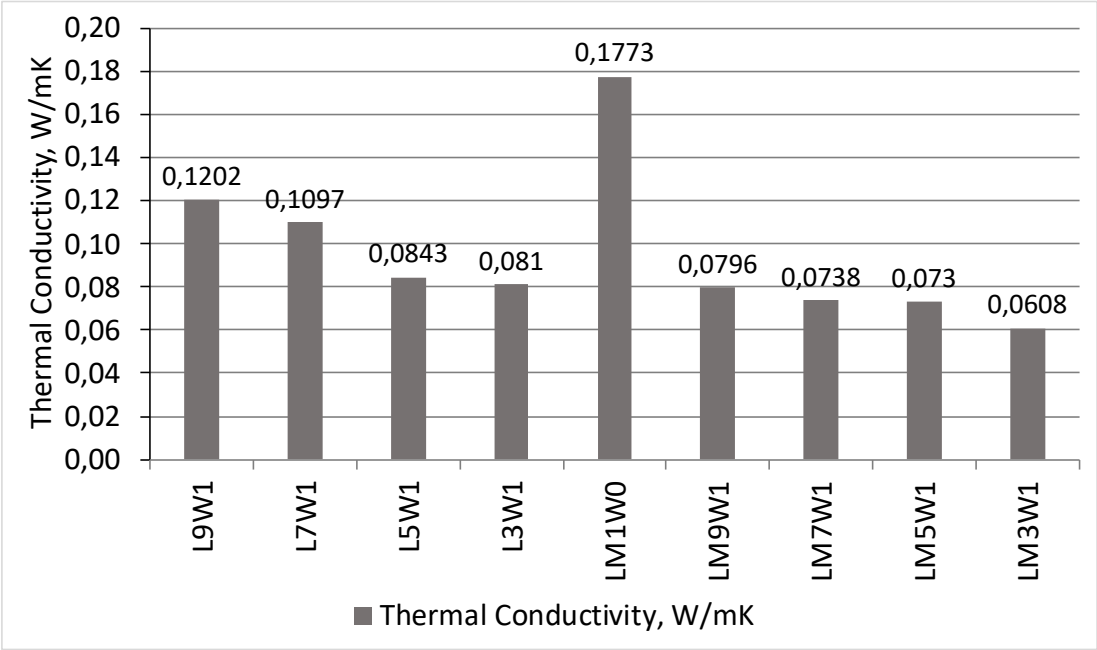


Figure 4.18. Thermal conductivity values of new material samples

Infrared thermography imaging analyses were conducted on newly-produced mortar samples together with marble, wood, rock wool, glass wool, expanded polystyrene (EPS), and autoclaved aerated concrete (AAC) thermal insulation samples. IR imaging tests on straw-mixed lime-pozzolan mortars together with some common building materials are shown in **Figure 4.19, 4.20, 4.21, 4.22**.

Temperature differences during 60 seconds of heating period and the heating rates of the studied material samples are presented in **Table 4.12.** IR images obtained during the heating sequence are shown in **Figure 4.19**. According to IR analyses, the heating rate of the studied materials, including newly-produced lime-based straw-mixed mortars (LW), are sorted as follows;

Rock wool> Glass wool= EPS > AAC insulation block > L3W1> Wood> L5W1= L7W1> L9W1> L1W0> Marble

Table 4.12. Temperature differences during 60 seconds of heating period and the heating rates of the straw-mixed lime-based mortar samples together with rock wool, glass wool, EPS, AAC insulation block, wood, and marble samples

Sample	Temperature Difference ΔT, °C	Duration t, s	Heating rate °C/s$^{1/2}$
L1W0	0.3	60	0.04
L9W1	0.7	60	0.09
L7W1	0.8	60	0.10
L5W1	0.8	60	0.10
L3W1	1.2	60	0.15
Rock wool	3.3	60	0.43
Glass wool	2.0	60	0.26
EPS	2.0	60	0.26
AAC Insulation Block	1.9	60	0.25
Wood	0.9	60	0.12
Marble	0.2	60	0.03

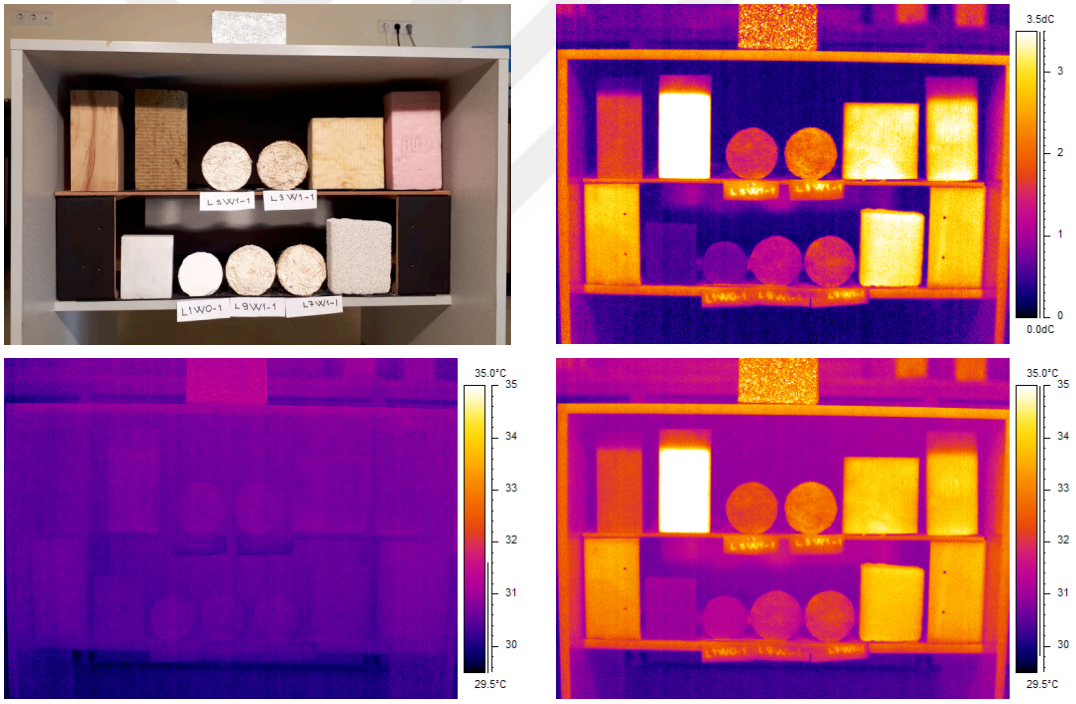


Figure 4.19. View of the straw-mixed lime-based mortar samples together with marble and wood samples and rock wool, glass wool, expanded polystyrene, autoclaved aerated concrete thermal insulation samples (on the left top), its IR image taken at the ambient conditions of 25.3ºC and 31%RH before heating period was started – initial IR image (on the left bottom); the last IR image of the heating period after the uniform heating with halogen lamp for a period of 200s (on the right bottom); and the differential IR image showing the temperature difference between the initial and the last IR images for the heating period of 200s (on the right top).

Temperature differences during 60 seconds of cooling period and the cooling rates of the studied material samples are presented in **Table 4.13.** IR images obtained during the cooling sequence are shown in **Figure 4.20**. According to IR analyses, the cooling rate of the studied materials, including newly-produced lime-based straw-mixed mortars (LW), are sorted as follows;

Rockwool > Glass wool> EPS> AAC insulation block > L3W1>L7W1> Wood= L5W1> L9W1> L1W0> Marble

IR analyses can reflect the thermal inertia properties of materials. Results show that the heating and cooling rates of the materials studied are not always parallel. All materials in this study heat faster and cool slower. Rock wool, glass wool, EPS, and AAC insulation block exhibit higher heating and cooling rates, as it is expected from thermal insulation materials. Newly-produced straw-mixed lime-based mortars (LW) have similar thermal inertia characteristics with the wood sample.

Table 4.13. Temperature differences during 60 seconds of cooling period and the cooling rates of the straw-mixed lime-based mortar samples together with rock wool, glass wool, EPS, AAC insulation block, wood, and marble samples

Sample	**Temperature Difference ΔT, °C**	**Duration t, s**	**Cooling rate °C/s$^{1/2}$**
L1W0	0.2	60	0.03
L9W1	0.5	60	0.06
L7W1	0.7	60	0.09
L5W1	0.6	60	0.08
L3W1	1.0	60	0.13
Rock wool	2.9	60	0.37
Glass wool	2.0	60	0.26
EPS	1.8	60	0.23
AAC Insulation Block	1.6	60	0.21
Wood	0.6	60	0.08
Marble	0.1	60	0.01

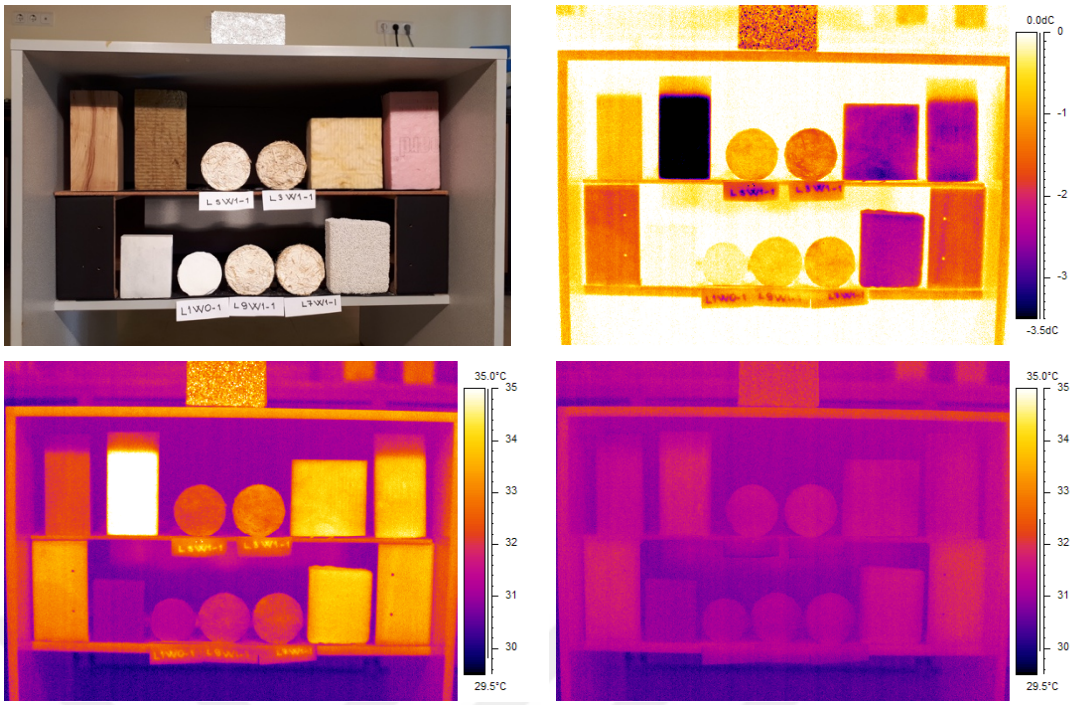


Figure 4.20. View of the straw-mixed lime-based mortar samples together with marble and wood samples and rock wool, glass wool, expanded polystyrene, autoclaved aerated concrete thermal insulation samples (on the left top), its IR image taken at the ambient conditions of 25.3ºC and 31%RH after the uniform heating with halogen lamp for a period of 200s – initial IR image (on the left bottom); the last IR image of the cooling period when halogen lamps were switched off for a period of 200s (on the right bottom); and the differential IR image showing the temperature difference between the initial and the last IR images for the cooling period of 200s (on the right top).

Temperature differences during 60 seconds of heating period and the heating rates of the studied material samples are presented in **Table 4.14.** IR images obtained during the heating sequence are shown in **Figure 4.21**. According to IR analyses, the cooling rate of the studied materials, including newly-produced straw-mixed lime-pozzolan mortars (LMW), are sorted as follows;

Rockwool> Glass wool= EPS > AAC insulation block > LM9W1= LM5W1> LM7W1= Wood= LM3W1> LM1W0> Marble

Table 4.14. Temperature differences during 60 seconds of heating period and the heating rates of the straw-mixed lime-pozzolan mortar samples together with rock wool, glass wool, EPS, AAC insulation block, wood, and marble samples

Sample	Temperature Difference ΔT, °C	Duration t, s	Heating rate °C/s$^{1/2}$
LM1W0	0.4	60	0.05
LM9W1	0.8	60	0.10
LM7W1	0.7	60	0.09
LM5W1	0.8	60	0.10
LM3W1	0.7	60	0.09
Rock wool	3.1	60	0.40
Glass wool	2.0	60	0.25
EPS	1.9	60	0.25
AAC Insulation Block	1.8	60	0.23
Wood	0.7	60	0.09
Marble	0.1	60	0.01

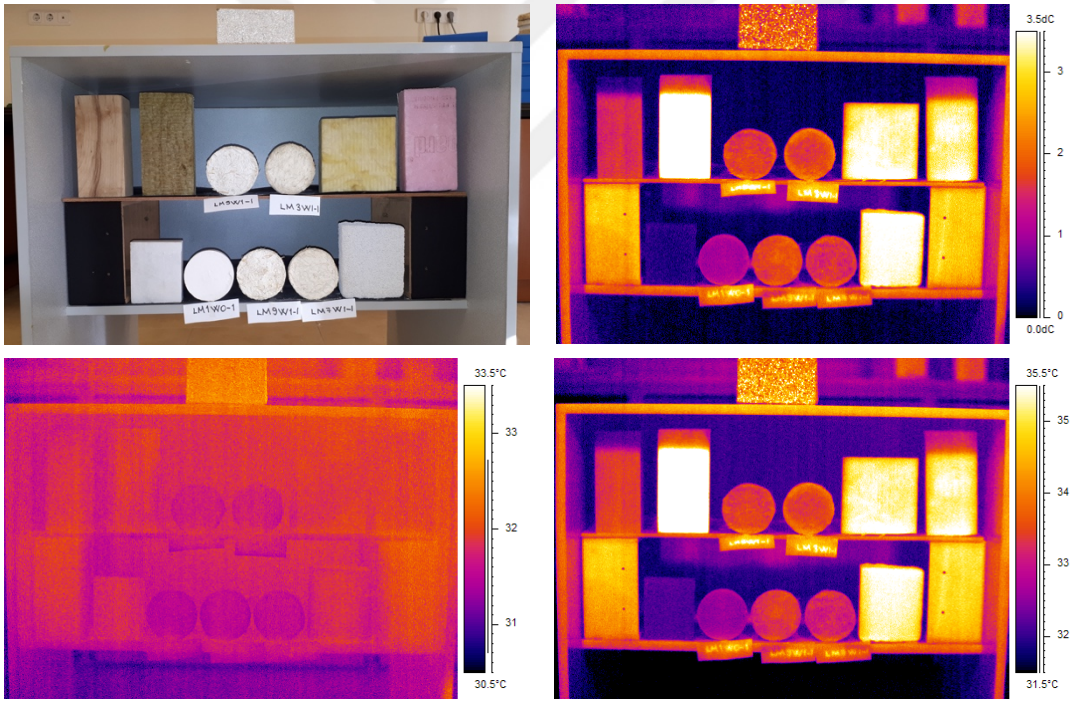


Figure 4.21. View of the straw-mixed lime-pozzolan mortar samples together with marble and wood samples and rock wool, glass wool, expanded polystyrene, autoclaved aerated concrete thermal insulation samples (on the left top), its IR image taken at the ambient conditions of 24.3ºC and 33%RH before heating period was started – initial IR image (on the left bottom); the last IR image of the heating period after the uniform heating with halogen lamp for a period of 218s (on the right bottom); and the differential IR image showing the temperature difference between the initial and the last IR images for the heating period of 218s (on the right top).

Temperature differences during 60 seconds of cooling period and the cooling rates of the studied material samples are presented in **Table 4.15.** IR images obtained during the cooling sequence are shown in **Figure 4.22**. According to IR analyses, the cooling rate of the studied materials, including newly-produced straw-mixed lime-pozzolan mortars (LMW), are sorted as follows;

Rockwool> EPS > Glass wool> AAC insulation block > LM9W1>LM5W1= Wood> LM7W1= LM3W1> LM1W0> Marble

Newly-produced straw-mixed lime-pozzolan mortars (LMW) have similar thermal inertia characteristics with the wood sample. Heating and cooling rates of straw-mixed lime-based mortars (LW) and straw-mixed lime-pozzolan mortars (LMW) are similar.

Table 4.15. Temperature differences during 60 seconds of cooling period and the cooling rates of the straw-mixed lime-pozzolan mortar samples together with rock wool, glass wool, EPS, AAC insulation block, wood, and marble samples

Sample	**Temperature Difference ΔT, °C**	**Duration t, s**	**Cooling rate °C/s$^{1/2}$**
LM1W0	0.4	60	0.05
LM9W1	0.7	60	0.09
LM7W1	0.5	60	0.06
LM5W1	0.6	60	0.08
LM3W1	0.5	60	0.06
Rock wool	2.8	60	0.36
Glass wool	1.7	60	0.22
EPS	1.8	60	0.23
AAC Insulation Block	1.6	60	0.21
Wood	0.6	60	0.08
Marble	0.1	60	0.01

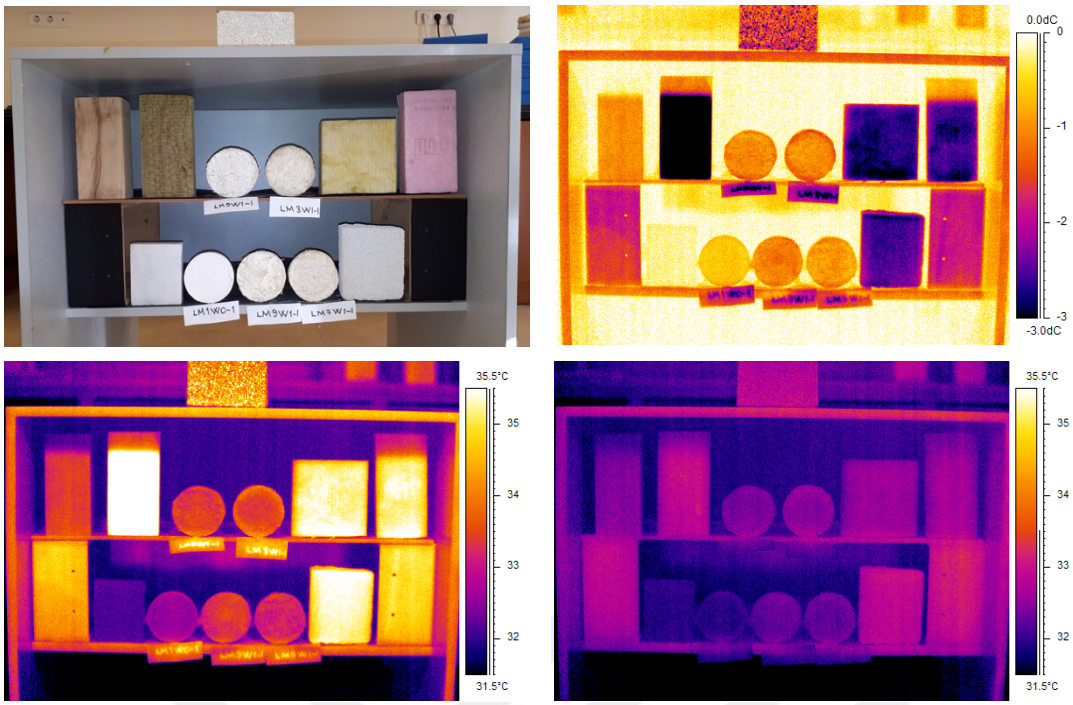


Figure 4.22. View of the straw-mixed lime-pozzolan mortar samples together with marble and wood samples and rock wool, glass wool, expanded polystyrene, autoclaved aerated concrete thermal insulation samples (on the left top), its IR image taken at the ambient conditions of 24.3ºC and 33%RH after the uniform heating with halogen lamp for a period of 218s – initial IR image (on the left bottom); the last IR image of the cooling period when halogen lamps were switched off for a period of 180s (on the right bottom);, and the differential IR image showing the temperature difference between the initial and the last IR images for the cooling period of 180s (on the right top).

4.8. XRD Analyses Results for the Confirmation of Pozzolanic Reaction Products Formation in New Mortar Samples

The XRD analyses were performed on powdered samples to confirm the formation of pozzolanic reaction products within new mortar compositions. Both interior and exterior powders of material samples were analyzed. Determined differences about type and the intensity values of detected minerals are related with the used raw materials, their proportions, and the favored chemical reaction which is either pozzolanic reaction or carbonation reaction. XRD results of newly-produced mortar samples are presented in **Figure 4.23, 4.24, 4.25, 4.26, 4.27, 4.28, 4.29, 4.30, 4.31, 4.32, 4.33, 4.34, 4.35, 4.36, 4.37, 4.38, 4.39, 4.40, 4.41,** and **4.42.**

Portlandite (P) and calcite (C) were detected in the XRD traces in all studied samples. Calcite was formed during the carbonation reaction of $Ca(OH)_2$. Comparison of mineralogical differences between L1W0, sample made from calcium hydroxide, and mortar samples produced with various lime: straw aggregate was used for the confirmation of pozzolanic activity of straw fibers.

- Tobermorite traces were detected in both inner and outer powders of samples prepared without metakaolin; which are L9W1, L7W1, L5W1, and L3W1.
- Tobermorite and calcite peaks often overlap.
- The intensity of the hydration products is directly related to the straw ratio in the mixture since it acts as a silica source.
- Different than amorphous silica existing inside straw fibers, crystalline phase SiO_2 was detected during XRD studies, which is one of the indicators of pozzolanic activity between straw aggregates and lime. Analyses on samples containing high percentages of straw and metakaolin in their mixture prove the formation of quartz.
- Generally, the intensity of tobermorite peaks is higher in inner sections, while calcite peaks are more dominant at the exterior surfaces of materials.
- Quartz traces are more dominant in lime-pozzolan mortars containing straw aggregate than mortar samples prepared without metakaolin.

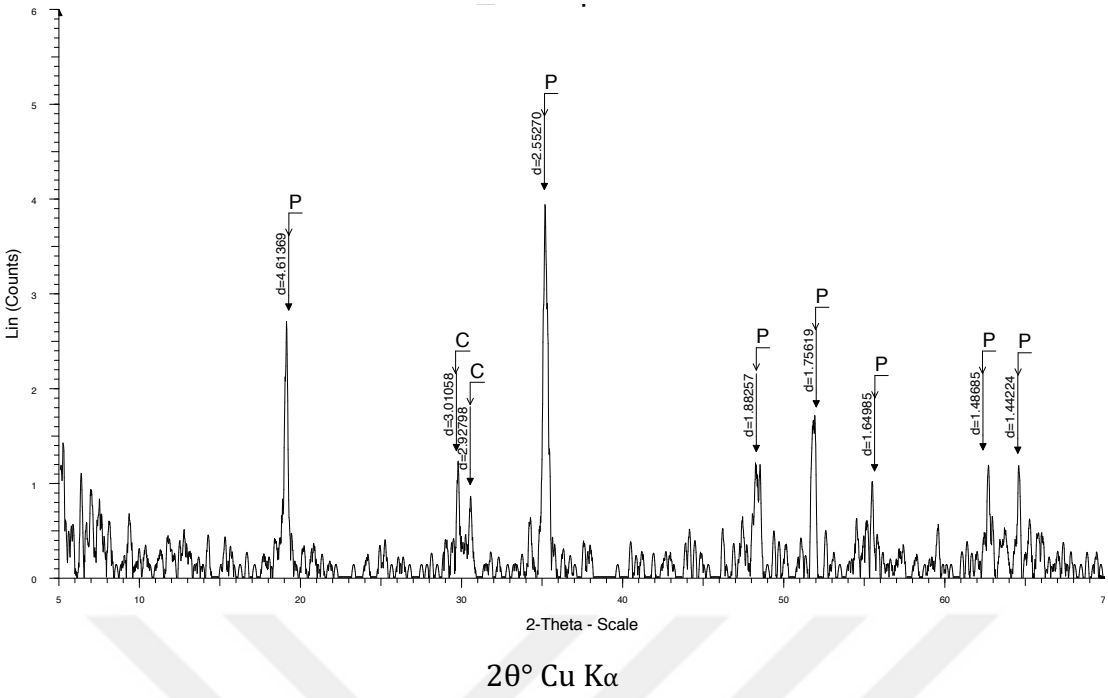


Figure 4.23. XRD traces of L1W0-outer powder (P: Portlandite, C: Calcite)

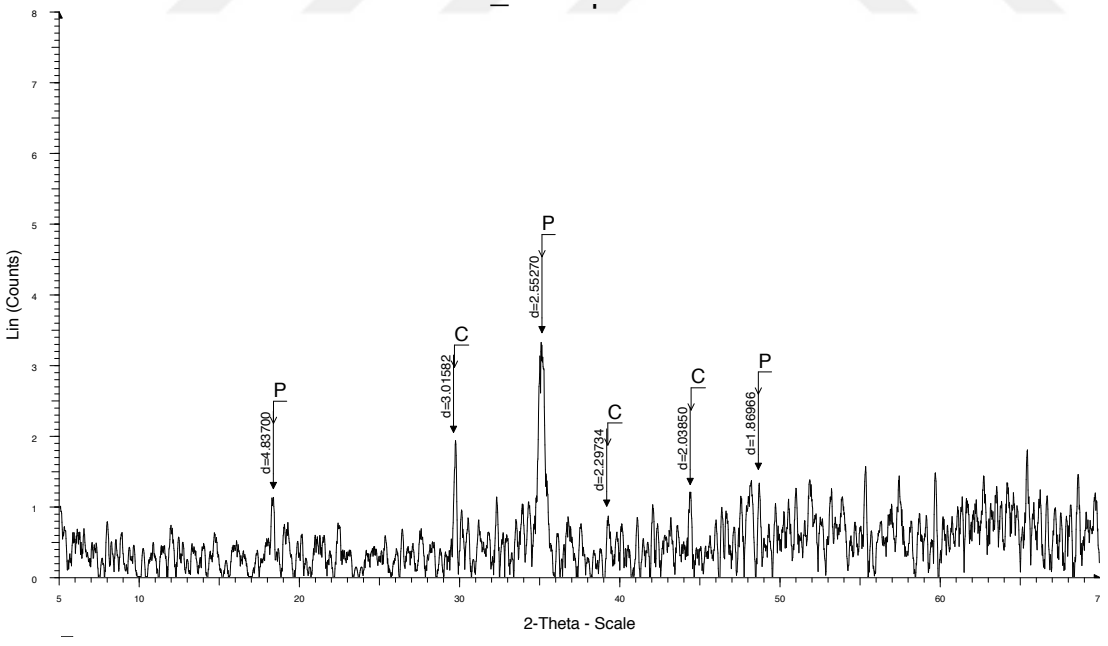


Figure 4.24. XRD traces of L1W0-inner powder (P: Portlandite, C: Calcite)

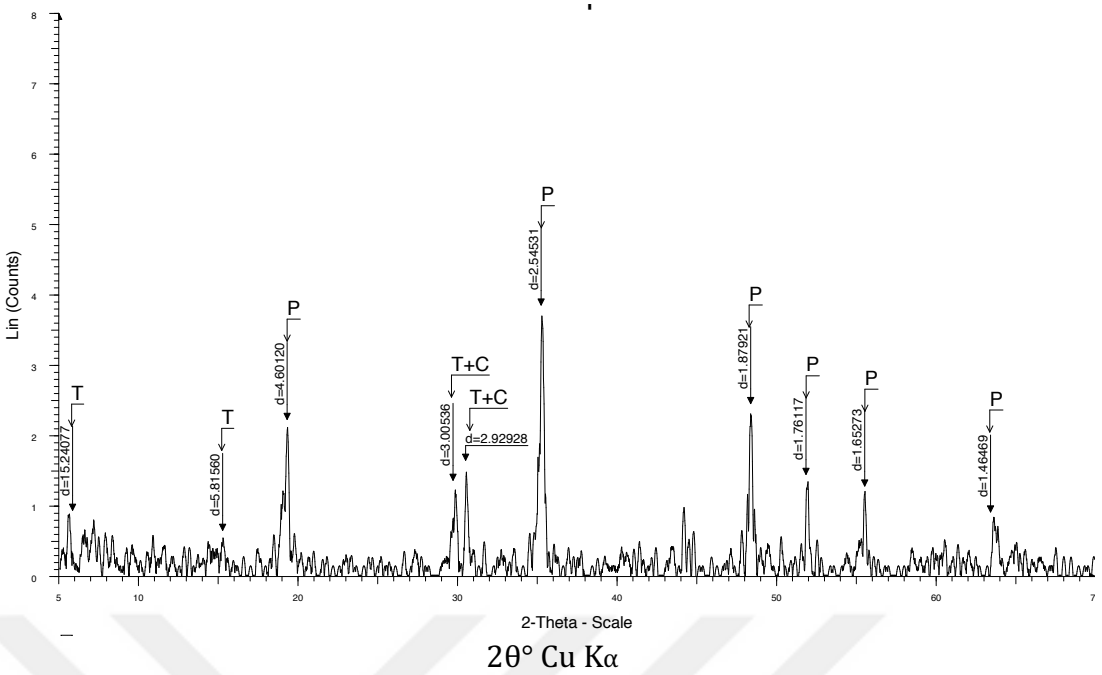


Figure 4.25. XRD traces of L9W1-outer powder (P: Portlandite, C: Calcite, T: Tobermorite)

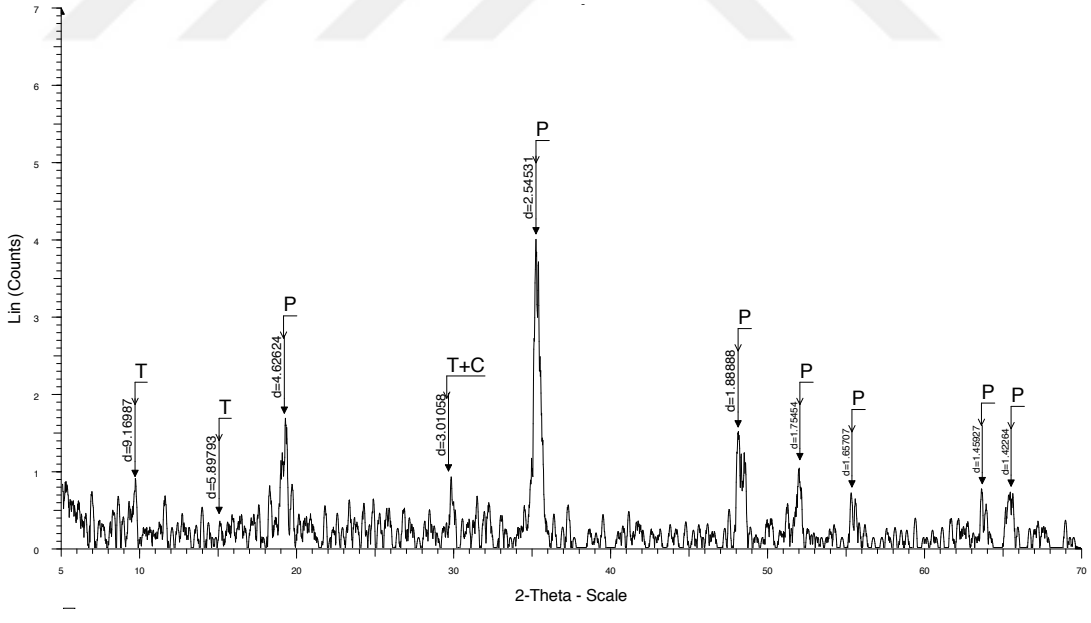
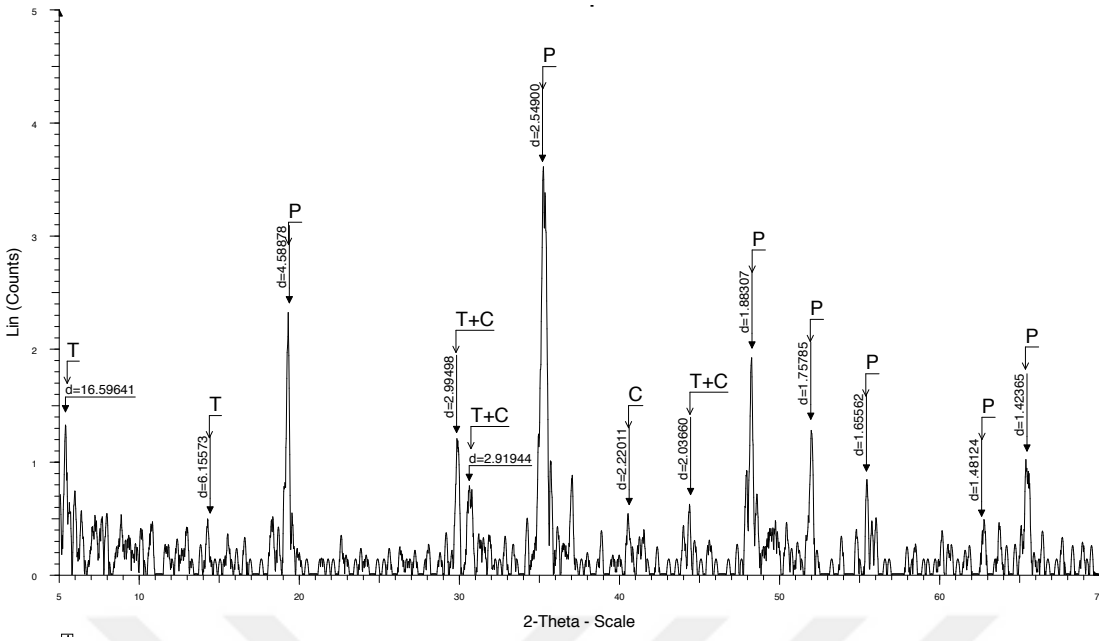
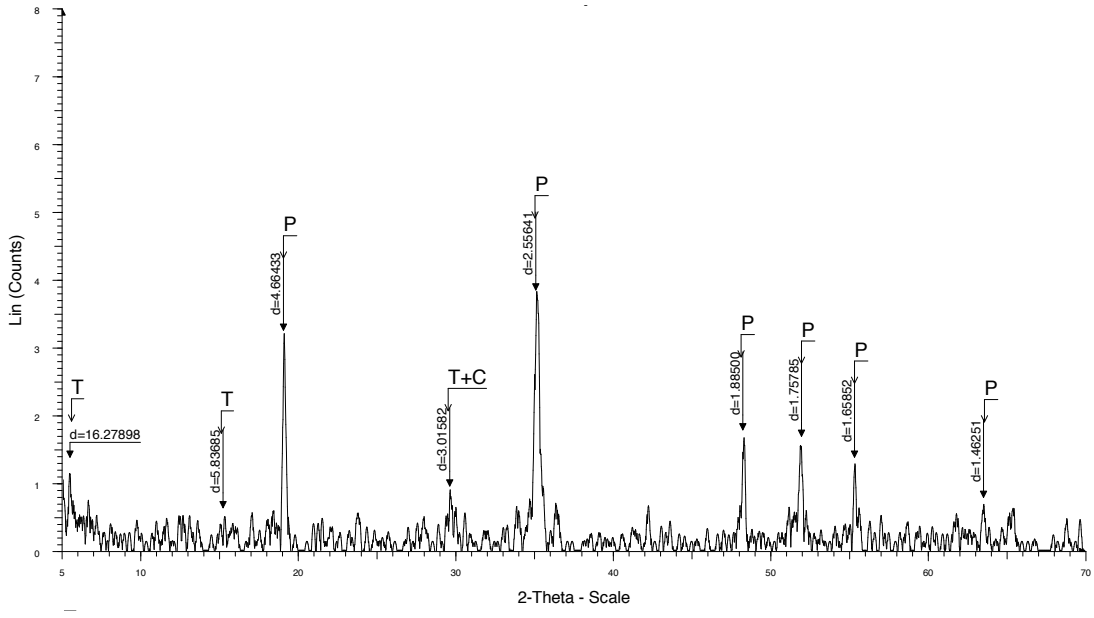


Figure 4.26. XRD traces of L9W1-inner powder (P: Portlandite, C: Calcite, T: Tobermorite)



2θ° Cu Kα

Figure 4.27. XRD traces of L7W1-outer powder (P: Portlandite, C: Calcite, T: Tobermorite)



2θ° Cu Kα

Figure 4.28. XRD traces of L7W1-inner powder (P: Portlandite, C: Calcite, T: Tobermorite)

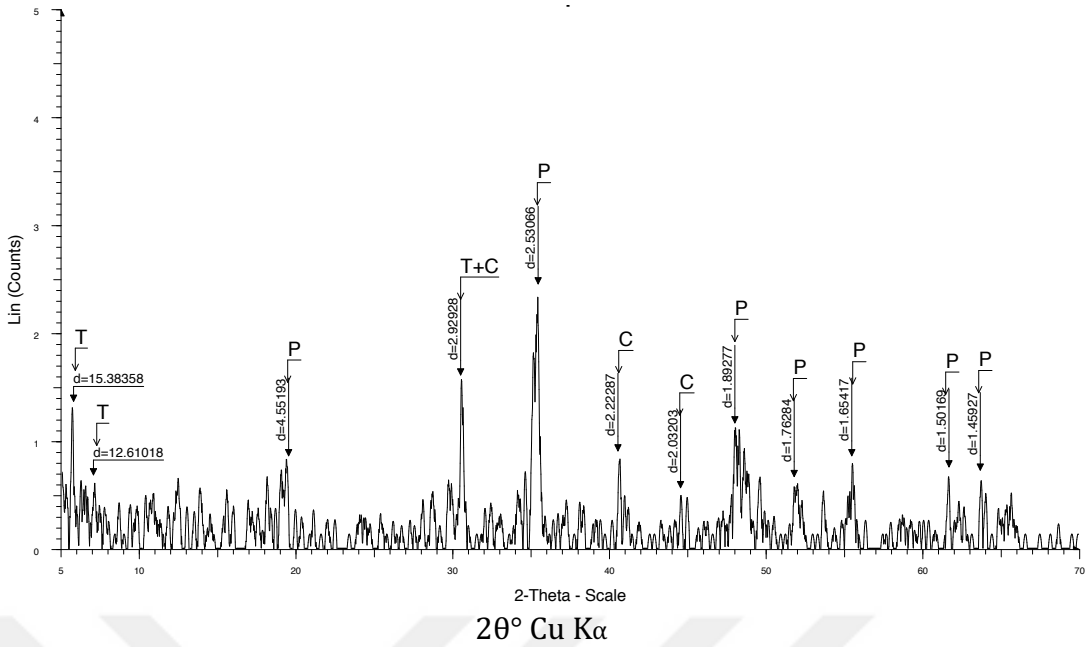


Figure 4.29. XRD traces of L5W1-outer powder (P: Portlandite, C: Calcite, T: Tobermorite)

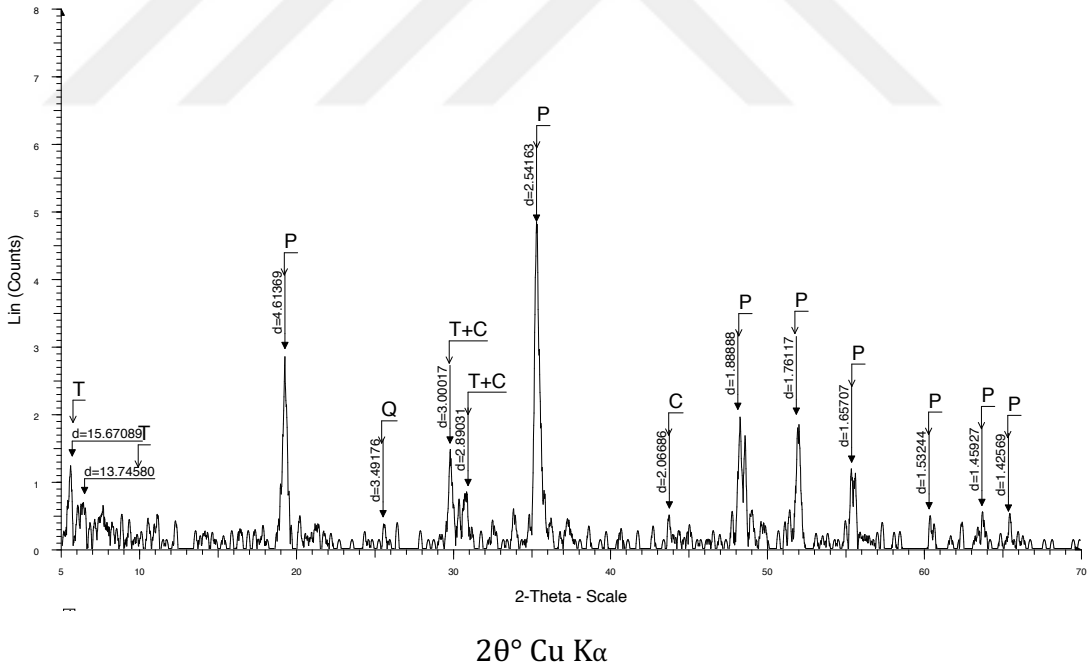


Figure 4.30. XRD traces of L5W1-inner powder (P: Portlandite, C: Calcite, T: Tobermorite, Q: Quartz)

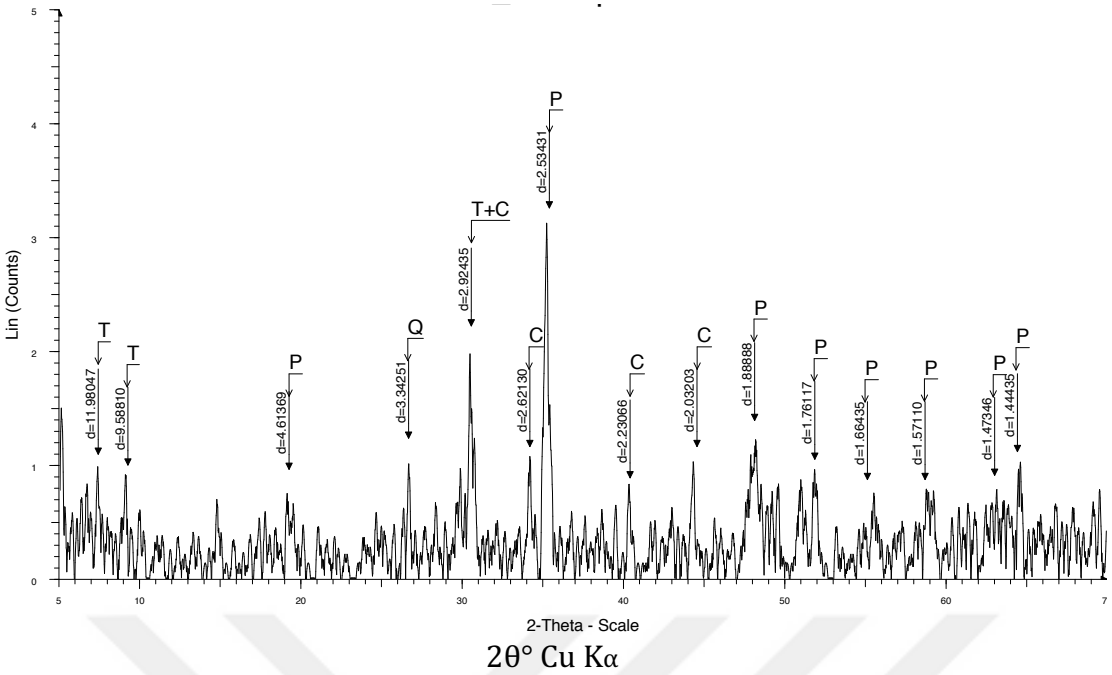


Figure 4.31. XRD traces of L3W1-outer powder (P: Portlandite, C: Calcite, T: Tobermorite, Q: Quartz)

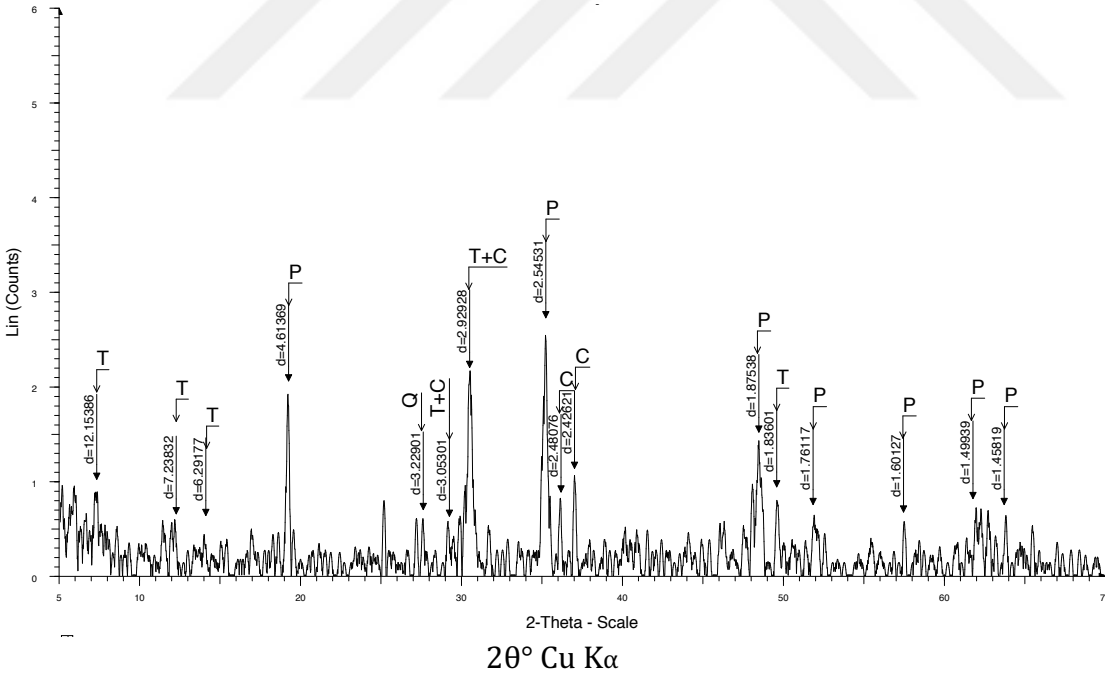


Figure 4.32. XRD traces of L3W1-inner powder (P: Portlandite, C: Calcite, T: Tobermorite, Q: Quartz)

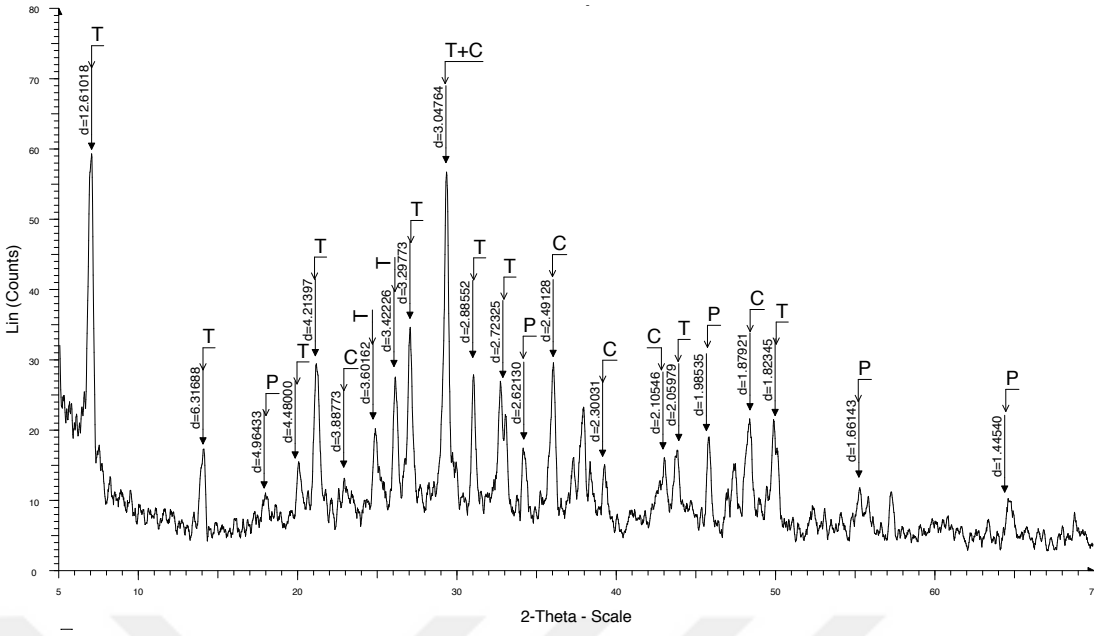


Figure 4.33. XRD traces of LM1W0-outer powder (P: Portlandite, C: Calcite, T: Tobermorite)

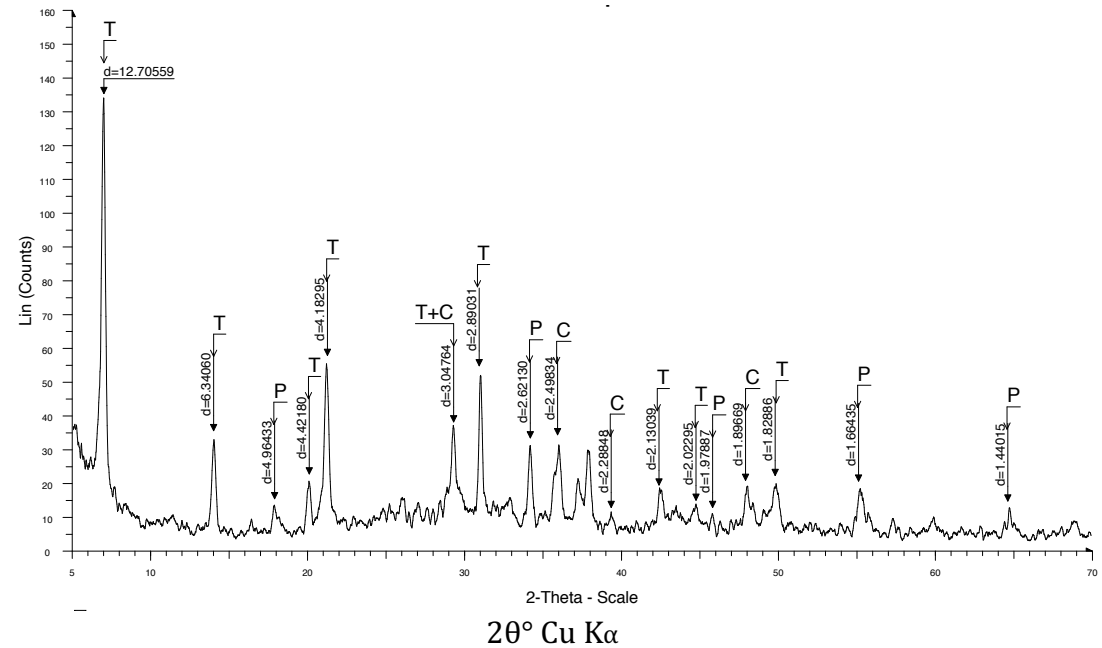


Figure 4.34. XRD traces of LM1W0-inner powder (P: Portlandite, C: Calcite, T: Tobermorite)

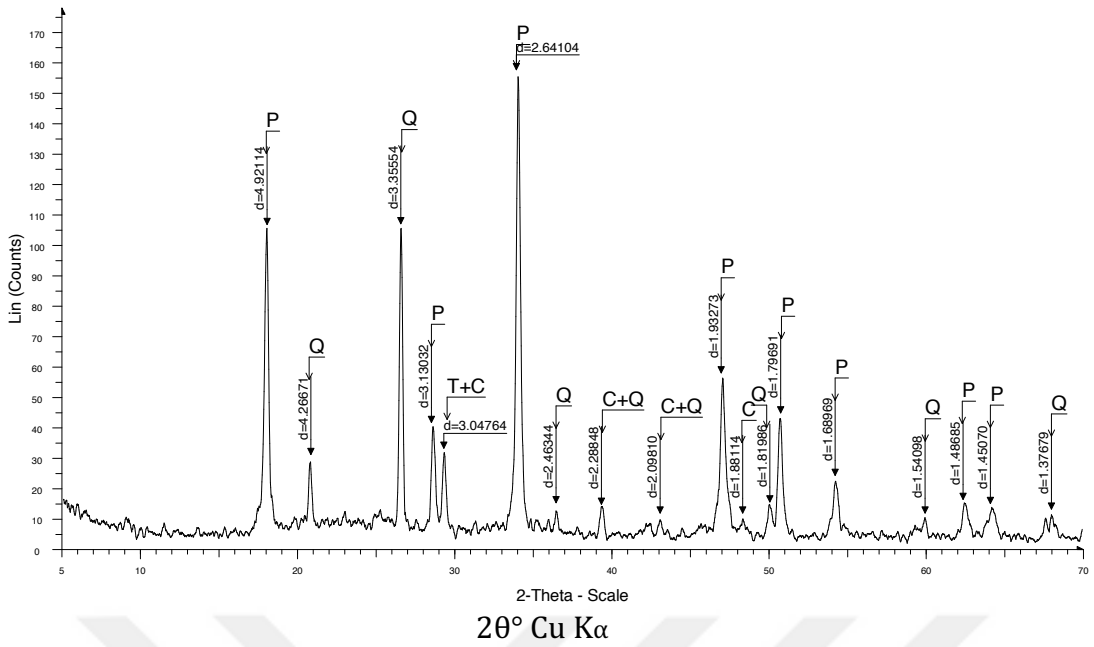


Figure 4.35. XRD traces of LM9W1-outer powder (P: Portlandite, C: Calcite, T: Tobermorite, Q: Quartz)

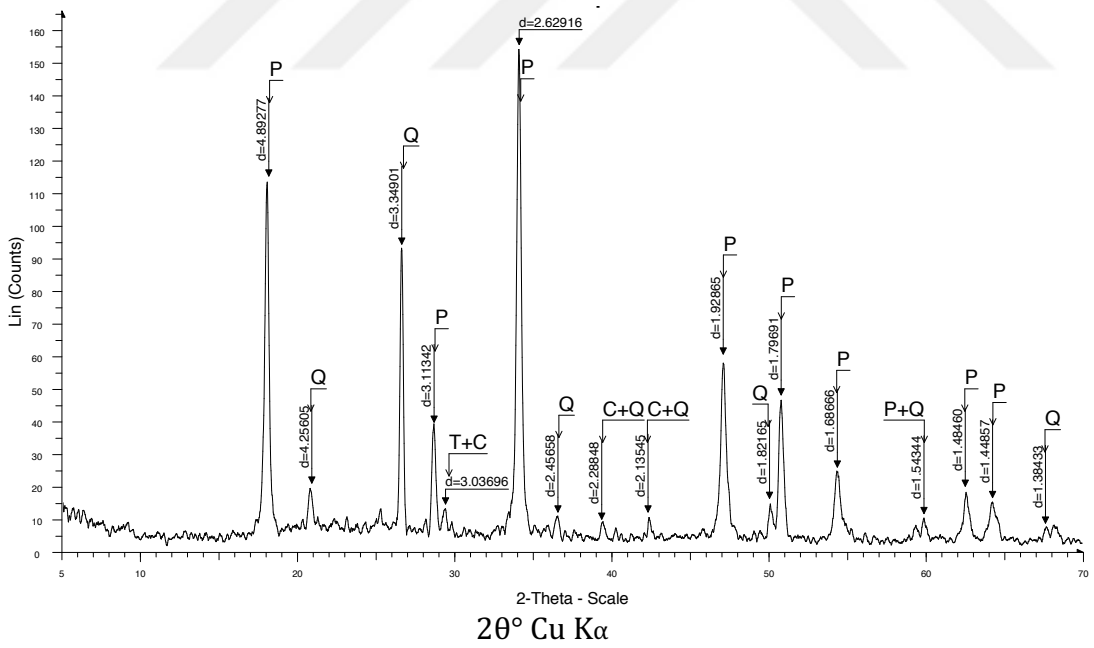


Figure 4.36. XRD traces of LM9W1-inner powder (P: Portlandite, C: Calcite, T: Tobermorite, Q: Quartz)

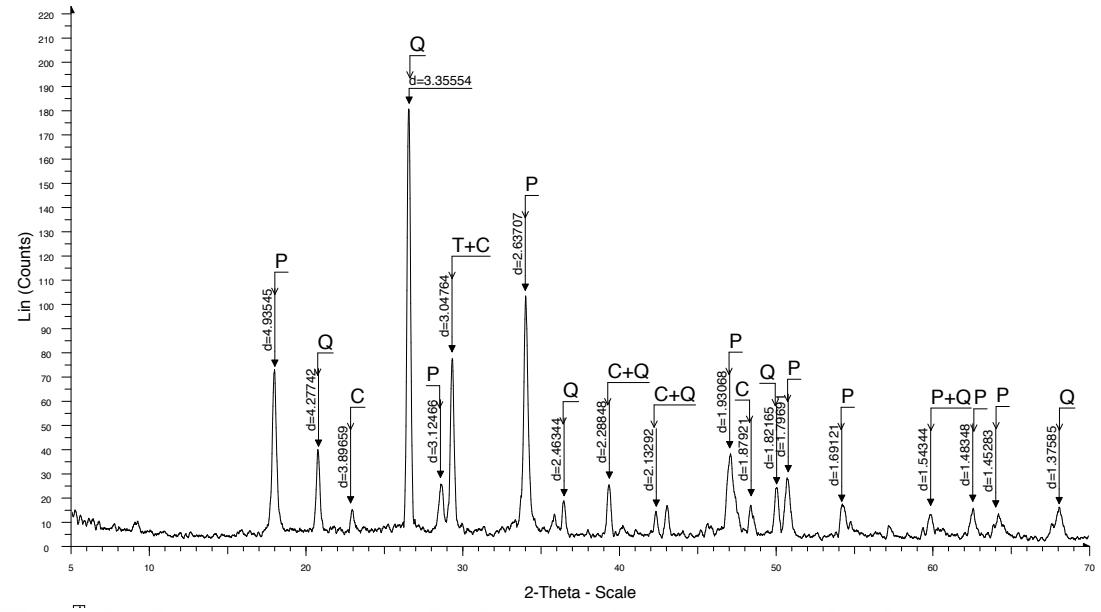


Figure 4.37. XRD traces of LM7W1-outer powder (P: Portlandite, C: Calcite, T: Tobermorite, Q: Quartz)

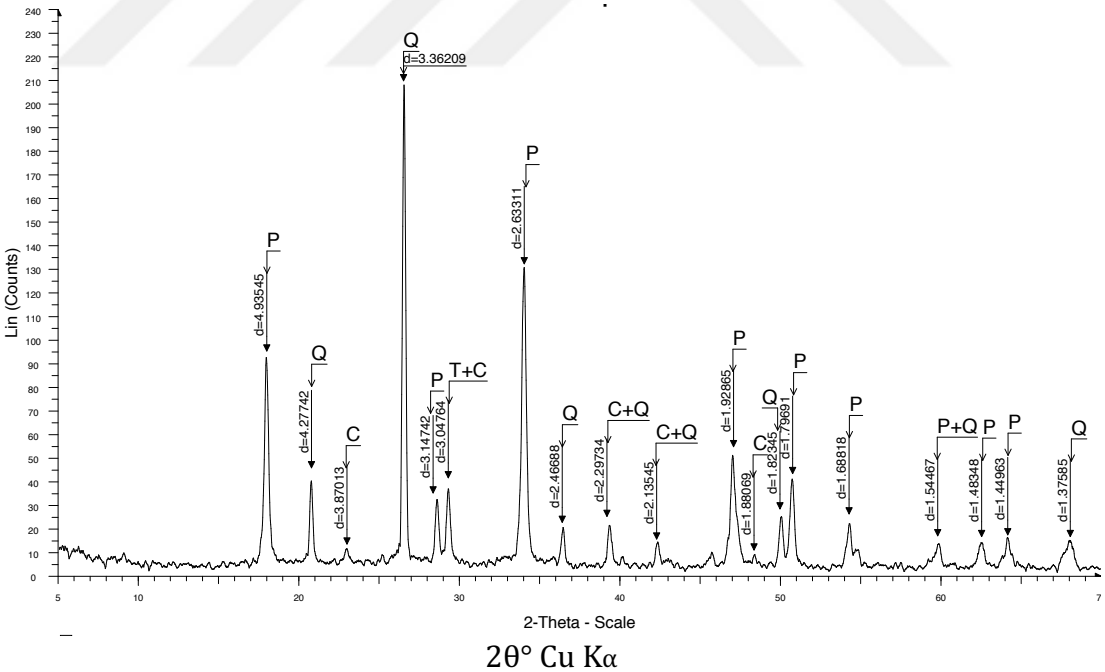


Figure 4.38. XRD traces of LM7W1-inner powder (P: Portlandite, C: Calcite, T: Tobermorite, Q: Quartz)

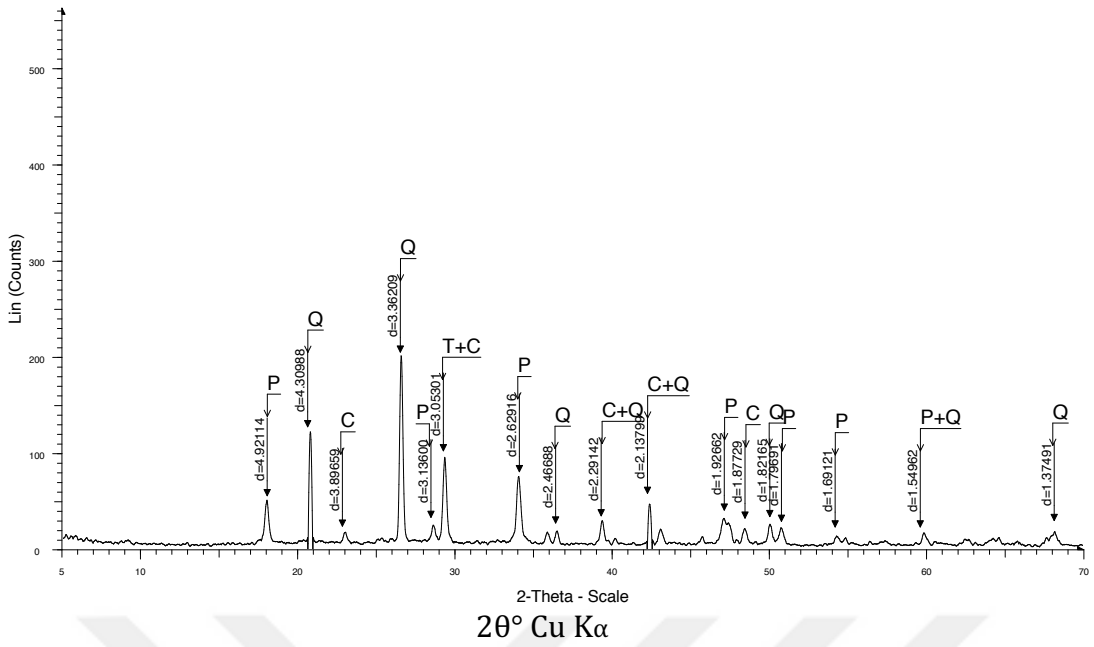


Figure 4.39. XRD traces of LM5W1-outer powder (P: Portlandite, C: Calcite, T: Tobermorite, Q: Quartz)

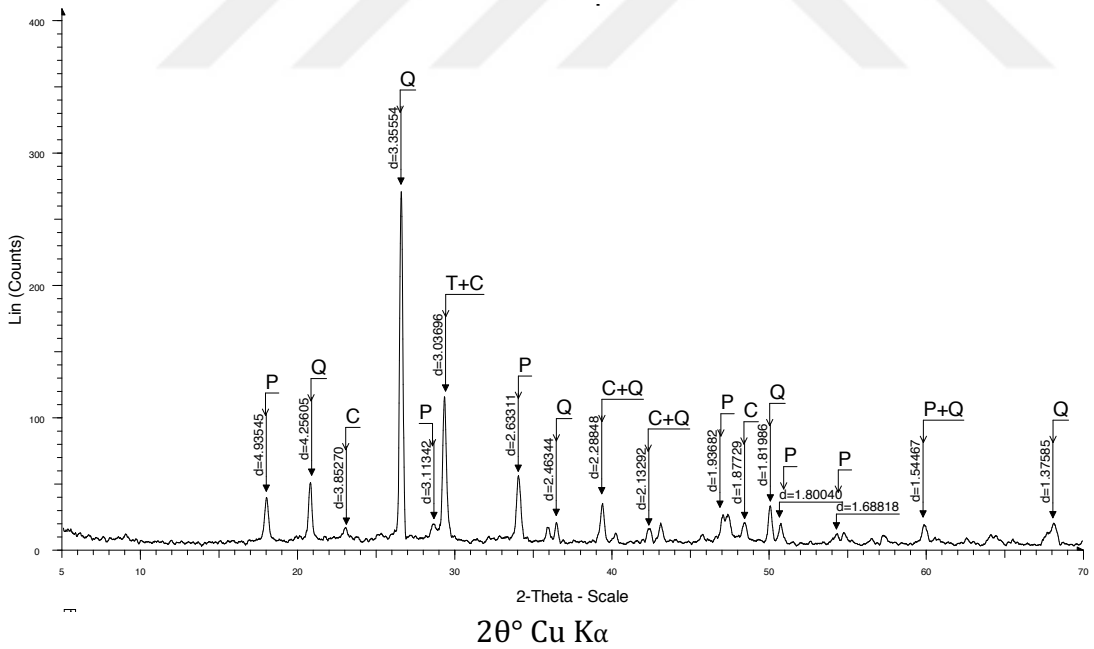


Figure 4.40. XRD traces of LM5W1-inner powder (P: Portlandite, C: Calcite, T: Tobermorite, Q: Quartz)

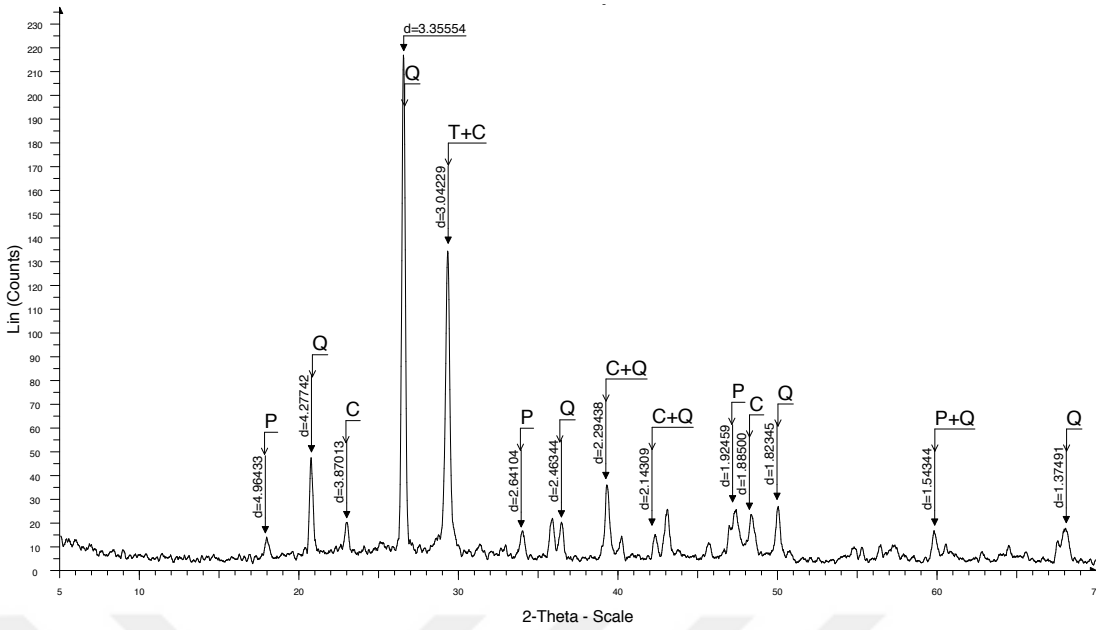


Figure 4.41. XRD traces of LM3W1-outer powder (P: Portlandite, C: Calcite, T: Tobermorite, Q: Quartz)

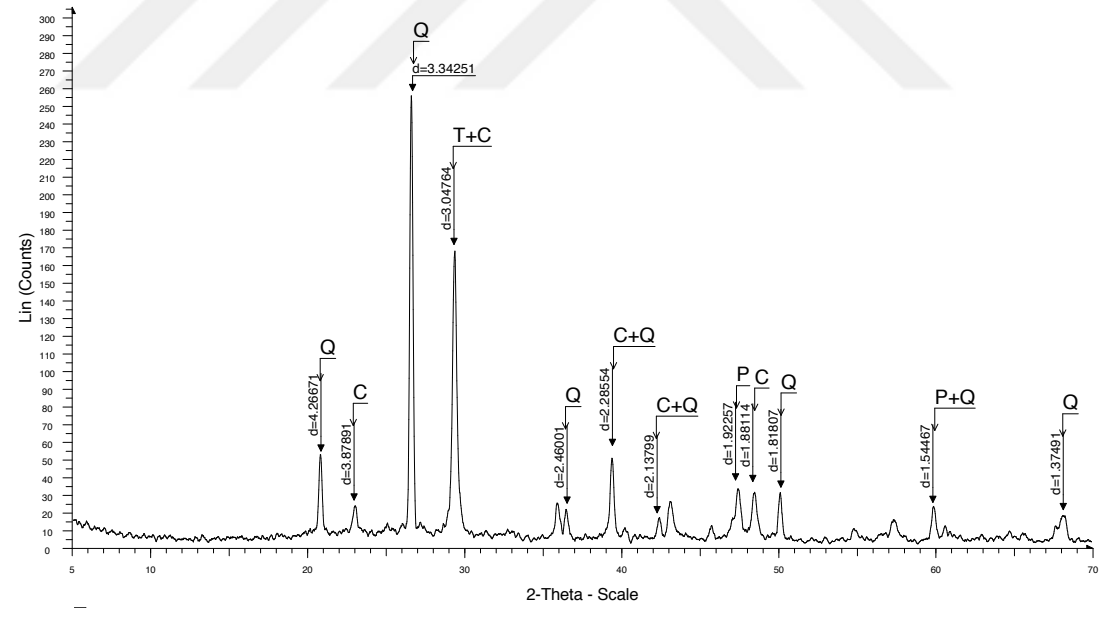


Figure 4.42. XRD traces of LM3W1-inner powder (P: Portlandite, C: Calcite, T: Tobermorite, Q: Quartz)

4.9. Cross-Section Image Analysis of New Mortar Samples

Image analyses were performed on the surfaces as well as cross-sections of new mortar specimens in 7x, 12.5x, and 25x magnification lenses by stereomicroscope to understand microstructures of new mortar samples. Visible pores were examined in terms of their size, shape, and distribution.

- Exterior surface image in 25x magnification and cross-section images in various scales of L1W0 are presented in **Figure 4.43**. Large pores varying in the range of 50 microns and 2000 microns are visible. Pores are often circular.
- Continuous and interconnected irregular-shaped and capillary-shaped pores are seen in the microscopic images of L9W1, L7W1, L5W1, and L3W1 which are presented in **Figure 4.44**, **Figure 4.45**, **Figure 4.46**, and **Figure 4.47**, respectively. Solid parts are in the form of granular deposits. Small grains of solid parts, which stick to the straw fiber surfaces, are visible. Straw fibers form a three-dimensional network within the material sample.
- Irregular-shaped pores are in the range of 0.15 mm and 2 mm, while capillary-pores are in the range of 0.1 mm and 0.3 mm in the L9W1, L7W1, L5W1, and L3W1 (**Figure 4.44, 4.45, 4.46, 4.47**).
- Large and circular pores varying in the range of 0.1 mm and 0.7 mm are visible in the stereomicroscope images of LM1W0 (**Figure 4.48**). Small shrinkage cracks up to 10 mm length and 0.1 mm width are detected which interconnect with large pores.
- Magnified images of straw-mixed lime-pozzolan mortar samples are presented in **Figure 4.49**, **Figure 4.50**, **Figure 4.51**, and **Figure 4.52**. Fibers intertwine with each other in three directions which produces voids. Those voids keep the fibers oriented in all directions altogether. The voids at some parts are filled with the solid matrix while other parts are shaped with fibers. All fibers are partially covered with the powders of the solid matrix. The crumbled form of solid parts is larger in scale with reference to material samples produced without metakaolin.
- There is no order on the distribution of straw fibers as well as pores.

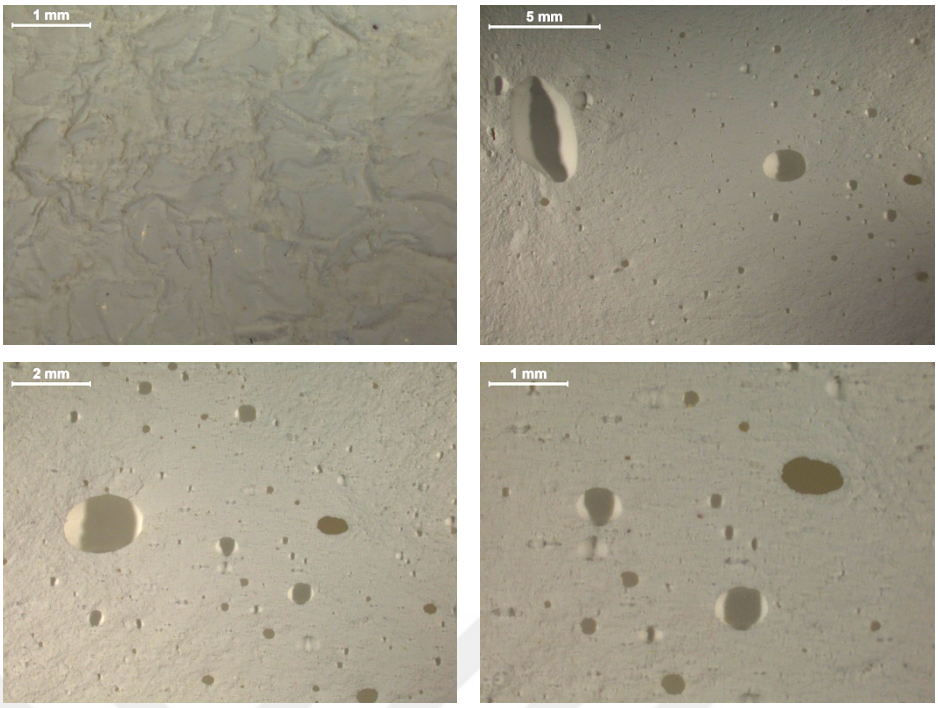


Figure 4.43. Magnified images of L1W0 taken by stereomicroscope (top left: exterior surface with 25x, top right: cross-section image with 7x, bottom left: cross-section image with 12.5x, bottom right: cross-section image with 25x)

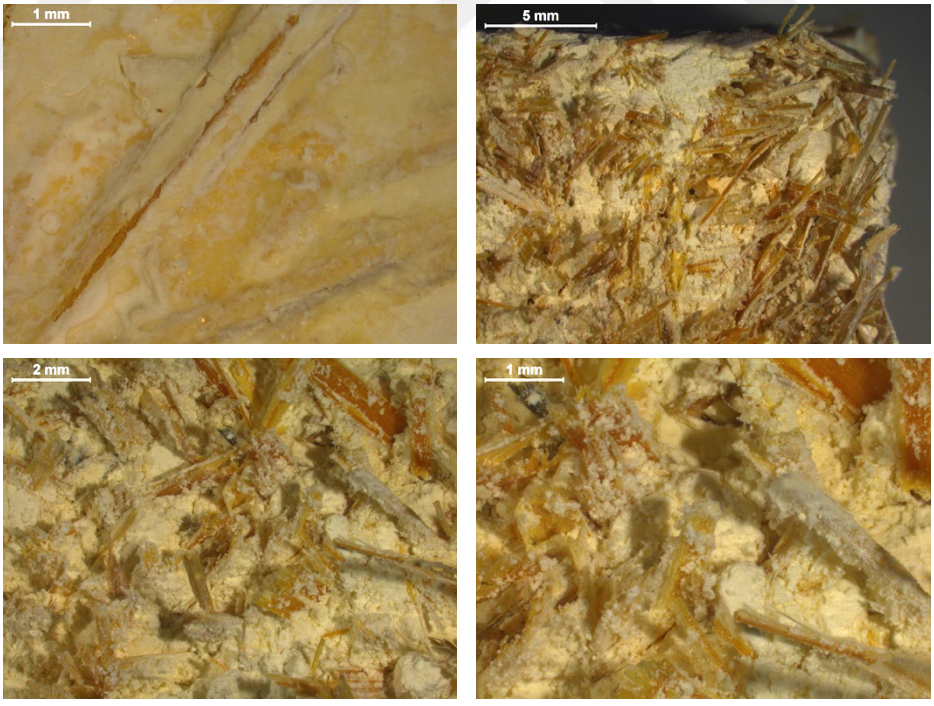


Figure 4.44. Magnified images of L9W1 taken by stereomicroscope (top left: exterior surface with 25x, top right: cross-section image with 7x, bottom left: cross-section image with 12.5x, bottom right: cross-section image with 25x)

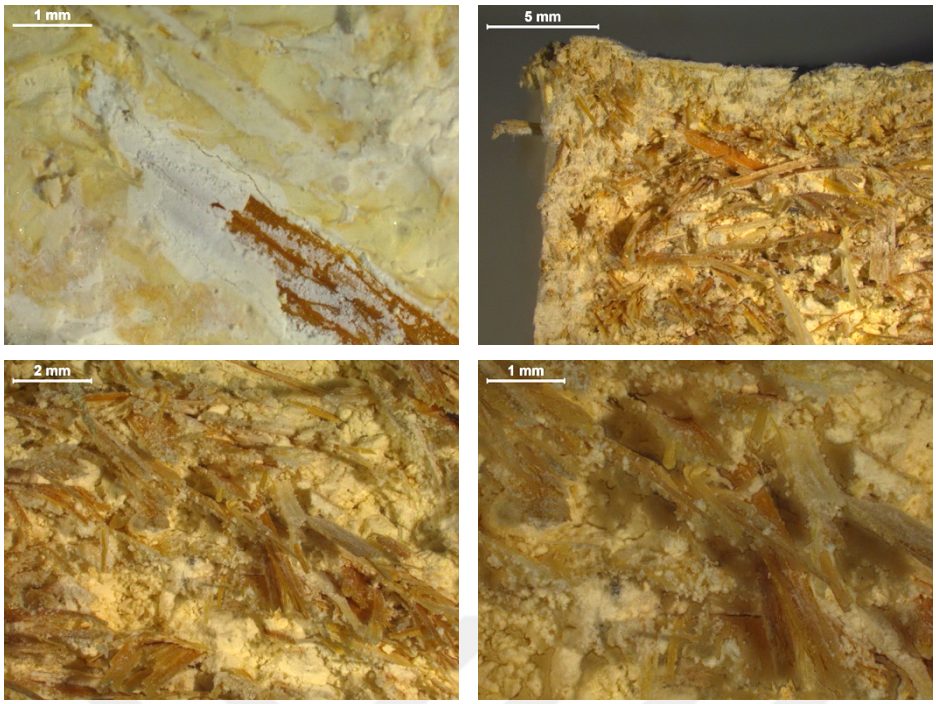


Figure 4.45. Magnified images of L7W1 taken by stereomicroscope (top left: exterior surface with 25x, top right: cross-section image with 7x, bottom left: cross-section image with 12.5x, bottom right: cross-section image with 25x)

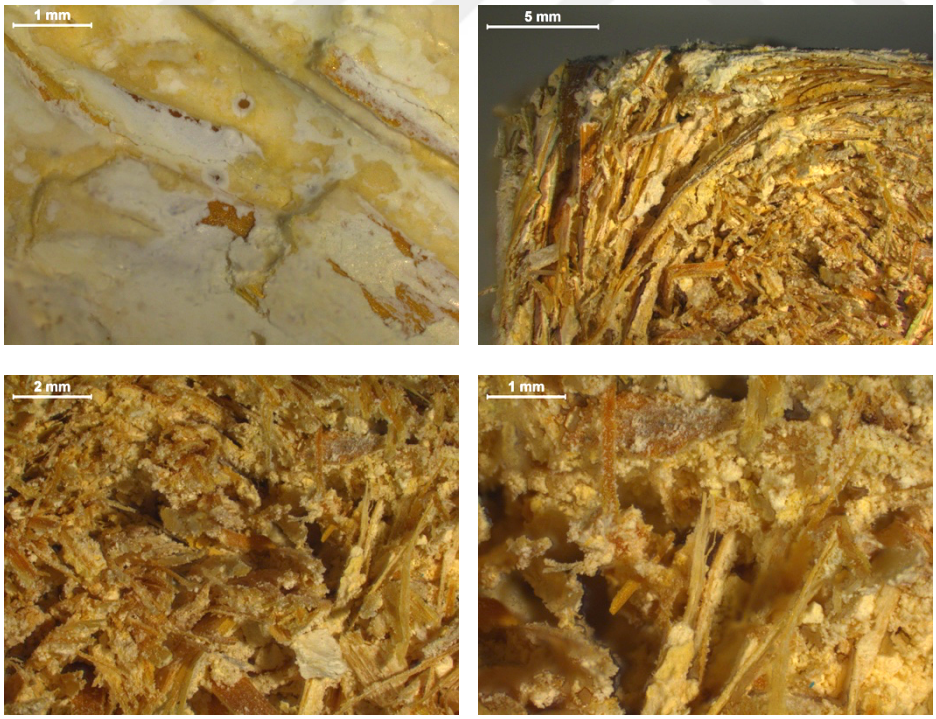


Figure 4.46. Magnified images of L5W1 taken by stereomicroscope (top left: exterior surface with 25x, top right: cross-section image with 7x, bottom left: cross-section image with 12.5x, bottom right: cross-section image with 25x)



Figure 4.47. Magnified images of L3W1 taken by stereomicroscope (top left: exterior surface with 25x, top right: cross-section image with 7x, bottom left: cross-section image with 12.5x, bottom right: cross-section image with 25x)

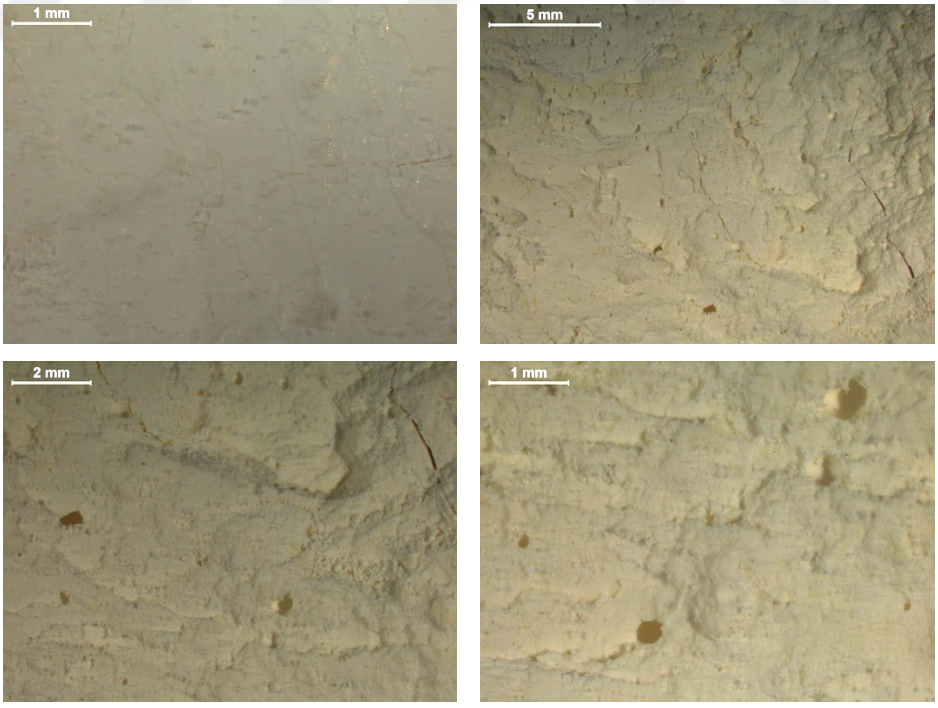


Figure 4.48. Magnified images of LM1W0 taken by stereomicroscope (top left: exterior surface with 25x, top right: cross-section image with 7x, bottom left: cross-section image with 12.5x, bottom right: cross-section image with 25x)

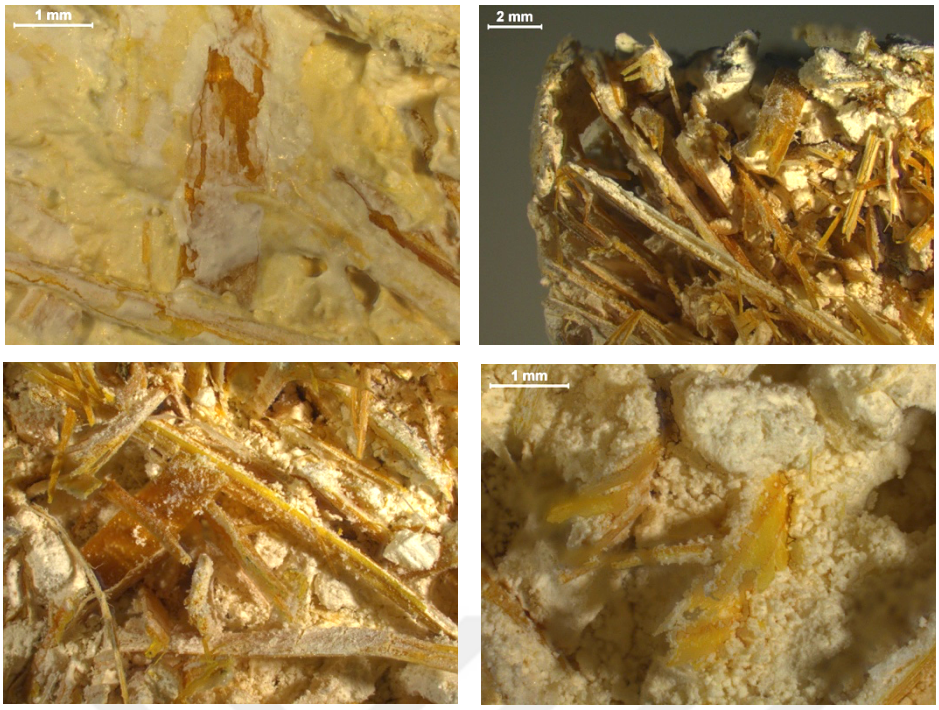


Figure 4.49. Magnified images of LM9W1 taken by stereomicroscope (top left: exterior surface with 25x, top right: cross-section image with 7x, bottom left: cross-section image with 12.5x, bottom right: cross-section image with 25x)

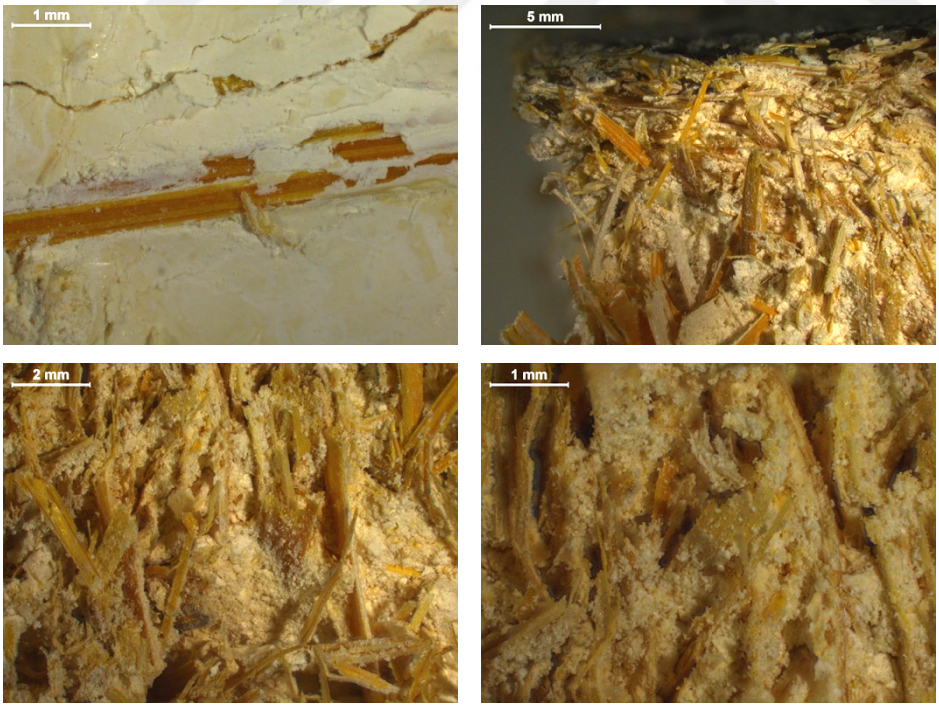


Figure 4.50. Magnified images of LM7W1 taken by stereomicroscope (top left: exterior surface with 25x, top right: cross-section image with 7x, bottom left: cross-section image with 12.5x, bottom right: cross-section image with 25x)

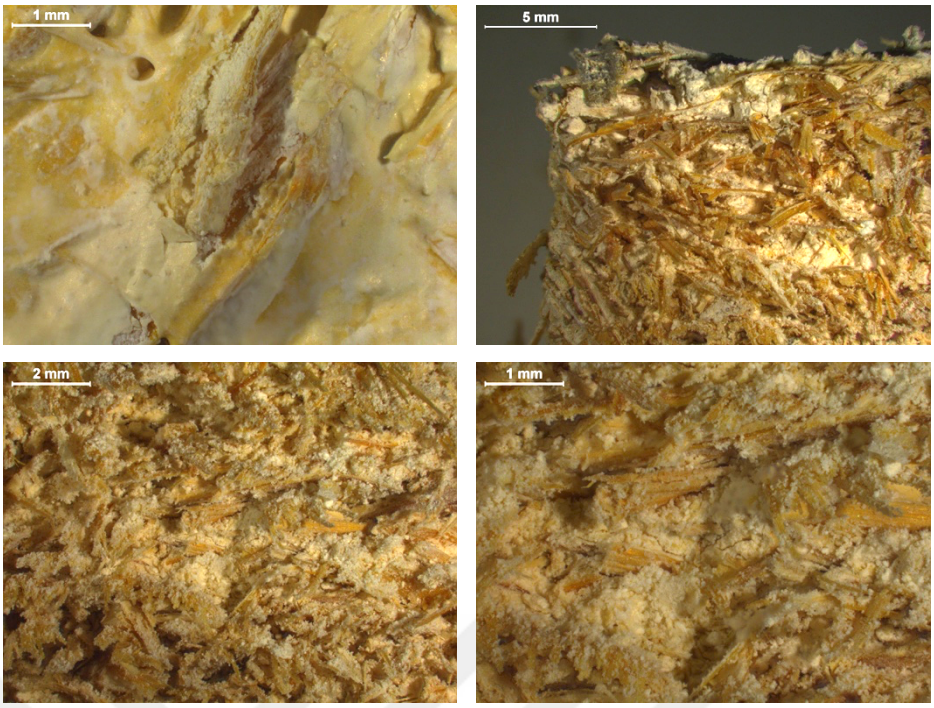


Figure 4.51. Magnified images of LM5W1 taken by stereomicroscope (top left: exterior surface with 25x, top right: cross-section image with 7x, bottom left: cross-section image with 12.5x, bottom right: cross-section image with 25x)

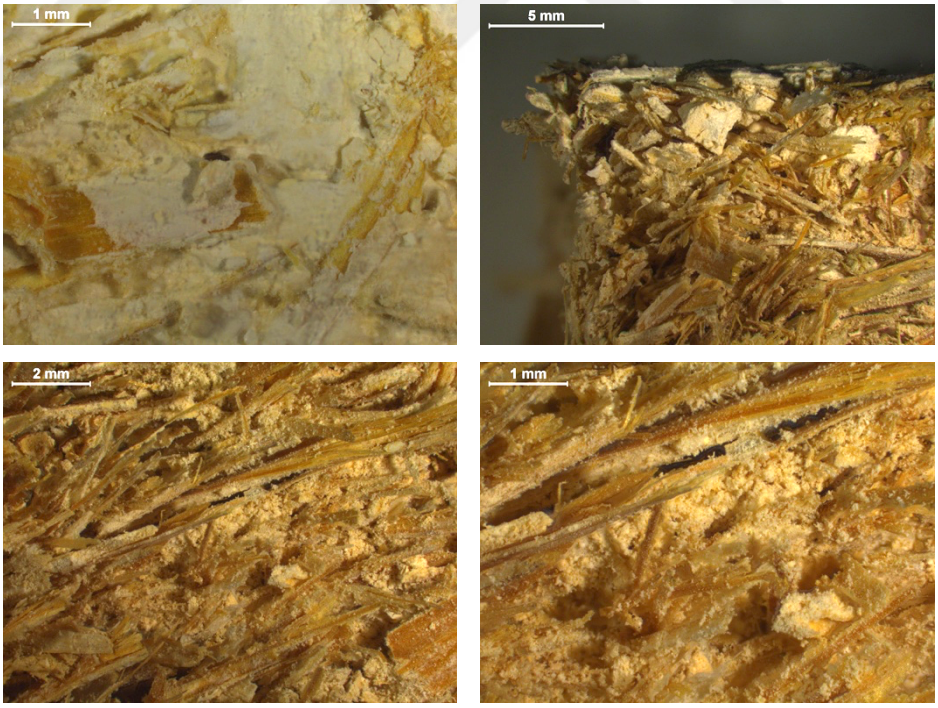


Figure 4.52. Magnified images of LM3W1 taken by stereomicroscope (top left: exterior surface with 25x, top right: cross-section image with 7x, bottom left: cross-section image with 12.5x, bottom right: cross-section image with 25x)

CHAPTER 5

DISCUSSION

In this section, the results obtained from the laboratory analyses are interpreted together to discuss potentials and limitations of newly-produced mortar samples for their possible use as building materials, to evaluate overall performance characteristics of straw-mixed lime-pozzolan mortars in comparison with commonly-used thermal and sound insulation materials, and to assess individual and combined contribution of straw aggregate and metakaolin on performance properties of new mortar samples.

5.1. Potentials and Limitations of Newly-Produced Mortar Samples to be Used as Construction Materials

The physical, physicomechanical, mechanical, acoustical, and thermal performances, as well as mineralogical and microstructural properties of newly-produced mortar samples, are evaluated in terms of their potentials and limitations.

The physical properties of all straw-mixed LW and LMW mortar samples show that those samples are highly-porous, lightweight, and highly water vapor permeable. Their effective porosity, bulk density, and water vapor diffusion resistance index vary in the ranges of 70–80% by volume, 0.42–0.68 g/cm^3, and 1.2–1.7, respectively (**Table 5.1.**). The concluded remarks on their physical properties can be summarized as follow:

— Among those samples, only the ones, which have the highest content of straw (L3W1 and LM3W1) with 3:1 binder to straw ratio, perform as the most lightweight and porous mortar samples reaching to the bulk density of 0.42 g/cm^3 and effective porosity of 80%. The same samples exhibit the lowest thermal conductivity and highest sound absorption coefficient, which correspond with the highest porous nature. Such a very-highly porous nature resulting in good thermal and acoustical characteristics is one of the potentials of those newly-produced materials.

— The water vapor permeability characteristics in terms of the equivalent air thickness of water vapor permeability (SD), water vapor diffusion resistance index (μ-value) and water vapor transmission rate (RT) data show that all straw-mixed mortar samples are highly-breathable. The μ-value is a unitless parameter showing vapor tightness of material and indicates how many times greater the resistance a material layer to vapor transmission is, compared to a static layer of air of the same thickness (ISO 12572:2016). The μ-value of the static air layer is accepted as 1.0 in the standards. The μ-value data show that the resistance to water vapor permeation of all straw-mixed samples is at most 1.7 times greater than the air layer. Such a very-highly water vapor permeation performance is one of the potentials of those newly-produced materials.
— Due to high levels of water absorption capacity, being in the range of 103% - 190% by weight, newly-produced materials require protection against getting washed/wet by precipitation or water exposure. Their highly water absorptive nature is one of the weaknesses of straw-mixed mortar samples. To strengthen those materials against water-exposed conditions, their exposed surfaces have to be protected with a less water-absorptive finishing layer. That protective plaster/coat, if being in direct contact with the backing straw-mixed mortars, is expected to be compatible with their physical and physicomechanical properties. This means that any protective layer should be lime-based, highly-breathable, porous, and pozzolanic to achieve good adherence and continuity in water-vapor permeation.

The physicomechanical and mechanical properties of all straw-mixed LM and LMW mortar samples show that the newly-produced mortar samples have low strength properties (**Table 5.1.**). The ultrasonic pulse velocity (UPV) data obtained from the straw-mixed mortars exhibit various ranges show that newly-produced mortars with straw aggregate have a heterogeneous nature. Those materials are compressible at a certain rate, and a slight compression was observed to enhance its physicomechanical properties. The strength tests present that even the most fibrous samples have compressive and flexural strength performances in certain amounts. The ultrasonic pulse velocity ($UPV_{W/PRESS}$) and modulus of elasticity ($MoE_{W/PRESS}$) of those samples, except L3W1, vary in the ranges of 490-663 m/s, 94-275 MPa, respectively.

The flexural strength and compressive strength of all straw-mixed samples vary in the ranges of 281-547 kPa and 257-491 kPa, respectively. The concluded remarks on their physicomechanical and mechanical properties can be summarized as follow:

— The sample L3W1 is the weakest sample in terms of physicomechanical properties since it was not possible to obtain any transit time data during measurements. On the other hand, the sample LM3W1 in which there is lime binder half in the amount and addition of metakaolin exhibited a certain physicomechanical strength. Both samples have the highest porosity characteristics with the potentials of higher thermal resistivity and sound absorption performances. However, the LM3W1 sample is stiffer than the L3W1 sample. Such stiffer and very-highly porous nature is one of the potentials of the LM3W1 sample in comparison to the L3W1 sample.

— The L3W1 sample has the highest uniaxial compressive strength and flexural strength among all straw-mixed mortar samples while it has the poorest physicomechanical properties. In comparison to the L3W1, the sample LM7W1, having a similar amount of binder and additional metakaolin additive, presents compressive and flexural strength close to the L3W1 sample with stiffer nature. Considering the overall physicomechanical and mechanical features of straw-mixed lime-based mortars, the performance of the LM7W1 samples is the strongest.

— The micro views obtained from the image analyses of cross-sections show the weakness in integration between straw fibers and lime-pozzolan binder. The considerable reduction in physicomechanical and mechanical properties in straw-mixed samples might be attributed to the low integration between bio-aggregate and binder. Therefore, further studies are needed to find out more effective mixing techniques for the preparation of straw-mixed lime-based samples to benefit more from pozzolanic characteristics of straw and to achieve higher strength at those highly-porous and highly-fibrous samples.

— In spite of its lower binder content and higher porosity, the sample LM1W0 has compressive strength two times higher than the L1W0 sample and has similar ultrasonic pulse velocity with the L1W0. The good physicomechanical and mechanical performances of lime-pozzolan mixed straw-free mortar signals that those types of mortars can be used as protective layers supporting the straw-mixed ones acting as insulation infill layers.

Table 5.1. Physical, physicomechanical, and mechanical properties of newly-produced straw-mixed lime-pozzolan mortar samples

Sample	Bulk Density ρ, g/cm³	Porosity φ, % by volume	Water Absorption Coefficient θ, % by weight	Water Vapor Diffusion Resistance Index μ, unitless	$UPV_{w/PRESS}$ m/s	$MoE_{w/PRESS}$ MPa	Flexural Strength σf, kPa	Compressive Strength σc, kPa
L1W0	1.13 ± 0.01	51.60 ± 1.47	45.57 ± 1.66	2.79 ± 0.18	1470 ± 193	2294 ± 624	1383 ± 23	2204 ± 187
L9W1	0.68 ± 0.01	69.56 ± 0.07	103.05 ± 2.14	1.39 ± 0.02	663 ± 54	275 ± 47	281 ± 36	341 ± 30
L7W1	0.62 ± 0.01	70.92 ± 0.06	113.50 ± 2.27	1.67 ± 0.02	593 ± 53	204 ± 35	405 ± 71	404 ± 60
L5W1	0.63 ± 0.03	72.03 ± 1.43	114.13 ± 7.08	1.63 ± 0.00	609 ± 78	206 ± 46	354 ± 0	295 ± 36
L3W1	0.49 ± 0.03	77.09 ± 1.19	158.34 ± 11.33	1.51 ± 0.05	N.A.	N.A.	547 ± 189	472 ± 96
LM1W0	0.79 ± 0.04	60.71 ± 3.83	77.13 ± 8.34	3.50 ± 0.08	1380 ± 93	1417 ± 128	N.A	5326 ± 619
LM9W1	0.55 ± 0.00	74.71 ± 0.78	135.22 ± 2.59	1.33 ± 0.09	553 ± 64	147 ± 36	313 ± 15	257 ± 58
LM7W1	0.63 ± 0.01	72.72 ± 0.46	115.92 ± 2.60	1.40 ± 0.05	528 ± 38	161 ± 57	416 ± 132	491 ± 62
LM5W1	0.53 ± 0.02	75.77 ± 0.12	144.14 ± 4.86	1.39 ± 0.15	522 ± 31	132 ± 18	409 ± 24	343 ± 70
LM3W1	0.42 ± 0.01	80.02 ± 1.06	190.80 ± 2.88	1.23 ± 0.02	490 ± 51	94 ± 20	368 ± 19	252 ± 19

The studied acoustic properties of all straw-mixed LW and LMW mortar samples show that they have variable sound absorption characteristics. Their noise reduction coefficient (NRC) and weighted sound absorption coefficient (αw) values vary in the ranges of 0.16–0.46 and 0.16–0.40, respectively (**Table 5.2.**). The concluded remarks on their acoustical properties can be summarized as follow:

- Under 125 Hz, all studied newly-produced mortar samples are sound reflective since the sound absorption coefficient (α) values at specific frequencies are lower than 0.1.
- For mid-frequencies (500 Hz and 1000 Hz), average sound absorption coefficients (α_{mid}) of straw-mixed LW and LMW mortar samples are in the range of 0.21-0.57.
- For high-frequencies (2000 Hz and 4000 Hz), average sound absorption coefficients (α_{high}) of straw-mixed LW and LMW mortar samples are in the range of 0.12-0.55.
- The average NRC values of straw-mixed LW and LMW samples are 0.31 and 0.19, respectively.
- The average αw values of straw-mixed LW and LMW samples are 0.34 and 0.23, respectively.
- The sample L1W0, which is the reference sample without straw aggregate and metakaolin, have lower NRC and αw values than the other straw-mixed lime-based (LW) mortar samples. The NRC and αw values of the sample L1W0 are 0.24 and 0.15, respectively.
- The sample LM1W0, which is the reference sample without straw aggregate and with metakaolin, have lower NRC and αw values than the other straw-mixed lime-pozzolan (LMW) mortar samples. The NRC and αw values of the sample LM1W0 are 0.10 and 0.17, accordingly.
- For 500 Hz, 1000 Hz, 2000 Hz, and 4000 Hz, newly-produced mortar sample L3W1 has the highest sound absorption coefficient values, which are 0.39, 0.76, 0.60, and 0.51, respectively. L3W1 has the highest NRC and αw values, which are 0.46 and 0.40, respectively.
- Newly-produced straw-mixed lime-based (LW) mortar samples have higher NRC and αw values than straw-mixed lime-pozzolan (LMW) mortar samples.

The thermal conductivity properties of all straw-mixed LW and LMW mortar samples show that those samples have low thermal conductivity values which are in the range of 0.0608 W/mK and 0.1202 W/mK (**Table 5.2.**). The concluded remarks on their thermal properties can be summarized as follow:

- The average thermal conductivity value of all straw-mixed lime-based mortar samples (LW) is 0.0988 W/mK. Among those mortars, the sample L3W1 has the lowest thermal conductivity value of 0.0810. The average thermal conductivity value of all straw-mixed lime-pozzolan mortar samples (LMW) is 0.0718 W/mK. Straw-mixed lime-pozzolan mortars (LMW) have higher thermal resistivity properties than straw-mixed lime-based mortar samples (LW).
- Among those mortars, the sample LM3W1 has the lowest thermal conductivity value of 0.0608. This sample also has the lowest bulk density and highest effective porosity values of 0.42 g/cm^3 and 80% by volume, respectively. The increase in the effective porosity is inversely proportional to thermal conductivity values. The only disagreement is in LM9W1 and LM7W1 since the density value of the latter is higher.
- The thermal conductivity value of LM1W0 is 0.1773 W/mK, which is the highest among all studied mortar samples.
- According to infrared thermography studies, the thermal inertia properties of straw-mixed lime mortars (LW) and straw-mixed lime-pozzolan mortars (LMW) exhibit similar characteristics with the wood sample. All newly-produced straw-mixed mortar samples (LW and LMW) have higher thermal inertia properties than commonly-used thermal insulation materials studied during IR analyses (rock wool, glass wool, EPS, and AAC insulation block). All materials studied during the IR thermography, heat faster and cools slower.

The mineralogical and microstructural properties of all straw-mixed LW and LMW mortar samples show that the existence of tobermorite traces, hydration reaction products, is the evidence of pozzolanic reaction between raw materials used during the production of newly-produced mortar samples. The data achieved is summarized below:

— X-ray diffraction (XRD) analyses were conducted to confirm the pozzolanic reaction. Especially pozzolanic reactivity of straw fibers was questioned. Specifically, tobermorite traces were searched in the new mortar samples produced without metakaolin (LW). Obtained results prove that straw fibers act as a silica source and reacts with $Ca(OH)_2$. As a result, hydration products having cementitious properties are formed.

— XRD traces of mortar samples produced without metakaolin are supported by the pozzolanic activity measurements performed with the saturated lime method on powdered straw samples. Naturally occurring amorphous silica inside plant tissues exhibit similar characteristics with opal-a, which is a highly-reactive form. During the pozzolanic reactions, amorphous silica was transformed into crystalline phase silica. The formation of SiO_2 is an indication of pozzolanic activity. The intensity of the tobermorite peaks is closely related to the percentage of pozzolanic additives inside material compositions.

— Cross-section image analyses employed on straw-mixed lime-pozzolan mortars show that continuous and irregular-shaped pores and capillary-shaped shrinkage cracks varying in different scales are visible. Straw fibers form a three-dimensional network inside material samples, and this formation produced voids around straw fibers. Solid parts are in the form of granular deposits; for material samples produced with metakaolin, they are larger in scale.

Table 5.2. NRC, αw, α_{mid}, α_{high}, and λ values of straw-mixed lime-pozzolan mortar samples

Sample	**NRC unitless**	**αw unitless**	**α_{mid} (500 Hz-1000 Hz) unitless**	**α_{high} (2000 Hz-4000 Hz) unitless**	**λ W/mK**
L1W0	0.17	0.22	0.24	0.15	N.A.
L9W1	0.22	0.29	0.26	0.22	0.12
L7W1	0.28	0.33	0.35	0.26	0.11
L5W1	0.28	0.34	0.34	0.29	0.08
L3W1	0.46	0.40	0.57	0.55	0.08
LM1W0	0.11	0.16	0.10	0.17	0.18
LM9W1	0.16	0.18	0.21	0.12	0.08
LM7W1	0.16	0.22	0.21	0.13	0.07
LM5W1	0.24	0.28	0.28	0.23	0.07
LM3W1	0.20	0.25	0.21	0.23	0.06

5.2. Performance Evaluation of Newly-Produced Mortar Samples in Comparison to Some Commonly-Used Thermal and Sound Insulation Materials

Newly-produced straw-mixed lime-pozzolan mortars exhibit different thermal and sound absorption characteristics among each other. A comparison between new mortar samples and some commonly-used conventional and alternative insulation materials was studied. Researched conventional insulation materials are rock wool, glass wool, polyurethane foam, EPS foam, and XPS foam. The thermal and sound absorption performance of alternative materials were also searched in the literature which are cellulose insulation, corkboard, wood fiber insulation, hemp mat, kenaf boards, flax mat, and sheep wool mat (**Table 5.3**, **Table 5.4**).

All new mortar samples have higher densities than studied conventional and alternative material samples. Except for L3W1, straw-mixed lime-based mortars (LW) and straw-mixed lime-pozzolan mortars (LMW) generally have lower sound absorption coefficients and NRC values than conventional and alternative materials (**Table 5.3**).

At 500 Hz, L3W1 has a higher sound absorption coefficient than XPS foam and wood fiber insulation. Considering the thickness of the mortar test specimen (18 cm), it may exhibit better characteristics than sheep wool mat (60 cm) and corkboard (50 cm) at this specific frequency. At 1000 Hz, L3W1 has a higher sound absorption coefficient than XPS foam, cellulose insulation, corkboard, hemp mat, wood fiber insulation, kenaf board, and sheep wool mat. L3W1 may exhibit similar characteristics with rock wool, glass wool, EPS foam, and flax mat if the comparison is performed with the same thickness value for each material sample. At 2000 Hz, L3W1 has a higher sound absorption coefficient than XPS foam, cellulose insulation, corkboard, hemp mat, and flax mat. L3W1 has a similar absorption performance with EPS foam and kenaf boards. L3W1 has higher noise reduction coefficient (NRC) values than XPS foam and corkboard for the studied thickness ranges. L3W1 has a resembling performance with EPS foam, wood fiber insulation, kenaf board, and sheep wool mat.

Table 5.3. Sound absorption coefficient and NRC values of straw-mixed lime-pozzolan mortar samples of this study and commonly-used conventional and alternative insulation materials

Sample	Thickness *(d)* mm	Density *(ρ)* kg/m^3	Sound Absorption Coefficient, (α) Frequency				
			250 Hz	500 Hz	1000 Hz	2000 Hz	NRC
Conventional Materials*							
Rock Wool	50	80	0.30	0.50	0.80	0.90	0.64
Glass Wool	50	50	0.50	0.50	0.80	0.90	0.68
Polyurethane Foam	50	30	0.30	0.70	0.90	0.80	0.67
EPS Foam	50	28	0.20	0.40	0.80	0.65	0.5
XPS Foam	50	25	0.15	0.25	0.40	0.50	0.33
Alternative Materials*							
Cellulose Insulation	50	28	0.60	0.90	0.75	0.55	0.70
Corkboard	50	105	0.15	0.40	0.60	0.40	0.41
Wood Fiber Insulation	25	n.a.	0.15	0.30	0.75	0.95	0.55
Hemp Mat	40	40	0.60	0.60	0.55	0.50	0.57
Kenaf Boards	50	20	0.39	0.52	0.58	0.62	0.53
Flax Mat	35	43	0.65	0.84	0.80	0.55	0.71
Sheep Wool Mat	60	25	0.21	0.40	0.65	0.82	0.52
New Mortar Samples							
L1W0	20	1130	0.04	0.17	0.31	0.17	0.17
L9W1	18	680	0.11	0.19	0.33	0.26	0.22
L7W1	19	620	0.12	0.28	0.42	0.30	0.28
L5W1	17	630	0.12	0.28	0.41	0.32	0.28
L3W1	18	490	0.10	0.39	0.76	0.60	0.46
LM1W0	24	790	0.02	0.06	0.15	0.20	0.11
LM9W1	18	550	0.08	0.14	0.28	0.12	0.16
LM7W1	19	630	0.11	0.22	0.20	0.13	0.16
LM5W1	19	530	0.15	0.20	0.36	0.25	0.24
LM3W1	17	420	0.13	0.15	0.28	0.24	0.20

*Sound Absorption coefficients, NRC values, and thicknesses were found in the literature. (Pedroso *et al*., 2017; Euchora, 2003; Heraklith, 2015).

The thermal conductivity *(λ)*, specific heat capacity (*c*), and thermal diffusivity (*D)* data of some conventional and alternative insulation materials, and newly-produced mortar samples are presented in **Table 5.4**. Investigated conventional insulation materials are rock wool, glass wool, polyurethane foam, EPS foam, XPS foam, cellulose insulation, corkboard, wood fiber insulation, hemp mat, kenaf boards, flax mat, and sheep wool mat. Varying with the density values, common conventional and alternative insulation materials have lower thermal conductivity, lower specific heat, and higher thermal diffusivity values than newly-produced straw-mixed lime-pozzolan mortar samples.

Thermal conductivity of LM3W1 is lower than some flax mats having higher densities. Thermal conductivity of LM3W1 exhibits similar characteristics with some hemp mats having higher densities. Specific heat values of new mortar samples are 5 to 20 times higher than studied common insulation materials. Thermal diffusivity values of new mortar samples are generally lower than studied common insulation materials. The closest relationship of diffusivity between new mortar samples and studied materials are with wood fiber insulation.

According to the obtained results and findings of the literature, straw-mixed lime-pozzolan mortars (LMW) have compatible thermal conductivity values with the alternative insulation materials which are available in the market. Both thermal diffusivity and infrared thermography (IR) results show that thermal inertia characteristics of all newly-produced mortar samples are higher than common insulation products.

Table 5.4. Thermal conductivity, specific heat, and thermal diffusivity values of straw-mixed lime-pozzolan mortar samples of this study and commonly-used conventional and alternative insulation materials

Sample	**Density *(ρ)*, kg/m^3**	**Thermal Conductivity *(λ)*, W/mK**	**Specific Heat *(c)*, kJ/kg K**	**Thermal Diffusivity *(D)*, m^2/s**
Conventional Materials*				
Rock Wool	40-200	0.033-0.040	0.8-1.0	1.25E^{-6} / 2.00E^{-7}
Glass Wool	15-75	0.031-0.037	0.9-1.0	2.30E^{-6} / 4.93E^{-7}
Polyurethane Foam	15-45	0.022-0.040	1.3-1.5	1.13E^{-6} / 5.93E^{-7}
EPS Foam	15-35	0.031-0.037	1.3	1.59E^{-6}/ 8.13E^{-7}
XPS Foam	32-40	0.032-0.037	1.5-1.7	6.67E^{-7} / 5.44E^{-7}
Alternative Materials*				
Cellulose Insulation	30-80	0.037-0.042	1.3-1.6	9.49E^{-7} / 3.28E^{-7}
Cork Board	110-170	0.037-0.050	1.5-1.7	2.24E^{-7} / 1.73E^{-7}
Wood Fiber Insulation	50-270	0.038-0.050	1.9-2.1	4.00E^{-7} / 8.82E^{-8}
Hemp Mat	20-90	0.038-0.060	1.6-1.7	1.19E^{-6} / 3.92E^{-7}
Kenaf Boards	30-180	0.034-0.043	1.6-1.7	7.08E^{-7} / 1.41E^{-7}
Flax Mat	20-100	0.038-0.075	1.4-1.6	1.36E^{-6} / 4.69 E^{-7}
Sheep Wool Mat	10-25	0.038-0.054	1.3-1.7	2.92E^{-6} / 1.27 E^{-6}
New Mortar Samples				
L1W0	1130	N.A.	5.16±0.03	N.A.
L9W1	680	0.1202	5.34±0.97	3.33E^{-8}
L7W1	620	0.1097	6.70±0.44	2.62E^{-8}
L5W1	630	0.0843	3.06±0.04	4.35E^{-8}
L3W1	490	0.0810	12.82±0.27	1.29E^{-8}
LM1W0	790	0.1773	8.22± 0.06	2.73E^{-8}
LM9W1	550	0.0796	5.97±1.13	2.41E^{-8}
LM7W1	630	0.0738	12.02±0.14	9.78E^{-9}
LM5W1	530	0.073	14.92±0.01	9.30E^{-9}
LM3W1	420	0.0608	20.27±2.60	7.14E^{-9}

* Thermal conductivity, specific heat and density values of the conventional and alternative materials were found in the literature. Thermal diffusivity values were calculated with respect to the literature data presented in this table. (Schiavoni *et al.*, 2016).

5.3. Impact of Straw Aggregate and Metakaolin Additive on Performance Properties of Newly-Produced Mortar Samples

Compared to the straw-free reference samples, the straw aggregate in all straw-mixed mortar samples, having a various binder to straw ratio, was observed to noticeably-decrease their bulk density and to noticeably-increase their effective porosity. Among the binder: straw ratios varying in the range of 9:1 to 3:1, the 3:1 binder: straw ratio has the largest impact on physical properties. The lowest bulk density and thermal conductivity, and the highest porosity and sound absorption characteristics were achieved at the straw mixed samples with the binder: straw ratio of 3:1. The main target is to achieve the most porous, the lowest thermal conductive, the highest sound absorptive mortar which has enough strength. Therefore, the focus was given here to the evaluation of the L3W1 and the LM3W1 samples.

When two samples of L3W1 and LM3W1 are compared with each other, the sample L3W1 is weaker than the sample LM3W1 in terms of physicomechanical properties since it was not possible to obtain any transit time data during measurements. The sample LM3W1 has metakaolin content as a pozzolanic additive in its mixture. Although the LM3W1 sample has the lime content half in the amount in comparison to the sample L3W1, it is stiffer than the L3W1 sample due to the presence of metakaolin in its mixture. That signals the contribution of pozzolanic additive to the physicomechanical properties of the mortar product. In short, the addition of metakaolin, even reducing binder half in the amount, was observed to increase the stiffness of the mortar.

When thermal conductivity and sound absorption performances of L3W1 and LM3W1 samples are compared with each other, the sample L3W1 has better sound absorption than LM3W1, while being more thermal conductive than the sample LM3W1. In brief, the sample L3W1 (with αw value of 0.40) has a higher sound absorption than the sample LM3W1 (with αw value of 0.25) while the sample L3W1 (with λ value of 0.08) has lower thermal resistance than the sample LM3W1 (with λ value of 0.06) (**Table 5.2**).

When two straw-free reference samples of L1W0 and LM1W0 are compared with each other, the sample L1W0 has lower compressive strength than the sample LM1W0 (**Table 5.1**). The LM1W0 sample has metakaolin content as a pozzolanic additive in its mixture. Although the LM1W0 sample has the lime content in half the amount in comparison to the sample L1W0, its compressive strength is two times higher than the L1W0 sample. That result supports that metakaolin as the pozzolanic additive contributes to the mechanical strength of the mortar product.

When water vapor transmission rate and water absorption characteristics of two straw-free reference samples are compared with each other, the sample LM1W0 has slower water vapor transmission than the sample L1W0 (as much as half of it), although its water absorption capacity in immersed conditions is almost twice of the water absorption capacity of L1W0 sample. That behavior, in other words, performing higher resistance to water vapor permeation while still having high water absorption capacity, signals that water impermeability performance of very porous and water absorptive mortars can be improved by encouraging the formation of pozzolanic products during the setting of mortar mixture.

The combined interpretation of performance properties and strength characteristics of lime-based straw mixed mortar samples with and without metakaolin additive show that the L3W1 and LM3W1 samples have low but still enough flexural and compressive strength (**Table 5.1**). The results highlight the sample LM3W1 as stiffer, more thermal resistive material than the sample L3W1 and while highlight the sample L3W1 as more sound absorptive and less stiff than the sample LM3W1.

Since stiffness and strength characteristics are crucial for building materials, further analyses can be performed to prepare lime-based straw-mixed pozzolanic mixtures with a higher content of straw for the development of more thermal resistive and sound absorptive materials coated with protective and breathable plasters having higher water impermeability. Preparation techniques for the mixing process need to be developed for benefitting more from the pozzolanic behavior of straw in direct contact with pure lime under high relative humidity and CO_2 exposure conditions.

CHAPTER 6

CONCLUSION

This study concerns the production of new straw-mixed lime-pozzolan materials for thermal and sound insulation purposes. Lime-based mortars with pozzolanic additives were used throughout history for several purposes and some of those materials are still durable and functioning. Inspired by traditional construction technology, new material sample compositions were formulated. The materials studied in this study are:

- A historical lime-based exterior plaster sample from Kemer Village, Manisa-Turkey, and
- Newly-produced straw-mixed lime-based mortar samples with or without pozzolanic additive.

Several laboratory analyses were conducted to reveal the physical, physicomechanical, compositional, mineralogical, and microstructural properties of the traditional sample. Obtained results formed a guideline for the production of new material samples. Materials are formulated with various lime: pozzolan: straw fiber ratios within two groups. The pre-determined binder to straw fiber ratios were kept identical in each group to observe the effect of metakaolin. The first group of materials were prepared without metakaolin. In the second group, the ratio of lime over metakaolin was 1:1, which is kept constant. Control samples without any aggregate were produced for each group to understand the combined and individual effects of straw fibers and metakaolin. Physical, physicomechanical, mechanical, acoustical, thermal, mineralogical, and microstructural properties of those material samples were revealed via laboratory analyses. Moreover, the pozzolanic activity of straw fibers was another area of interest which was confirmed via the saturated lime test, electrical conductivity method and X-ray diffraction analyses. Results show that straw fibers are also pozzolanic and act as a silica source within compositions.

The physical properties of new material samples show that those materials are highly-porous, lightweight, and highly water vapor permeable. UPV results conducted with different methods revealed that newly-produced mortar samples are still compressible. Results fluctuations during measurements suggest heterogeneous characteristics of new mortar samples. Material samples have low but still enough physicomechanical properties. The mechanical strength of the new material samples is low, which is attributed to the inadequate level of integration between the binder and straw fibers. Materials are weak under compressive and flexural stress. X-ray diffraction analyses were performed to prove the pozzolanic activity of straw fibers via the formation of hydration products. Both inner and outer powders of the samples were investigated to observe the existence of tobermorite and calcite and their intensities. Cross-section analyses were performed with a stereomicroscope to understand the microstructure of produced mortar samples. Straw fibers form a three-dimensional network that produces several voids and microcracks around fibers.

The sound absorption coefficient and thermal conductivity values of the material samples varies depending on the straw and metakaolin content in the mixtures. Infrared thermography analyses were performed to reveal thermal inertia characteristics of material samples in comparison with some common building materials together with certain types of building insulation materials. Experimentations revealed that heating and cooling rates of materials are different from each other.

Cross-interpretation between newly-produced mortar samples and some commonly-used thermal and sound insulation materials were performed to understand the overall performance of the samples in terms of insulation properties. Regarding sound insulation properties, except for material sample L3W1, newly-produced mortar samples generally have lower sound absorption coefficient, noise reduction coefficient, and weighted sound insulation coefficient values than conventional and alternative insulation materials available in the market. The sound absorption capacity is closely related to the density of materials, for this reason, evaluation should be done under identical thicknesses values to reveal real comparison. The straw-mixed lime-based mortar sample L3W1 has higher sound absorption coefficient values than some conventional materials even with thinner sections. The noise reduction coefficient and

weighted sound absorption coefficient of the sample L3W1 are higher than XPS foam and corkboard insulation. It exhibits similar characteristics with EPS foam, wood fiber insulation, kenaf board, and sheep wool mat in terms of sound absorption. Thermal conductivity values of LM3W1 exhibit similar characteristics with flax mat and hemp mat.

Results on material samples from two groups were interpreted together to reveal individual and combined effects of straw fibers and metakaolin. It is concluded that the increase in the straw fiber content within the compositions reduces the bulk density, ultrasonic pulse velocity, modulus of elasticity, compressive strength, and tensile strength values and increases the effective porosity, water absorption coefficient, water vapor permeability, sound absorption coefficient, noise reduction coefficient, weighted sound absorption coefficient, thermal conductivity, and thermal diffusivity characteristics.

Replacement of half of the binder content with metakaolin within the compositions reduces the bulk density, water vapor permeability, sound absorption coefficient, noise reduction coefficient, and weighted sound absorption coefficient values. Usage of lime binder half in the amount and addition of metakaolin increase the effective porosity, water absorption coefficient, compressive strength, and tensile strength values and thermal conductivity and thermal diffusivity characteristics. Metakaolin has a positive impact on the ultrasonic pulse velocity and modulus of elasticity properties.

Considering revealed performance properties, straw-mixed lime-based mortars with or without pozzolanic additive are valid alternatives to the conventional building insulation materials to be used for thermal and sound insulation purposes. Depending on the specific needs, especially mortar samples produced with the highest amounts of wheat straw fiber with or without metakaolin (L3W1 and LM3W1), new mortar samples provide desirable thermal and acoustic performances. Physicomechanical and mechanical characteristics of mortars can be improved via ensuring better integration between the binder and aggregate context within the material matrix. Newly-produced mortar samples in this study can be used for renovations of historical buildings and new constructions due to their good performance properties.

The knowledge achieved by this research highlight the potentials of the lime-based straw-mixed pozzolanic mortar products in terms of their thermal resistive, sound absorptive, highly-breathable, self-healing, insect-resistive, and long-term durable features contributing to qualified indoor air quality and indoor physical comfort conditions. In addition, protective lime-based breathable coats with particular performances are needed to improve its fire resistance and water impermeability. Therefore, further studies are needed to develop the performance properties of straw-mixed pozzolanic lime-based products, multi-layered compositions with particular performances, and appropriate preparation techniques to benefit from additives at the highest level.

REFERENCES

Adams, T. (2016). *Sound materials: a compendium of sound absorbing materials for architecture and design*. Amsterdam: Frame Publishers.

Alemdar, A. & Sain, M. (2007). Isolation and characterization of nanofibers from agricultural residues: wheat straw and soy hulls. *Bioresource Technology, 99,* 1664-1671. doi:10.1016/j.biortech.2007.04.029

Antonio, J. (2011). Acoustic behaviour of fibrous materials. In R. Fangueiro (Ed.), *Fibrous composite materials for civil engineering applications* (pp. 306-324). Cambridge: Woodhead Publishing.

Arenas, J. & Asdrubali, F. (2018). Eco-materials with noise reduction properties.In Martinez, L. *et al.* (Eds.), *Handbook of Ecomaterials.* (pp. 1-26). Springer. https://doi.org/10.1007/978-3-319-48281-1_137-1

Arizzi, A. & Cultrone, G. (2012). Aerial lime-based mortars blended with pozzolanic additive and different admixtures: a mineralogical, textural and physical-mechanical study. *Construction and Building Materials, 31*, 135-143. doi:10.1016/j.conbuildmat.2011.12.069

Arizzi, A. & Cultrone, G. (2013). The influence of aggregate texture, morphology and grading on the carbonation of non-hydraulic (aerial) lime-based mortars. *Quarterly Journal of Engineering Geology and Hydrogeology, 46*, 507-520. doi:10.1144/qjegh2012-017

Asdrubali, F. (2006). *Survey on the acoustical properties of new sustainable materials for noise control*. Paper presented at the Euronoise 2006, Tampere, Finland.

Asdrubali, F. (2009). *The role of life cycle assessment (LCA) in the design of sustainable buildings: thermal and sound insulating materials*. Paper presented at the Euronoise 2009, Edinburg, Scotland.

Asdrubali, F., D'Alessandro, F., & Schiavoni, S. (2015). A review of unconventional sustainable building insulation materials. *Sustainable Materials and Technologies, 4,* 1-17. http://dx.doi.org/ 10.1016/j.susmat.2015.05.002

Asdrubali, F., Schiavoni, S. & Horoshenkov, K. (2012). A review of sustainable materials for acoustic applications. *Building Acoustics, 19* (4), 283-312.

ASTM C125-19, *Standard Terminology Relating to Concrete and Concrete Aggregates*, ASTM International, West Conshohocken, PA, 2019, www.astm.org

ASTM C351-92b(1999)e1, *Standard Test Method for Mean Specific Heat of Thermal Insulation* (Withdrawn 2008), ASTM International, West Conshohocken, PA, 1992, www.astm.org

ASTM C518-17, *Standard Test Method for Steady-State Thermal Transmission Properties by Means of the Heat Flow Meter Apparatus*, ASTM International, West Conshohocken, PA, 2017, www.astm.org

ASTM C597-16, *Standard Test Method for Pulse Velocity Through Concrete*, ASTM International, West Conshohocken, PA, 2016, www.astm.org

ASTM E96 / E96M-16, *Standard Test Methods for Water Vapor Transmission of Materials*, ASTM International, West Conshohocken, PA, 2016, www.astm.org

Aydın, A., Tavukçuoğlu, A. & Çalışkan, M. (2008). *Assessment of acoustical characteristics for historical baths (hammams)*. Paper presented at the Euronoise 2008, Paris, France.

Bakolas, A., Aggelakopoulou, E., Moropoulou, A. & Anagnostopoulou, S. (2006). Evaluation of pozzolanic activity and physico-mechanical characteristics in metakaolin-lime pastes. *Journal of Thermal Analysis and Calorimetry, 84*, 157-163.

Barbero-Barrera, M., Maldonado-Ramos, L., Van Balen, K., Garcia-Santos, A. & Neila-Gonzalez, F. (2013). Lime render layers: an overview of different properties. *Journal of Cultural Heritage.* http://dx.doi.org/10.1016/j.culher.2013.07.004

Berardi, U. & Iannace, G. (2015). Acoustic characterization of natural fibers for sound absorption applications. *Building and Environment, 94*(2), 840-852. https://doi.org/10.1016/j.buildenv.2015.05.029

Black, C. (Ed.). (1965). *Methods of soil analysis part 2: chemical and microbiological properties*. Madison, Wis: American Society of Agronomy.

Bouasker, M., Belayachi, N., Hoxha, D. & Al-Mukhtar, M. (2014). Physical characterization of natural straw fibers as aggregates for construction materials applications. *Materials, 7,* 3034-3048. doi:10.3390/ma7043034

Böke, H., Akkurt, S., İpekoğlu, B. & Uğurlu, E. (2006). Characteristics of brick used aggregate in historic brick-lime mortars and plasters. *Cement and Concrete Research, 36,* 1115-1122. doi:10.1016/j.cemconres.2006.03.011

Bribian, I., Capilla, A. & Uson, A. (2011). Life cycle assessment of building materials: Comparative environmental impacts and evaluation of the eco-efficient potential. *Buildings and Environment, 46,* 1133-1140. doi:10.1016/j.buildenv.2010.12.002

Brundtland, G. (1987). *Report of the World Commission on Environment and Development: Our common future.* Oxford: Oxford University Press.

Cabrera, J. & Rojas, M. (2001). Mechanism of hydration of the metakaolin-lime-water system. *Cement and Concrete Research, 31*, 177-182.

Cerny, R., Kunca, A., Tydlitat, V., Drchalova, J. & Rovnanikova, P. (2006). Effect of pozzolanic admixtures on mechanical, thermal and hygric properties of lime plasters. *Construction and Building Materials, 20*, 849-857. doi:10.1016/j.conbuildmat.2005.07.002

Cheng, P., Kim, H. & Lin, T. (1992). The study of silica deposition in the leaf blade of Zea mays L. by X-Ray contact microradiography and confocal microscopy. In: A. Michette, G. Morrison & C. Buckley (Eds.), *X-Ray Microscopy III.* Heidelberg: Springer.

Corklink. (2012). *Technical data sheet* [Data File]. Retrieved from http://www.corklink.com/wp-content/uploads/2012/09/expanded-cork-technical-data.pdf

Çizer, Ö., Van Balen, K., Elsen, J. & Van Gemert, D. (2012). Real-time investigation of reaction rate and mineral phase modification of lime carbonation. *Construction and Building Materials, 35*, 741-751. http://dx.doi.org/10.1016/j.conbuildmat.2012.04.036

Degryse, P., Elsen, J. & Waelkens, M. (2002). Study of ancient mortars from Sagalassos (Turkey) in view of their conservation. *Cement and Concrete Research, 32,* 1457-1463.

Desarnaulds, V., Constanzo, E., Carvalho, A. & Arlaud, B. (2005). *Sustainability of acoustic materials and acoustic characterization of sustainable materials.* Paper presented at the Twelfth International Congress on Sound and Vibration, Lisbon, Portugal.

Ding, G. (2014). Life cycle assessment (LCA) of sustainable building materials: an overview. In F. Pacheco-Torgal *et al.* (Eds.), *Eco-efficient construction and building materials* (pp. 38-62). Cambridge: Woodhead Publishing.

Euchora. (2003). *Rapporto di prova* [Data File]. Retrieved from https://www.euchora.com/certificati_EN.html

Errman, M. (2015). *Architectural acoustics illustrated.* Haboken, NJ: Wiley & Sons Inc.

European Union, European Environment Agency. (2014). *Noise in Europe 2014.* Luxembourg: Publications Office of the European Union. doi:10.2800/763331

European Union, Eurostat. (2018). *Energy, transport and environment indicators.* Luxembourg: Publications Office of the European Union. Retrieved from https://ec.europa.eu/eurostat/web/products-statistical-books/

Frias, M. & Cabrera, J. (2001). Influence of MK on reaction kinetics in MK/lime and MK-blended cement systems at 20ºC. *Cement and Concrete Research, 31*, 519-527.

Frias, M., Villar-Cocina, E., Sanchez de Rojas, M. & Valencia-Morales, E. (2005). The effect that different pozzolanic activity methods has on the kinetic constants of the pozzolanic reaction in sugar cane straw–clay ash/lime systems: application of a kinetic-diffusive model. *Cement and Concrete Research, 35*, 2137-2142. doi:10.1016/j.cemconres.2005.07.005

Fortes-Revilla, C., Martinez-Ramirez, S. & Blanco-Varela, M. (2006). Modelling of slaked lime-metakaolin mortar engineering characteristics in terms of process variables. *Cement & Concrete Composites, 28*, 458-467. doi:10.1016/j.cemconcomp.2005.12.006

Gamerio, A., Santos-Silva, A., Veiga, R. & Velosa, A. (2012). Hydration products of lime-metakaolin pastes at ambient temperature. *Thermochimica Acta, 535*, 36-41. doi:10.1016/j.tca.2012.02.013

Global Alliance for Buildings and Construction. (2018). *2018 global status report: towards a zero-emission, efficient and resilient buildings and construction sector.* Retrieved from www.globalabc.org

Grist, E., Paine, K., Heath, A., Norman, J. & Pinder, H. (2013). Compressive strength development of binary and ternary lime-pozzolan mortars. *Materials and Design, 52*, 514-523. http://dx.doi.org/10.1016/j.matdes.2013.05.006

Güleç, A. & Tulun T. (1997). Physico-chemical and petrographical studies of old mortars and plasters of Anatolia. *Cement and Concrete Research, 27*(2), 227-234.

Hain, M., Bartl, J. & Jacko, V. (2009). *Active infrared thermography in non-destructive testing*. Paper presented at the Measurement 2009, Smolenice, Slovakia.

Heraklith. (2015). *Woodwool insulation: inspired by nature* [Data File]. Retrieved from https://heraklith.co.uk/

Huberman, N., Pearlmutter, D. (2008). A life-cycle energy analysis of building materials in the Negev desert. *Energy and Buildings, 40*(5), 837-848. doi:10.1016/j.enbuild.2007.06.002

Iannace, G. (2017). The acoustic characterization of green materials. *Building Acoustics, 24*(2), 101-113. doi: 10.1177/1351010X17704624

IEA. (2018). *World energy statistics.* Paris: OECD Publishing. Retrieved from https://doi.org/10.1787/world_energy_stats-2018-en

International Organization for Standardization. (1998). *Determination of sound absorption coefficient and impedance in impedance tubes – Part 2: transfer function method* (ISO Standard No. 10534-2). Retrieved from https://www.iso.org/standard/22851.html

International Organization for Standardization. (2016). *Hygrothermal performance of building materials and products – determination of water vapour transmission properties – cup method* (ISO Standard No. 12572). Retrieved from https://www.iso.org/standard/64988.html

International Organization for Standardization. (2017). *Non-destructive testing – infrared thermographic testing – general principles* (ISO Standard No. 10880). Retrieved from https://www.iso.org/standard/61881.html

İpekoğlu, B., Böke, H. & Çizer, Ö. (2007). Assessment of material use in relation to climate in historical buildings. Building and Environment, 42, 970-978. doi:10.1016/j.buildenv.2005.10.029

Jelle, B. (2011). Traditional, state-of-the-art and future thermal insulation materials and solutions: Properties, requirements and possibilities. *Energy and Buildings, 43*, 2549-2563. doi:10.1016/j.enbuild.2011.05.015

Kingery, D., Vandiver, P. & Prickett, M. (1988). The beginning of pyrotechnology, part II: production and use of lime and gypsum plaster in the pre-pottery neolithic near east. *Journal of Field Archaeology, 15*(2), 219-244.

Kreith, F. & Black, W. (1980). *Basic heat transfer*. New York, NY: Harper & Row.

Long, M. (2006). *Architectural acoustics*. M. Levy & R. Stern (Eds.). Boston, MA: Elsevier Academic Press.

Luxan, M., Madruga, F. & Saavedra, J. (1988). Rapid evaluation of pozzolanic activity of natural products by conductivity measurement. *Cement and Concrete Research, 19*, 63-68.

Matias, G., Faria, P. & Torres, I. (2014). Lime mortars with heat treated clays and ceramic waste: a review. *Construction and Building Materials, 73*, 125-136. http://dx.doi.org/10.1016/j.conbuildmat.2014.09.028

Meadows, D. H., Meadows, D. L., Randers, J., & Behrens, W. W. (1972). *The limits to growth*. New Yok, NY: Universe Books.

Meadows, D. H., Meadows, D. L., & Randers, J. (1992). *Beyond the limits: confronting global collapse envisioning sustainable future*. Post Mills, VT: Chelsea Green Publishing Company.

Moretti, E., Belloni, E. & Agosti, F. (2016). Innovative mineral fiber insulation panels for buildings: thermal and acoustic characterization. *Applied Energy, 169*, 421-432. http://dx.doi.org/10.1016/j.apenergy.2016.02.048

Moropoulou, A., Bakolas, A. & Aggelakopoulou, E. (2004). Evaluation of pozzolanic activity of natural and artificial pozzolans by thermal analysis. *Thermochimica Acta, 420*, 135-140. doi:10.1016/j.tca.2003.11.059

Naik, T., Malhotra, V. & Popovics, J. (2004). The ultrasonic pulse velocity. In V. Malhotra and N. Carino (Eds.)., *Handbook on Nondestructive testing of concrete*. CRC Press LLC

Nunes, L. (2017). Nonwood bio-based materials. In D. Jones & C. Brischke (Eds.), *Performance of Bio-based Building Materials* (pp. 97-186). Woodhead Publishing. https://doi.org/10.1016/B978-0-08-100982-6.00003-3.

Nunes, C. & Slizkova, Z. (2014). Hydrophobic lime based mortars with linseed oil: characterization and durability assessment. *Cement and Concrete Research, 61-62,* 28-39. http://dx.doi.org/10.1016/j.cemconres.2014.03.011

Oates, J. (1998). *Lime and limestone: chemistry and technology, production and uses*. Weinheim: Wiley-VCH.

Oldham, D., Egan, C. & Cookson, R. (2011). Sustainable acoustic absorbers from the biomass. *Applied Acoustics, 72*, 350-363. doi:10.1016/j.apacoust.2010.12.009

Pacheco-Torgal, F. (2014). Introduction to the environmental impact of construction and building materials. In F. Pacheco-Torgal *et al.* (Eds.), *Eco-efficient construction and building materials* (pp. 1-10). Cambridge: Woodhead Publishing.

Pavlik, V. & Uzakova, M. (2016). Effect of curing conditions on the properties of lime, lime-metakaolin and lime-zeolite mortars. *Construction and Building Materials, 102*, 14-25. http://dx.doi.org/10.1016/j.conbuildmat.2015.10.128

Pedroso, M., De Brito, J. & Silvestre, J. (2017). Characterization of eco-efficient acoustic insulation materials. *Construction and Building Materials, 140*, 221-228. http://dx.doi.org/10.1016/j.conbuildmat.2017.02.132

Pfundstein, M., Gellert, R., Spitzner, M. & Rudolphi, A. (2007). *Insulating materials: principles materials applications.* Munich: Birhauser & Edition Detail.

Rashad, A. (2013). Metakaolin as cementitious material: history, scours, production and composition – a comprehensive overview. *Construction and Building Materials, 41*, 303-318. http://dx.doi.org/10.1016/j.conbuildmat.2012.12.001

Sain, M. & Panthapulakkal, S. (2006). Bioprocess preparation of wheat straw fibers and their characterization. *Industrial Crops and Products, 23,* 1-8. doi:10.1016/j.indcrop.2005.01.006

Schiavoni, S., D'Alessandro, F., Bianchi, F., & Asdrubali, F. (2016). Insulation materials for the building sector: A review and comparative analysis. *Renewable and Sustainable Energy Reviews, 62*, 998-1011. doi:10.1016/j.rser.2016.05.045

Shvarzman, A., Kovler, K., Grader, G. & Shter, G. (2003). The effect of dehydroxylation/amorphization degree on pozzolanic activity of kaolinite. *Cement and Concrete Research, 33*, 405-416.

Siddique, R. & Klaus, J. (2009). Influence of metakaolin on the properties of mortar and concrete. *Applied Clay Science, 43*, 392-400. doi:10.1016/j.clay.2008.11.007

Silva, B., Ferreira-Pinto, A. & Gomes, A. (2014). Influence of natural hydraulic lime content on the properties of aerial lime-based mortars. *Construction and Building Materials, 72*, 208-218. http://dx.doi.org/10.1016/j.conbuildmat.2014.09.010

Stefanidou, M., Papachristoforou, M. & Kesikidou, F. (2016). *Fiber-reinforced lime mortars.* Paper presented at the 4th Historic Mortars Conference, Santorini, Greece.

Tavukçuoğlu, A., Caner-Saltık, E. & Erol, F. (2018). *Kemer Köyü'ndeki (Salihli, Manisa) geleneksel evlerin tamirinde kullanılacak malzemelerin tarifine yönelik analizler: kerpiç harcı ve sıvalar* [Performance analysis of building materials to be used as repair materials in the restoration of traditional houses in Kemer Village (Salihli, Manisa): adobe mortars and plasters]. Paper presented at the 4th National Building Congress, Antalya, Turkey.

Tavukçuoğlu, A., Çiçek, P. & Grinzato, E. (2008). Thermal analysis of an historical Turkish bath by quantitative IR thermography. *QIRT Journal, 5*(2), 151-173. https://doi.org/10.3166/qirt.5.151-173

Teutonico, J. (1988). *A laboratory manual for architectural conservators*. Rome: ICCROM.

Thermonature. (2015). *High performance insulation materials* [Data File]. Retrieved form www.thermo-nature.de

Tunçoku, S. & Caner-Saltık, E. (2006). Opal-A rich additives used in ancient lime mortars. *Cement and Concrete Research, 36*, 1886-1893. doi:10.1016/j.cemconres.2006.06.012

Turkish Standards Institution. (1984). *Determination of specific heat of thermal insulating materials* (Withdrawn Standard) (TS Standard No. 4048). Ankara: Turkish Standards Institution.

Turkish Standards Institution. (2000). *Methods of test for mortar for masonry – Part 1: determination of particle size distribution (by sieve analysis)* (TS Standard No. 1015-1). Ankara: Turkish Standards Institution.

Turkish Standards Institution. (2000). *Methods of test for mortar for masonry – Part 3: Determination of consistence of fresh mortar (by flow table)* (TS Standard No. 1015-3). Ankara: Turkish Standards Institution.

Turkish Standards Institution. (2000). *Methods of test for mortar for masonry – Part 11: Determination of flexural and compressive strength of hardened mortar* (TS Standard No. 1015-11). Ankara: Turkish Standards Institution.

Turkish Standards Institution. (2000). *Methods of test for mortar for masonry – Part 19: Determination of water vapour permeability of hardened rendering and plastering mortars* (TS Standard No. 1015-19). Ankara: Turkish Standards Institution.

Turkish Standards Institution. (2001). *Methods of test for mortar for masonry – Part 10: Determination of dry bulk density of hardened mortar* (TS Standard No. 1015-10). Ankara: Turkish Standards Institution.

Turkish Standards Institution. (2002). *Acoustics: sound absorbers for use in buildings-rating of sound absorption* (TS Standard No. 11654). Ankara: Turkish Standards Institution.

Turkish Standards Institution. (2003). *Thermal performance of building materials and products – determination of thermal resistance by means of guarded hot plate heat flow meter methods: products of high and medium thermal resistance* (TS Standard No. 12667). Ankara: Turkish Standards Institution.

Turkish Standards Institution. (2004). *Testing concrete – Part 4: Determination of ultrasonic pulse velocity* (TS Standard No. 12504-4). Ankara: Turkish Standards Institution.

Turkish Standards Institution. (2012). *Paints and varnishes: determination of water-vapour transmission properties – cup method* (TS Standard No. 7783). Ankara: Turkish Standards Institution.

Turkish Standards Institution. (2013). *Thermal insulation requirements for buildings* (TS Standard No. 825). Ankara: Turkish Standards Institution.

Valero-Delgado, A. (2014). Mineral resource depletion assessment. In F. Pacheco-Torgal *et al.* (Eds.), *Eco-efficient construction and building materials* (pp. 13-37). Cambridge: Woodhead Publishing.

Van Balen, K. (2005). Carbonation reaction of lime, kinetics at ambient temperature. *Cement and Concrete Research, 35*, 647-657. doi:10.1016/j.cemconres.2004.06.020

Veiga, R. (2017). Air lime mortars: what else do we need to know to apply them in conservation and rehabilitation interventions: a review. *Construction and Building Materials, 157*, 132-140. https://doi.org/10.1016/j.conbuildmat.2017.09.080

WeiDong, Y. & Yan, L. (2012). Sound absorption performance of natural fibers and their composites. *Science China Technological Sciences, 55*(8), 2278-2283. doi: 10.1007/s11431-012-4943-1

World Health Organization, International Agency for Research on Cancer. (2002). Man-made vitreous fibres. *IARC monographs on the evaluation of carcinogenic risks to humans, 81*. Lyon: IARCPress

Zach, J., Hroudova, J., Brozovsky, J., Krejna, Z. & Gailius, A. (2013). Development of thermal insulating materials on natural base for thermal insulation systems. *Procedia Engineering, 57,* 1288-1294. doi:10.1016/j.proeng.2013.04.162

Zhang, D., Zhao, J., Wang, D., Xu, C., Zhai, M. & Ma, X. (2018). Comparative study on the properties of three hydraulic lime mortar systems: natural hydraulic lime mortar, cement-aerial lime-based mortar and slag-aerial lime-based mortar. *Construction and Building Materials, 186*, 42-52. https://doi.org/10.1016/j.conbuildmat.2018.07.053